


8-2017

Gcn5 Impacts FGF Signaling At Multiple Levels And Activates C-Myc Target Genes During Early Differentiation Of Embryoid Bodies

Li Wang

Follow this and additional works at: https://digitalcommons.library.tmc.edu/utgsbs_dissertations

 Part of the [Biological Factors Commons](#), [Cell Biology Commons](#), [Developmental Biology Commons](#),
and the [Molecular Biology Commons](#)

Recommended Citation

Wang, Li, "Gcn5 Impacts FGF Signaling At Multiple Levels And Activates C-Myc Target Genes During Early Differentiation Of Embryoid Bodies" (2017). *The University of Texas MD Anderson Cancer Center UTHealth Graduate School of Biomedical Sciences Dissertations and Theses (Open Access)*. 799.
https://digitalcommons.library.tmc.edu/utgsbs_dissertations/799

This Dissertation (PhD) is brought to you for free and open access by the The University of Texas MD Anderson Cancer Center UTHealth Graduate School of Biomedical Sciences at DigitalCommons@TMC. It has been accepted for inclusion in The University of Texas MD Anderson Cancer Center UTHealth Graduate School of Biomedical Sciences Dissertations and Theses (Open Access) by an authorized administrator of DigitalCommons@TMC. For more information, please contact digitalcommons@library.tmc.edu.

**GCN5 IMPACTS FGF SIGNALING AT MULTIPLE LEVELS AND
ACTIVATES C-MYC TARGET GENES DURING EARLY
DIFFERENTIATION OF EMBRYOID BODIES**

by

Li Wang, B. Sc.

APPROVED:

Sharon Y.R. Dent, Ph.D. Advisory Professor

Mark T. Bedford, Ph.D.

David G. Johnson, Ph.D.

Xiaobing Shi, Ph.D.

Pierre D. McCrea, Ph.D.

APPROVED:

Dean, The University of Texas

MD Anderson Cancer Center UTHealth Graduate School of Biomedical Sciences

**GCN5 IMPACTS FGF SIGNALING AT MULTIPLE LEVELS AND
ACTIVATES C-MYC TARGET GENES DURING EARLY
DIFFERENTIATION OF EMBRYOID BODIES**

**A
DISSERTATION**

Presented to the Faculty of
The University of Texas MD Anderson Cancer Center UTHealth

And
Graduate School of Biomedical Sciences

in Partial Fulfillment
of the Requirements
for the Degree of
DOCTOR OF PHILOSOPHY

by
Li Wang, B. Sc.
Houston, Texas

August 2017

ACKNOWLEDGMENTS

Ph.D. graduation marks a milestone in life, and it reminds me of everyone who has touched my life during this long, yet extremely rewarding and never-short-of-surprise journey. I would not be here today without the help and support from those who had stood by my side along this path.

I would like to express my sincere gratitude to my advisory professor, Dr. Sharon Dent, for her continuous support of my Ph.D. study and research. Sharon has always encouraged me to think outside the box and given me the freedom to pursue my scientific interests, yet she has kept me on track through her constructive criticisms. Despite her hectic schedule as the director of Science Park, she has always made herself available to help me, from evaluating detailed experimental results to insightful discussions over career plans. During my preparation for graduation, she has been an instrumental force to support and motivate me in crafting a quality research article and a scholarly dissertation, all in less than two months. It is because of her that my graduate life has been such a rewarding experience filled with enlightenment and positivity. I am proud, as I am grateful to have Sharon as my Ph.D. mentor.

Besides my advisor, I would like to thank the rest of my advisory committee, Dr. Mark Bedford, Dr. David Johnson, Dr. Pierre McCrea, Dr. Xiaobing Shi (2012-2017) and Dr. Michelle Barton (2011-2012). They have

offered insightful suggestions and comments to help shape my project. They have also asked hard questions, driving me to delve further in the literature and think more in order to refine my project. Although I have had members located both in Smithville and Houston, my committee has made it easy for me to arrange meetings timely in compliance with GSBS requirements. I sincerely appreciate their flexibility and willingness to help all these years.

The Dent Lab has been a nourishing environment for me to grow in for the past 6 years. This is a lab that appreciates and promotes hard work, creative ideas, critical thinking, individuality and teamwork. I have always felt supported and encouraged during my time in the lab. In particular, Dr. Calley Hirsch, a previous lab member, introduced me to stem cell biology, which eventually set the stage for me to build a project exploring gene regulation mechanisms in stem cell differentiation. I will always appreciate her for opening my eyes to this exciting research field. Dr. Andria Schibler (NIH) had been my lab “buddy” while she was here getting her Ph.D. We worked through countless late night hours together. Her creative ideas, resourcefulness in problem solving, and her humorous personality had been and will always be part of the fond memories of my grad-school life. Dr. Evangelia Koutelou has been my go-to person ever since I started diving into the world of stem cell differentiation (or embryonic development). She is well versed in many disciplines and techniques ranging from biochemistry to cell biology and to embryonic development. I learned many skills from her that

proved to be instrumental for my research, for instance, isolating stem cells from early stage mouse embryos, differentiating stem cells into specific lineages (we made neurons and vessels from stem cells!), preserving the EBs for cryosections/imaging, basic techniques to create stable cell lines, and so on. But more importantly, I find her enthusiasm toward science and her passionate, positive attitude toward life to be the most inspiring and encouraging. I feel so fortunate to have come to know Andria and Lia as great companions at work, also wonderful friends in life.

I would like to also extend my appreciation to our lab manager, Mr. Andrew Salinger, and our mouse expert, Amanda Martin. They have provided critical logistic and material support for my research.

Throughout the years, I had the opportunity to collaborate with scientists outside our lab. For instance, I worked with Dr. Ryan McCarthy (Barton Lab) for mass cytometry experiments, also collaborated with Dr. Junya Tomida (Wood Lab) to create the ES cells expressing GCN5 tagged with Flag-HA. These collaborations proved to be very educational and helpful.

The core facilities of MD Anderson Cancer Center, particularly, at Science Park have been very important for me to carry out my research. We have an amazing next generation sequencing (NGS) team and strong bioinformatics support here in Science Park, also a very capable confocal imaging core. And I had the opportunity to work with the CyTOF team (mass cytometry) in Houston. Their quality and timely services made it possible for

me to generate reliable data fundamental for my publication and this dissertation.

Science Park, a reclusive research institute surrounded by beautiful pine forests, has been a wonderful place for me to experience graduate life. I was able to concentrate on my study and research in the quiet, safe campus, yet also disengage anytime by simply stepping into wonderful natural world, or to explore city life close by. My overall grad-school experience proved that I had made the absolutely right decision to come here in the first place.

Finally, the love and support of my family has been always assuring and comforting all these years. Although I wish my father were alive to witness this achievement in my career, he would have been very proud.

As Nobel Laureate Dr. Bruce Beutler pointed out, it is important for scientists, especially the rising scientists, to develop an area of research, make progressive discoveries, and earn reputation for solid work. Graduate study/research made a great start on this course for me, I am excited and enthusiastically anticipate the journey ahead.

**GCN5 IMPACTS FGF SIGNALING AT MULTIPLE LEVELS AND
ACTIVATES C-MYC TARGET GENES DURING EARLY
DIFFERENTIATION OF EMBRYOID BODIES**

Li Wang, B.Sc.

Advisory Professor: Sharon Y.R. Dent, Ph.D.

Precise control of gene expression during development is orchestrated by transcription factors, signaling pathways and co-regulators, with complex cross-regulatory events often occurring. Growing evidence has identified chromatin modifiers as important regulators for development as well, yet how particular chromatin modifying enzymes affect specific developmental processes remains largely unclear. Embryonic stem cells (ESCs) are self-renewing, pluripotent, and have the abilities to generate almost all cell types in adult tissues. The dual capacity of ESCs to self-renew and differentiate offers unlimited potential for studying gene regulation events at specific developmental stages *in vitro* that parallel developmental events during embryogenesis *in vivo*.

In this dissertation project, we use a murine ESC aggregation assay (embryoid body formation, EB) to model the early development stages that proceed gastrulation, and report that GCN5, a histone acetyltransferase

(HAT) essential for embryonic development, is required for proper expression of multiple genes encoding components of the FGF signaling pathway, and for normal activation of ERK and p38 downstream of FGF signaling at early stages of EB formation. Loss of *Gcn5* is associated with disorganized cytoskeletal networks, and compromised capacity of ESCs to differentiate toward mesodermal and endodermal lineages. We identified 7 genes as putative direct targets of GCN5 during early differentiation by using RNAseq and H3K9ac ChIPseq. These genes are reportedly involved in signaling and metabolism, and most interestingly, 4 of them are c-MYC targets. These findings established a novel link between GCN5 and FGF signaling pathway, and highlighted the GCN5-MYC partnership in gene regulation during early differentiation.

TABLE OF CONTENTS

	PAGE
APPROVAL PAGE	i
TITLE PAGE	ii
ACKNOWLEDGMENTS	iii
ABSTRACT	vii
TABLE OF CONTENTS	ix
LIST OF FIGURES	xii
LIST OF TABLES	xiv
LIST OF APPENDIXES	xv
Chapter 1. Introduction	1
1.1 Chromatin and gene transcription: Histone acetylation	2
1.2 GCN5 functions: from gene transcription to embryonic development.....	4
1.3 Embryonic stem cells: <i>in vitro</i> model system for developmental gene expression studies.....	9
1.4 GCN5 – MYC partnership in the stem cell state	13
1.5 Is GCN5 important in ESC differentiation?	17
1.6 Significance	19
Chapter 2. Materials and Methods	21
Chapter 3. <i>Gcn5</i> loss leads to defective morphogenesis of EBs at epiblast stage.....	46

3.1 Embryoid body (EB) assay models embryogenesis leading to gastrulation.....	47
3.2 <i>Gcn5</i> ^{-/-} EBs do not exhibit defective proliferation or apoptosis at day5 ..	47
3.3 <i>Gcn5</i> ^{-/-} epiblast is severely disorganized at day 5.....	53
Chapter 4. <i>Gcn5</i>^{-/-} EBs have impaired capacities in differentiation	56
4.1 <i>Gcn5</i> ^{-/-} expresses lower levels of epiblast-specific marker genes at day 5	57
4.2 Delineating heterogenic populations in day5 <i>Gcn5</i> ^{-/-} EBs by mass cytometry	59
4.3 <i>Gcn5</i> ^{-/-} EBs have impaired abilities to differentiate into germ layers	66
Chapter 5. Gene expression profiling points to a regulatory role of <i>Gcn5</i> in FGF signaling pathway	68
5.1 Overview of differentially expressed genes upon <i>Gcn5</i> loss at day 3 and day 5	69
5.2 Gene ontology and pathway analysis reveal deregulated FGF signaling in <i>Gcn5</i> ^{-/-} EBs at day5	72
5.3 Validating Changes in Expression of FGF pathway genes by qRT-PCR.	72
Chapter 6. Deregulation of FGF signaling in <i>Gcn5</i>^{-/-} EBs	83
6.1 Abnormal FGF signaling in day5 <i>Gcn5</i> ^{-/-} EBs	84
6.2 Deficient activation of ERK and p38 is associated with crippled cytoskeletal networks in <i>Gcn5</i> ^{-/-} EBs at day 5	85
Chapter 7. GCN5 regulates selective c-MYC target genes in early differentiation.....	89

7.1 Attempts of ChIPs for GCN5 in differentiating EBs not successful.....	90
7.2 H3K9ac ChIPs in <i>Gcn5^{fx/fx}</i> and <i>Gcn5^{-/-}</i> EBs at day5	101
7.3 GCN5 is required for activating c-MYC target genes in day 5 EBs	101
Chapter 8. Conclusions, Discussion and Future Directions	113
8.1 Conclusions.....	114
8.2 Possible contributions to the observed EB phenotypes by non- transcriptional targets of GCN5.....	122
8.3 Potential compensatory effects from GCN5/ATAC or PCAF	129
8.4 Potential novel roles of GCN5 during early differentiation	130
8.5 Concluding remarks and perspectives	132
APPENDIXES.....	135
BIBLIOGRAPHY	185
VITA.....	208

LIST OF FIGURES

Figure 1 GCN5 containing complexes in mammalian systems	5
Figure 2 Creation of the pairing <i>Gcn5^{fx/fx}</i> and <i>Gcn5^{-/-}</i> ESCs	11
Figure 3 GCN5 – MYC partnership to promote gene transcription in various developmental/differentiation contexts	16
Figure 4 <i>Gcn5^{-/-}</i> EBs have abnormal morphology during early stages of differentiation.....	49
Figure 5 Loss of <i>Gcn5</i> does not inhibit proliferation or promote apoptosis at an early differentiation stage.....	51
Figure 6 Severely disorganized epiblast of <i>Gcn5^{-/-}</i> EBs at day 5	55
Figure 7 Epiblast marker genes are expressed at lower levels in <i>Gcn5^{-/-}</i> EBs.....	58
Figure 8 Using mass cytometry to delineate heterogeneous cell populations in differentiating ESCs.....	63
Figure 9 Changes in cell population composition in <i>Gcn5^{-/-}</i> EBs at the epiblast stage.....	65
Figure 10 Impaired differentiation abilities of <i>Gcn5^{-/-}</i> EBs.....	67
Figure 11 Overview of altered gene expression profiles in early stage <i>Gcn5^{-/-}</i> EBs	71
Figure 12 Top enriched processes identified by GSEA in the control EBs compared to <i>Gcn5^{-/-}</i> EBs at day 5	74

Figure 13 Altered gene expression profiles of FGF signaling pathway components in <i>Gcn5</i> ^{-/-} EBs at day 5	82
Figure 14 Deficient activation of the FGF pathway in the day 5 <i>Gcn5</i> ^{-/-} EBs.....	88
Figure 15 Attempts of GCN5 ChIPs for EBs are not successful	93
Figure 16 Creation of Flag-HA-GCN5 expressing J1 ESCs using targeted insertion mediated by CRISPR/CAS9	97
Figure 17 FLAG-HA-GCN5 interacts with subunits of SAGA complex in ESCs	99
Figure 18 Putative target genes of GCN5 during early EB differentiation	112
Figure 19 GCN5 impacts multiple components of the FGF signaling pathway and activates MYC targets during early differentiation.....	116
Figure 20 Acetylation of tubulin is not overtly affected by <i>Gcn5</i> loss in day 5 EBs	124
Figure 21 GCN5 expression is regulated during early differentiation..	128
Figure 22 Increased immune response in day 5 <i>Gcn5</i> ^{-/-} EBs.....	131

LIST OF TABLES

Table 1 Antibodies used in this study	38
Table 2 Primers used for PCR analyses	42
Table 3 Lineage markers used for mass cytometry	62
Table 4 Gene list of GSEA set Multicellular Organismal Development ..	76
Table 5 Gene list of GSEA set Cell Surface Receptor Linked Signal Transduction	79
Table 6 Mapping rates of the tags from the H3K9ac ChIPseq to mouse genome assembly mm10	102
Table 7 Peak calling for differential test between <i>Gcn5^{fx/fx}</i> and <i>Gcn5^{-/-}</i> samples	104
Table 8 Comparison of H3K9ac peaks and associated genes in <i>Gcn5^{fx/fx}</i> and <i>Gcn5^{-/-}</i> EBs at day 5.....	107
Table 9 Top ranked transcription factors or regulators reported to bind genes with decreased H3K9ac identified in <i>Gcn5</i> null EBs at day 5	108

LIST OF APPENDIXES

Appendix 1 List of genes with altered expression levels upon <i>Gcn5</i> loss in day 5 EBs identified by RNAseq (FDR 0.05, FC2).....	135
Appendix 2 List of genes with altered expression levels upon <i>Gcn5</i> loss in day 3 EBs identified by RNAseq (FDR 0.05, FC2).....	172
Appendix 3 List of genes with decreased H3K9ac levels in promoter region upon <i>Gcn5</i> loss in day 5 EBs (FDR0.05).....	180

Chapter 1. Introduction

1.1 Chromatin and gene transcription: Histone acetylation

In eukaryotes, genomic DNA is highly compacted to fit into the nucleus. To accomplish this, 146 base pairs (bps) of DNA wrap an octamer of core histone proteins (H2A, H2B, H3 and H4) to form a nucleosome, which is the basic unit of chromatin. Repeating arrays of nucleosomes interconnected by linker DNA and histone H1 are further packed into higher-order chromatin structures. The relaxation or condensation of chromatin exposes or limits the genetic information to be accessed by transcriptional machineries, which in turn control transcription from the DNA.

At the center of chromatin structure are the highly conserved core histone proteins. Both the N-terminal tail domains and the globular domains of histones are subject to a variety of post-translational modifications, however the tail domains are more heavily modified, including acetylation, phosphorylation, methylation, ubiquitination, sumoylation and ADP-ribosylation ([1](#), [2](#)). These modifications influence chromatin organization by affecting histone – DNA, nucleosome – nucleosome, and nucleosome – chromatin modifier interactions, and therefore provide multiple levels of chromatin state remodeling, and thus regulate gene transcription, DNA replication and DNA damage repair.

Histone acetylation has long been associated with open-states of chromatin and active gene transcription. The histone tail domains are rich in lysine (K) residues including H3K9, H3K14, H3K18, H4K5, H4K8 and H4K12, to name a few (3). The addition of the acetyl group effectively neutralizes the positive charge of histone tails, perturbing the histone-DNA interaction and the interactions between neighboring histones, which then lead to a more relaxed chromatin state, allowing for the access of transcriptional machineries. Acetylated lysines (K-ac) can also serve as docking sites for chromatin regulators to facilitate transcription (4). For instance, K-ac can be “read” by bromodomain containing chromatin modifiers, which often are HAT, methyltransferases, or chromatin remodeling complexes, to “open up” the chromatin for transcription (5, 6). K-ac can be bound by YEATS domain containing proteins like AF9 as shown in a recent report (7), which also promotes active transcription.

The level of histone acetylation is dynamic, and is regulated by the opposing actions of two families of chromatin modifiers, histone acetyltransferases (HATs) and histone deacetylases (HDACs). Although many HATs and HDACs have been identified to date, we still know very little about the specific biological processes regulated by particular enzymes. This dissertation project focuses on one such enzyme, GCN5, and its functions during early differentiation stages of embryonic stem cells.

1.2 GCN5 functions: from gene transcription to embryonic development

GCN5 was the first HAT to be linked to active transcription, and it exerts the fullest enzymatic activity when incorporated into multimember complexes ([8](#)). The main subunits and structures of GCN5 containing complexes are highly conserved across evolution ([9](#), [10](#)). In yeast, Gcn5 is part of the SAGA (SPT-ADA-GCN5 acetyltransferase) and ADA complexes. In mammalian systems, GCN5 is also a subunit of another complex called ATAC (ADA2A containing complex), although SAGA has until recently been the better defined GCN5 containing complex in terms of its subunits, modular organization and functions in gene transcription ([11](#)) (Figure 1). GCN5 has a highly related homolog protein, PCAF, which is a subunit of another multimember complex similar to SAGA ([11-13](#)).

The mammalian SAGA complex is organized into four functional submodules, including two enzymatic modules, a HAT module (including GCN5, the ADA proteins and SGF29) and a deubiquitinating (DUB) module containing USP22 as the catalytic subunit, along with ENY2, ATXN7 and ATXN7L3. Several substrates have been defined for SAGA, including acetylation on K9, K14, and K18 of H3 and ubiquitination on K120 of H2B. SAGA has two other submodules, the SPT module and the TAF module, which are essential for SAGA integrity and its interactions with transcriptional machinery ([11](#), [14](#)).

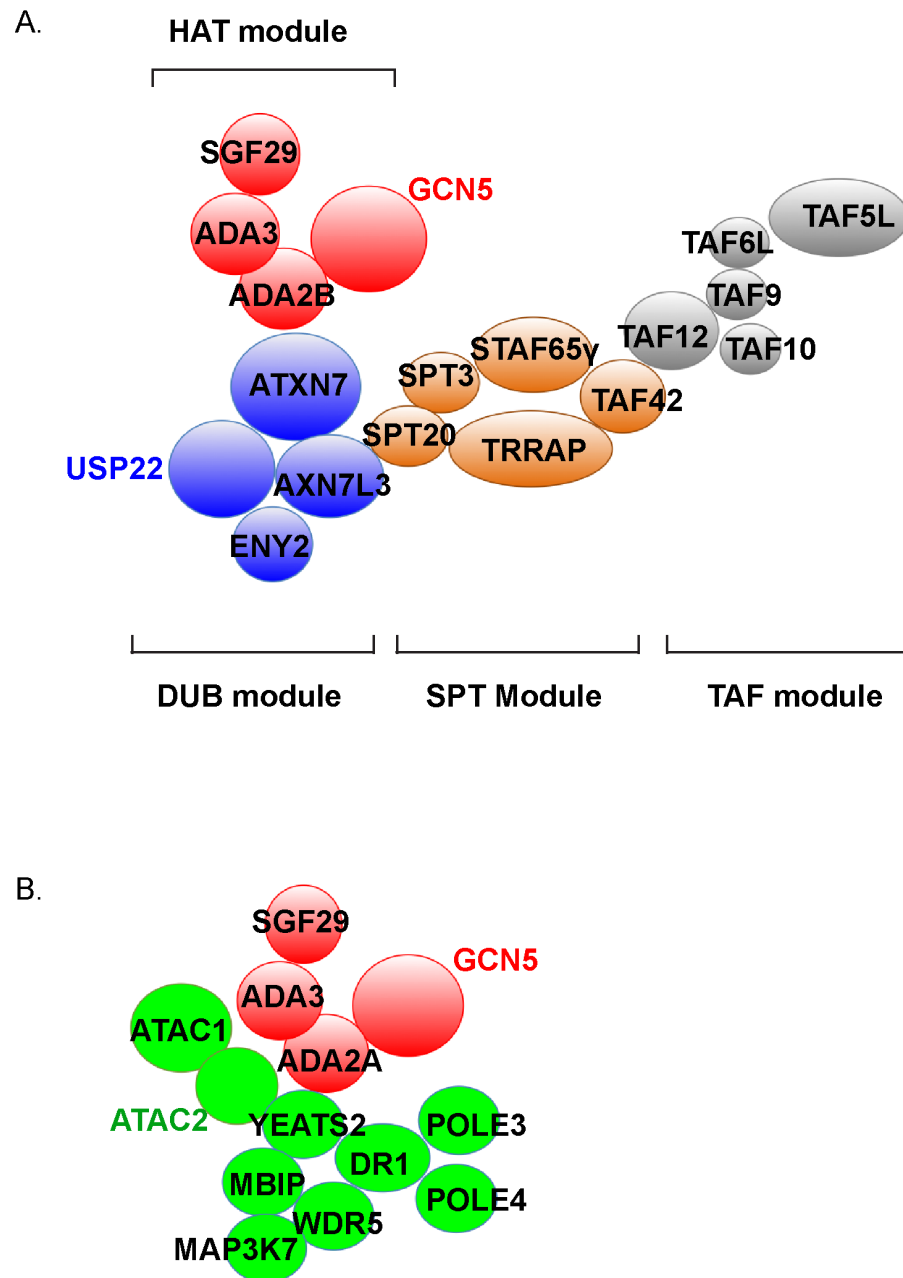


Figure 1 GCN5 containing complexes in mammalian systems

(A) The SAGA complex is composed of four submodules: SPT (orange), TAF (grey), DUB (blue) and HAT (red). GCN5 is the enzymatic center of the HAT

module and ADA2B is specific to the SAGA complex. USP22 is the deubiquitinase of the DUB module.

(B) ATAC complex has a similar GCN5 containing HAT module (red) with a unique ADA2A, and subunits (green) unique from SAGA. ATAC2 is a weak HAT that acetylates H4. YEATS2 is a reader for both acetylation and crotonylation of histones ([7](#), [15](#)).

Text color codes: the enzymes are highlighted in colors corresponding to the modules to which they belong.

This figure is adapted from my review in 2014 ([11](#)).

Both enzymatic activities of SAGA facilitate gene transcription. Although SAGA does not bind DNA directly, it is recruited by specific transcription factors (TFs), such as c-MYC, E2F and p53 ([16-20](#)), through the SPT module to their target gene promoters, allowing the GCN5/HAT-module to acetylate the nearby lysines on histone H3. Meanwhile, the TAF module interacts with the transcriptional machinery to promote the initiation of transcription. SAGA also facilitates transcript elongation after transcription is initiated, which is accomplished by actions of both HAT and DUB (USP22) modules ([14](#)).

Growing evidence indicates that the mammalian SAGA acts as a gene-specific co-activator ([21](#), [22](#)), but may also promote global gene transcription by recruiting RNA polymerase II (pol II) to all transcribed genes ([23](#)). Genetic studies of GCN5, however, support a selective role of GCN5/SAGA in gene regulation. For instance, both GCN5 and its catalytic activity are essential for normal development and survival of mouse embryos. *Gcn5* null embryos die soon after gastrulation and exhibit increased apoptosis in mesodermal lineages ([24](#)). *Gcn5* catalytic mutants, however, survive until mid-gestation, but develop cranial neural tube closure defects (NTDs) ([25](#)) due to abnormal retinoic acid (RA) signaling involving a non-histone substrate of GCN5 ([26](#)). These findings indicate that GCN5-containing complexes have both HAT dependent and independent functions during early development. The phenotypes of *Gcn5* mutant mice also indicate specific requirement for this

HAT in gene regulation during development, as loss of general transcription factors often leads to very early, preimplantation, death (27).

A conditional, “floxed” allele of *Gcn5* was also generated by the Dent lab to aid investigations of GCN5 functions in specific tissues or cell populations, at particular developmental stages. The *Gcn5*-floxed allele behaves as wild type, and mice homozygous for this allele (*Gcn5^{fx/fx}*) show no overt phenotypes (28). After exposure to Cre recombinase, exons 3-18 of *Gcn5* are deleted, creating a null allele. By crossing *Gcn5^{fx/fx}* mice with mice bearing *Cre* alleles driven by tissue specific promoters, *Gcn5* can be deleted in the tissues of interest, providing the opportunities to define the tissue specific requirements of *Gcn5* in gene regulation. For instance, a *Nestin-Cre*-mediated *Gcn5* deletion in neural stem cells (NSC) in the developing brain leads to reduced brain mass with microcephaly, a phenotype similar to that of *c-Myc* or *n-Myc* NSC conditional knockouts (29). Gene expression analysis shows that about 1/6 of genes impacted by *Gcn5* loss are also N-MYC targets, suggesting that GCN5 is a co-activator for N-MYC target gene expression in NSCs of the developing brain (29). Another study from our lab also reported the requirement for *Gcn5* in adipose tissue development. *Myf5-Cre*-mediated *Gcn5* deletion in precursors of brown adipose tissue of *Pcaf^{-/-}* mice results in postnatal lethality due to impaired brown adipose tissue development. Furthermore, GCN5/PCAF facilitate adipogenesis through

regulation of *PPAR γ* expression and regulate brown adipogenesis by influencing *Prdm16* expression (30).

Collectively, these findings indicated that GCN5 is essential for embryogenesis, and is required for normal development of neural tissues and brown adipose tissues by regulating the expression of specific gene programs. It was still unclear, though, what gene programs are regulated by GCN5 during early stages of development, as the early lethality of the *Gcn5* mutant embryos posed significant challenges for detailed molecular studies.

1.3 Embryonic stem cells: *in vitro* model system for developmental gene expression studies

Mouse embryonic stem cells (ESC) are derived from the inner cell mass (ICM) of a blastocyst, which is an early stage of a preimplantation embryo (31). ESCs are self-renewing and can be propagated in culture while retaining pluripotency. Pluripotency refers to the capacity of a single cell to differentiate into all cell lineages in the course of development, from a developing embryo to the fully developed organs in an adult. Self-renewal refers to the ability of a cell to proliferate and generate an identical daughter cell (31). Gene expression programs controlling pluripotency and self-renewal of ESCs *in vitro* are regulated by intricate networks of TFs (e.g. the OCT4-SOX2-NANOG network)(32, 33), growth factor or cytokine signaling (e.g. leukemia inhibitory

factor, LIF) (34) and an array of cofactors including chromatin regulators (e.g. Polycomb group and TIP60-p400)(35). These regulatory events are executed in a manner proven to be largely similar to that observed *in vivo*, which make the ESCs an attractive *in vitro* system modeling self-renewal, pluripotency maintenance and differentiation.

In light of these technical advances, *Gcn5* null ES cells were created in order to define the roles of GCN5 in self-renewal and/or pluripotency/differentiation *in vitro* (36). To do so, *Gcn5^{fx/fx}* ES cell isolates were derived from blastocysts of *Gcn5^{fx/fx}* mouse intercrosses, and then were transiently exposed to an EGFP-Cre recombinase by transfection (36) (Figure 2A). The GFP⁺ cells were sorted and selected by flow cytometry, and individual colonies propagated from the GFP⁺ cells were collected to confirm *Gcn5* deletion and to determine karyotypes (a term for the number and appearance of chromosomes in the nucleus of a eukaryotic cell). Two independent *Gcn5^{-/-}* ES clones were generated by this means (Figure 2, B and C), and together with their parental *Gcn5^{fx/fx}* isolates, were confirmed to have normal karyotypes.

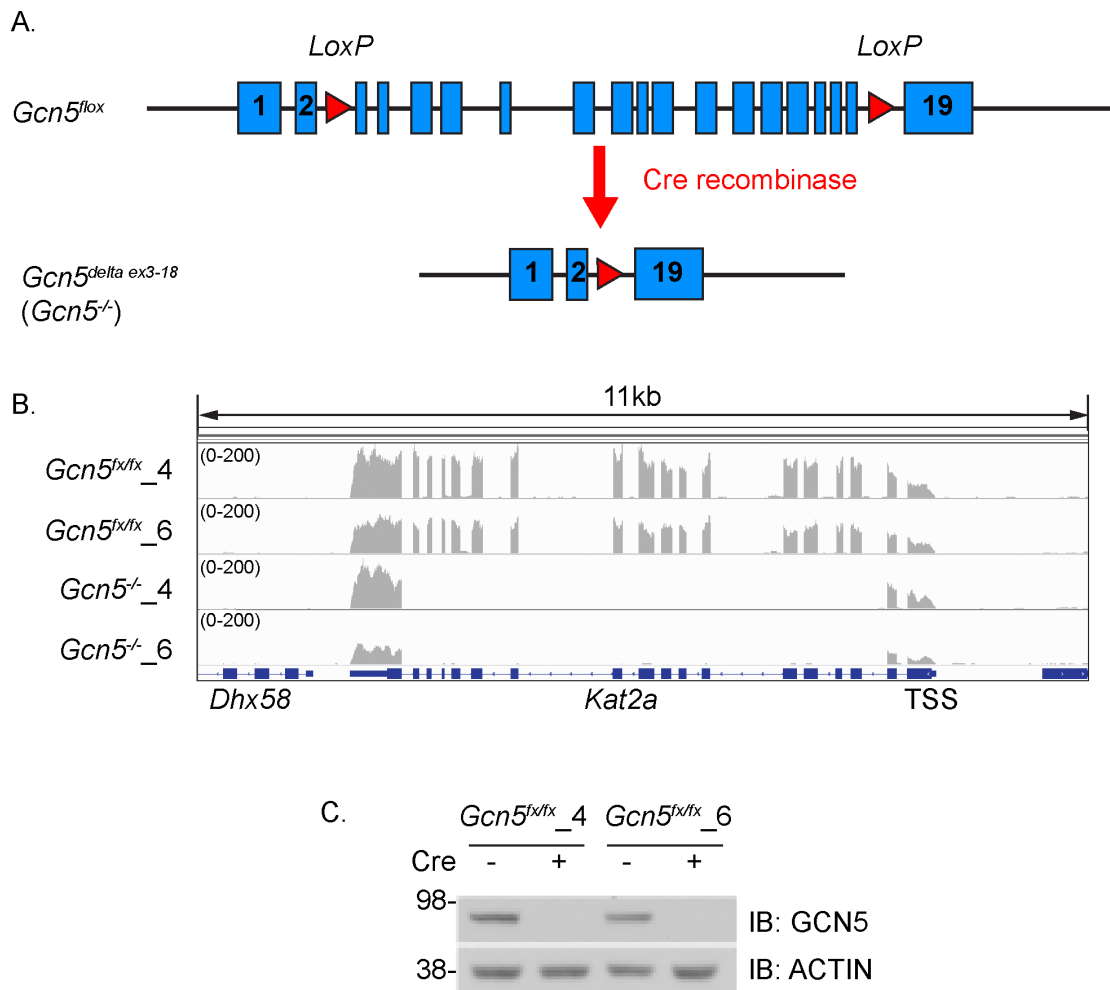


Figure 2 Creation of the pairing *Gcn5^{fx/fx}* and *Gcn5^{-/-}* ESCs

(A) A diagram illustrating the creation of a *Gcn5^{-/-}* allele after exposure of the *Gcn5^{fx/fx}* to Cre recombinase.

(B) and (C) RNA transcripts (B) and immunoblots (C) showing deletion of *Gcn5* and loss of GCN5 protein in the two null isolates.

This figure is adapted from an article (36) published in *Genes & Development*, for which I was an author.

Of note, these *Gcn5*^{-/-} ES clones have the same genome as the parental *Gcn5*^{fx/fx} ES cells, except for lack of exons 3-18 of *Gcn5* gene. Such genomic match should reduce the individual variance between the control and null cells, as would have been observed in isolates from wild type and null mice. Thus, in theory any defect observed in these *Gcn5*^{-/-} ES cells should be exclusively due to *Gcn5* loss.

In order to determine the genome wide association of GCN5 in wild type ESCs, AB1 mouse ESCs stably expressing *in vivo* biotinylated GCN5 (BirAV5-FLBioGcn5) were generated ([36](#), [37](#)) with a control cell line (BirAV5-FLBio) that stably expressed BirA and FLBio alone. This approach was used due to the absence of a suitable GCN5-specific antibody for efficient and specific chromatin immunoprecipitation (ChIP). The *in vivo* biotinylation system has two advantages; first, the biotinylated GCN5 can be immunoprecipitated by streptavidin, which is extremely efficient; second, the FLBioGCN5-stable-ESCs were selected for lower or equal protein level of FLBioGCN5 relative to that of endogenous GCN5, reducing potential artifacts due to exogenous protein expression.

These resources made it possible to define the gene expression programs regulated by GCN5 in undifferentiated ESCs.

1.4 GCN5 – MYC partnership in the stem cell state

Gcn5^{-/-} ES cells could be maintained in media conditioned for stem cell growth, and did not exhibit overt abnormalities ([28](#), [36](#)), suggesting that *Gcn5* is not required for ESC survival in undifferentiated culture conditions.

Streptavidin-ChIP coupled with deep sequencing (bioChIPseq) using the FLBioGCN5 ES cells showed that average binding profile of GCN5 strongly correlates that of RNA polymerase II (pol II), and that 59% of GCN5 binding sequences are active promoters, in keeping with its known co-activator role in transcription. Interestingly GCN5 also binds to a cluster of bivalent domains, which refer to promoter regions, largely of developmental genes, simultaneously marked by both activating (H3K4me3) and repressing (H3K27me3) histone modifications ([38](#)). Bivalent domains keep genes at a poised state, allowing for rapid activation by losing H3K27me3 or continued silencing by losing H3K4me3 upon appropriate developmental cues ([39](#)). The association of GCN5 with bivalent domains indicates that GCN5 maybe involved in regulating genes specific for pluripotency or differentiation in the ES cells. Comparison to published ChIP data in mouse ESCs revealed a striking correlation between GCN5 binding sites with those of MYC-E2F1, but not NANOG -OCT4-SOX2 TF network ([33](#), [40](#)). In addition, these sites primarily fell into the genes actively transcribed in the ESCs. These findings suggested that GCN5 co-activates MYC and E2F1 transcriptional networks in

pluripotent cells. Integration with the altered gene expression profiles generated from *Gcn5*^{fx/fx} and *Gcn5*^{-/-} ES cells further confirmed these findings, showing that a significant portion of the putative target genes directly activated by GCN5 (genes bound by GCN5, and with expression down regulated upon *Gcn5* loss) are also MYC/E2F targets, which largely regulate cell cycle. These results strongly indicate that GCN5 is an important co-factor for MYC/E2F TF network to regulate proliferation/self-renewal in ESCs ([36](#)).

The GCN5-MYC partnership defined in ESCs raised the possibility that GCN5 might also engage MYC during somatic cell reprogramming to induce pluripotent stem cell state from differentiated adult cells. Indeed, a functional RNAi screen for the earliest epigenetic regulators required for reprogramming identified GCN5 and several other SAGA subunits as critical regulators of reprogramming initiation. Genome wide analysis of gene expression events upon reprogramming initiation in MEFs (mouse embryonic fibroblasts) showed that, GCN5 and MYC form a positive feed-forward loop that activates a distinct alternative splicing gene network, which promotes the acquisition of the alternative slicing events essential for establishing pluripotency in early steps of reprogramming ([36](#)).

In concordance with the GCN5/N-MYC connection in NSC gene regulation ([29](#)), these collective studies highlight a GCN5 – MYC partnership in

regulating gene expression in self-renewal of the ESCs and in initiation steps of somatic cell reprogramming (Figure 3).

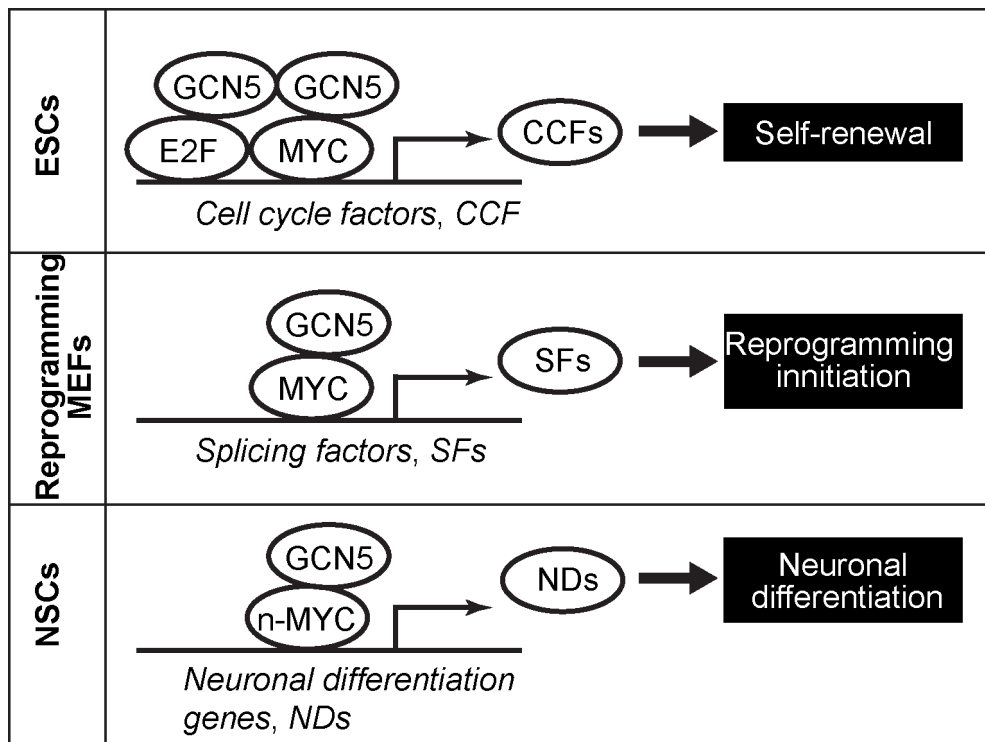


Figure 3 GCN5 – MYC partnership to promote gene transcription in various developmental/differentiation contexts

A cartoon showing GCN5 interactions with MYC family or related (E2F) factors to promote gene transcription in ESCs, reprogramming of MEFs (mouse embryonic fibroblasts) and NSCs (neural stem cells) in the developing brain ([29](#), [36](#)).

1.5 Is GCN5 important in ESC differentiation?

Our previous studies indicated the involvement of *Gcn5* in early differentiation events of ESCs, as *Gcn5* null ESCs (isolates derived from *Gcn5*^{-/-} blastocysts, which are different from the isogenic *Gcn5*^{-/-} ESCs made from *Gcn5*^{fx/fx} ESCs) form smaller aggregates compared to the wild type at day 6 of differentiation, and prematurely down regulated select pluripotency genes such as *Oct4* and *Nodal* in the absence of LIF. The expression of a mesoderm marker *Flk1*, but not the ectodermal markers tested, was lower in the *Gcn5* null EBs relative to the wild type EBs ([28](#)). These observations indicate that loss of *Gcn5* does not completely halt differentiation, but does affect the normal expression dynamics of specific genes during the process. The early loss of mesodermal lineages shortly after gastrulation in *Gcn5* null embryos also suggested that *Gcn5* might be important for specific lineage development. However, the early developmental processes and associated signaling pathways modulated by GCN5 have not yet been clearly defined.

By the time of implantation during mammalian development, the blastocyst has formed distinct lineages, including the trophoblast cells outlining the blastocyst that will give rise to extra-embryonic tissues, and the ICM, which develops into the epiblast, a columnar epithelial structure in a shape of an egg cylinder. The epiblast further differentiates into three germ layers,

ectoderm, endoderm and mesoderm. The process by which germ layers are formed from the epiblast is termed gastrulation ([34](#)).

Fibroblast growth factor (FGF) signaling is essential for these multiple stages during early embryonic development, from segregation of trophectoderm and primitive endoderm from the ICM ([41-46](#)) to specifications of primitive ectoderm and primitive streak ([47](#)), which in turn determine the fate of epiblast. ESC-based studies indicate that FGF signaling is involved in both pluripotency maintenance and neural ectodermal and mesodermal lineage specification ([48-50](#)) *in vitro*. However, how or if chromatin regulators contribute to FGF pathway regulation of gene expression programs during early developmental events is not yet clear.

This dissertation project employed an embryoid body differentiation protocol to define the functions of GCN5 in ESC differentiation. Embryoid bodies are 3-dimensional aggregates formed by ESCs in suspension upon withdrawal of LIF and inhibitors for ERK and GSK3 β (2i-s), which block differentiation. Hallmark events of this process include endodermal differentiation (visceral endoderm, VE) and basement membrane (BM) assembly at days 2-3, followed by polarized epiblast formation from the inner cells and the clearance of a central cavity (days 4-6) ([51](#)). These sequential events recapitulate transitions from formation of the inner cell mass (ICM) through embryonic

gastrulation, thereby providing opportunities to define molecular events in vitro that might contribute to the death of *Gcn5* null embryos shortly after gastrulation *in vivo*.

Using the *Gcn5*^{fx/fx} and *Gcn5*^{-/-} ESCs aforementioned, we find that *Gcn5* loss leads to severe disorganization of cytoskeletal networks in epiblasts. Gene expression profiling by RNA sequencing indicates that these phenotypes are associated with defective FGF signaling in the *Gcn5* null EBs. Several genes in the FGF and ERK pathways that are down regulated in *Gcn5* null EBs are known targets of c-MYC, consistent with our findings in undifferentiated ESCs. Disruption of these pathways in turn is associated with defective endoderm and mesoderm differentiation in *Gcn5* null EBs.

1.6 Significance

This work provides evidence for a novel role for GCN5 in the regulation of FGF signaling during early stage differentiation of EBs. It builds on previous links between GCN5 and MYC in undifferentiated ES cells, during neural development in embryos, and during somatic cell reprogramming, and reinforces the GCN5-MYC partnership in regulating gene expression in yet another important developmental process.

As abnormal regulation of growth factor regulated pathways drive oncogenesis ([52](#)), and MYC has long been linked to malignant transformation and growth ([53](#)), our findings here predict that GCN5 may also be important in cancers associated with over-activation of FGFs and/or MYC. Future work will explore this possibility, as well as the therapeutic potential of targeting GCN5 to inhibit growth or progression of these cancers.

Chapter 2. Materials and Methods

ES cell culture and differentiation

Gcn5^{fx/fx} and *Gcn5^{-/-}* ES lines were generated and characterized previously (36). ESCs were routinely grown on gelatin-coated plates in DMEM/High glucose (HyClone™, SH3002201) medium supplemented with 15% (v/v) ES-screened FBS (HyClone™, SH3007003E), 2mM L-glutamine (Hyclone, SH3003401), 0.1mM non-essential amino acids (Corning™, MT25025CI), 1% (v/v) penicillin/streptomycin (Hyclone, SV30010), 0.1 mM β-mercaptoethanol (Fisher, 03446I-100), 1000U/mL of LIF/ESGRO (Millipore, ESG1107), 1μM PD0325901 (Sigma, PZ0162) and 3 μM 1-Azakenpaullone (Sigma, A3734) (2i-s), and passaged with 0.25% Trypsin (HyClone™, SH3004201) every 2-3 days.

For EB differentiation, 3×10^5 cells were plated in a well of an ultra-low attachment 6-well plate (Corning, 07-200-601) in 3mL of differentiation media at 37°C with 5% CO₂. Media were replaced every other day by settling the EBs at low speed centrifugation (100g for 1 minute). The differentiation medium is composed of DMEM/High glucose:F12 (Cellgro™, MT10080CV):Neurobasal media (Gibco™, 21103049) (1:1:2) supplemented with 10% KnockOut Serum Replacement medium (Gibco™, A3181502), 2mM L-glutamine, 1% (v/v) penicillin/streptomycin and 0.1 mM β-mercaptoethanol.

Immunofluorescence and Confocal imaging

2-3 wells of EBs were collected in a 1.5mL tube, and 1.3mL of a given solution was used in the following steps of washes and sucrose incubation. EBs were washed once in PBS/1%BSA and fixed in 4% paraformaldehyde (PFA) for 30 minutes at room temperature. The fixed EBs were incubated in 7.5% sucrose/PBS for at least one hour at room temperature, then in 15% sucrose/PBS at 4°C overnight. Afterward, the EBs were embedded in Tissue-Tek® O.C.T. compound (Electron microscopy sciences, 62550-12) and incubated for 10 minutes at room temperature with agitation before frozen in liquid nitrogen (LN2). Frozen sections (8µM) were cut on a cryostat (Thermo) and mounted on glass slides. Air-dried sections were defined by drawing a square or circle around using a PAP-pen, and 200µL of a given solution was used the following steps of staining and washing. Sections were washed once with PBS, fixed in 2% PFA for 2 minutes then blocked with PBS containing 0.1% Tween-20 (Fisher, BP337-500) (PBT) and 5% Normal donkey serum (Millipore, S30-100ML) for 30 minutes at room temperature. The blocked sections were incubated with primary antibodies diluted in blocking buffer overnight at 4°C. The slides then were washed with PBT 3 times for a total 15 minutes, followed by incubations with fluorescence conjugated secondary antibodies for 40 minutes at room temperature. DAPI staining was performed after washing off the secondary antibodies. The slides then were washed with PBT 3 times, 5 minute each, and cover-slipped in a drop (8-12µL) of ProLong® Gold Antifade mounting media (Invitrogen™, P36930), then cured

overnight at room temperature. The slides were imaged on a Zeiss LSM 880 laser-scanning microscope. Airyscan detector array was used to image the cytoskeletons. Standard pinhole was used to image the various markers for lineages, proliferation and apoptosis. Antibodies used here are listed in the Table 1.

Expression analysis

EBs were harvested and total RNA was isolated using an RNeasy mini plus kit (Qiagen, 74134) following the manufacturer's instructions. 10-20 ng of total RNA was used per reaction, and quantitative RT-PCRs were performed on a 7500 Fast Real-Time PCR System (Applied Biosystems™, 4351107) using the Power SYBR Green RNA-to-CT1-Step Kit (Life technologies, 4389986). Three technical replicates were performed for each gene target tested and quantification using *Pbgd* as a reference gene. A two-tailed Student t-test was used for pair-wise comparisons. The expression primer sequences are listed Table 2.

RNA sequencing and data analysis

Total RNA was isolated as described above. The libraries were prepared using the Illumina TruSeq stranded total RNA kit according to the manufacturer's protocol, except that the PCR amplification cycle was reduced to 8. The libraries were loaded on cBot (Illumina) at final concentration of 10

pM to perform cluster generation, followed by 76 bp pair-ended sequencing on HiSeq 2500 (Illumina). Three independent experiments were included. 25-41 million pairs of reads were generated per sample. Each pair of reads represents a cDNA fragment from the library.

Data analysis

Mapping: The reads were mapped to mouse genome (mm10) by TopHat (version 2.0.10) ([54](#)) with an overall mapping rate of 84-94%. 72-91% fragments have both ends mapped to mouse genome.

Differential Expression: The number of fragments in each known gene from GENCODE Release M8 ([55](#)) was enumerated using htseq-count from HTSeq package (version 0.6.0) ([56](#)). Genes with less than 10 fragments in all the samples were removed before differential expression analysis. The differential expression between conditions was statistically assessed by R/Bioconductor package DESeq ([57](#)) (version 1.16.0). Genes with FDR (false discovery rate) ≤ 0.05 , fold change ≥ 2 and length $> 200\text{bp}$ were called as differentially expressed.

Principle Component Analysis (PCA): PCA was performed by R function prcomp using cpm (count of fragments in each gene per million of fragments mapped to all exons) values. The scale option was set as TRUE.

Heatmap: The normalized counts from DESeq were used to generate heatmap by Cluster 3.0 ([58](#)) and Java Treeview ([59](#)). The values in each

gene were centered by median and rescaled so that the sum of the squares of the values is 1.0.

Gene Function and Pathway Analysis: The differential genes called by DESeq were used for Ingenuity Pathway Analysis (IPA) and Gene Set Enrichment Analysis (GSEA) ([60](#)).

Chromatin immunoprecipitation, qPCR and deep sequencing

5×10^6 ESCs (*Gcn5^{fx/fx}* and *Gcn5^{-/-}*) were seeded in 15mL differentiation media in a 10cm ultra-low attachment plate (Corning, 5539101) for differentiation. Cells were fed every other day. At day 5, EBs were collected in a 15mL falcon tube and washed once with 5mL PBS, then incubated with 1mL Accutase™ cell dissociation reagent (Gibco™, A1110501) at 37°C for 10 minutes. EBs were dissociated by pipetting then diluted 1:4 by the differentiation media to stop digestion, and pelleted at 200g for 5 minutes. The pellets were washed once in 1mL PBS, and chromatin immunoprecipitation (ChIP) was performed as previously described ([61](#)) with some modifications. Briefly, for crosslinking, each EB cell pellet was resuspended in 1.5mL media, a small aliquot (10μL) was set aside for cell count, then 100μL of 16% formaldehyde (Thermo Scientific™, PI28906) was added to make a final concentration of 1%, and the mixture was incubated for 10 minutes at room temperature on a rotator. 178μL of 125 mM glycine was added to quench the crosslinking for 5 minutes. Cells were washed with 1mL ice-cold PBS containing protease inhibitor

cocktail (PI, Sigma, P8340). The washed, cross-linked cells were resuspended in swelling buffer (5 mM PIPES pH 8.0, 85 mM KCl and 1% NP40) at a concentration of 10^6 cell/mL, and incubated for 20 minutes on ice. The crude nuclei were pelleted and lysed in nuclei lysis buffer (50 mM Tris-HCl pH 8.0, 10 mM EDTA and 1% SDS) at a concentration of 10^6 cell-nuclei/200 μ L and sonicated using a Bioruptor® Plus sonication device (Diagenode B01020001). Total 15 minutes of sonication (3 rounds of 10 cycles with 30 seconds on and 30 seconds off per cycle on the high setting) were applied to obtain chromatin fragments in the size of 150-300 bps. Sonicated samples were centrifuged to remove insoluble debris. 30 μ g of chromatin fragments were diluted 1:10 in ChIP Dilution Buffer (0.01% SDS, 1% TritonX-100, 1mM EDTA, 20mM Tris-HCl, pH8.0 and 150mM NaCl) and were precleared with Dynabeads Protein A (Invitrogen™, 10002D) for 1 hour at 4°C. Precleared lysates were incubated with 1 μ g of anti-H3 or 3 μ g of anti-H3K9ac overnight, followed by incubation with Dynabeads™ Protein A for 1 hour at 4°C. Immunoprecipitates were washed as previously described ([61](#)). All solutions used in steps above were supplemented with PI. DNA was eluted in elution buffer (50mM NaHCO₃ and 1% SDS) at room temperature for 15 minutes, de-crosslinked at 65°C overnight, treated with RNaseA for 1 hour at 37°C and purified using a PCR purification kit (Qiagen, 28104).

For qPCR analysis, 2µL of input (2% input diluted 100 x in water) or ChIP DNA was used for each reaction using a SYBR green PCR master mix kit (Life technologies, 4367659). Primers used for qPCR analysis are listed in Table 2.

ChIP DNA from 4 independent replicative experiments, including 2 replicates for each isogenic pair (*Gcn5^{fx/fx}* and *Gcn5^{-/-}*), were used for deep sequencing. ChIP libraries were prepared using Kapa Hyper Preparation kit (KAPA Biosystems, Wilmington, MA) protocol for Illumina Platforms. Briefly, for each library, 5ng of ChIP DNA was end-repaired and 3' adenylated using a proprietary master mix, and ligated to the specific NextFlex adaptors from Bioo Scientific (Bioo Scientific, Austin, TX). The adaptor ligated DNA was enriched using a KAPA Hyper Library Preparation kit (KAPA Biosystems, KK8502) with 5 cycles of PCR (1 cycle at 98°C for 45 seconds; 4 cycles of 98°C for 15 seconds, 60°C for 30 seconds, and 72°C for 30 seconds; 1 cycle at 72°C for 1 minute), and purified with AmpureXP beads (Beckman Coulter, A63881). The library quality was validated on a 2200 TapeStation from Agilent Technologies (Agilent, Santa Clara, CA). Libraries concentrations were determined using a Kapa Library Quantification Kit (KAPA Biosystems, KK4933) and loaded on cBOT (Illumina) at final concentration of 1.5nM for cluster generation, then sequenced with 50bp single-read on a HiSeq3000 sequencer (Illumina).

Data analysis

Mapping: Sequenced DNA reads were mapped to mouse genome mm10 using bowtie (version 1.1.2) (62) with at most 2 mismatches allowed and only the reads that were mapped to unique position were retained. 34-47 million reads were generated per sample. 90-94% reads were mapped to mouse genome, with 73-84% uniquely mapped. To avoid PCR bias, for multiple reads that were mapped to the same genomic position, only one copy was retained for further analysis. 19-29 million reads were used in the final analyses.

Peak Calling: H3K9ac peaks were detected by MACS (version 1.4.2) (63). The window size was set as 500 bp and the p-value cutoff was 1e-5. H3K9Ac peaks were initially called by comparing to the corresponding total H3. Then the peaks that overlapped ENCODE blacklisted regions (64) or were not called by comparing to the corresponding total input were removed.

Differential Peak Calling: The peaks of all H3K9ac samples were merged and the numbers of reads in these merged peaks were counted for each H3K9ac sample. The count table was used to call differential H3K9ac peaks between *Gcn5^{fx/fx}* and *Gcn5^{-/-}* by edgeR (65). Batch effect among the 4 replicates was corrected following edgeR user's guide. Peaks with FDR (false discovery rate) ≤ 0.05 were called as changed between *Gcn5^{fx/fx}* and *Gcn5^{-/-}*. Genes with differential peaks in promoter (defined as -1000 bp to +500bp from TSS) were called as associated with changed H3K9Ac.

Signal Landscape: Each read was extended by 150bp to its 3' end. The number of reads on each genomic position was rescaled to normalize the effective library size by edgeR to 10M and averaged over every 10bp window. The normalized values were displayed in UCSC genome browser ([66](#)).

Transcription Factor Binding: ENCODE ChIP-Seq Significance Tool ([67](#)) was used to identify enriched ENCODE transcription factors in the promoters of the genes associated with changed H3K9Ac. The promoter was defined as -5000 bp to +2000 bp from TSS.

Mass cytometry

Sample preparation for mass cytometry was performed as in ([68](#)). Briefly, EBs were dissociated using Accutase, stained with cisplatin for viability at 25µM for 1 minute at room temperature and then quenched using PBS containing 1%BSA. The cells were fixed 1.5% PFA for 10 minutes at room temperature, then permeabilized with methanol (1mL per million cells) and incubated overnight at 4°C. Samples were barcoded according to ([69](#)), pooled and antibody stained with the panel of antibodies in Table 2. Cells were stained with 1:2000^{191/193} Iridium (Ir) DNA intercalator (Fluidigm), 62.5nM final, for 10 minutes at room temperature. Samples and EQ Four Element Calibration Beads (Fluidigm) were combined and diluted with water to a concentration of 5×10^5 cells/ml and run at 45ul/min a CyTOF 2 mass

cytometer (Fluidigm). Data were normalized on bead passport using CyTOF software (v6.0.626, Fluidigm).

Initial data processing and gating was done with FlowJo vX10.0. EQ Four Element Calibration Beads were removed and data were gated on singlets by Ir193 and Event Length parameters. Removal of dead cells was done in the Pt198 channel. SPADE analysis of the data was performed using SPADE V3.0 in MATLAB r2015b (Mathworks). SPADE tree construction was performed using agglomerative clustering on all markers listed in Table 1. Annotation of SPADE tree regions was done according to marker distribution and cell percentages in each region were calculated for all samples. Percentages were normalized relative to mean $Gcn5^{fx/fx}$ and statistical significance was determined by the Wilcoxon rank sum test performed in MATLAB using the ranksum function.

Whole cell lysates and Nuclear extracts preparation

For preparation of whole cell lysates (WCL), 5-10 million cells (EB or ESCs) were lysed in 1mL RIPA buffer (150mM NaCl, 50mM Tris-HCl pH7.9, 1% Triton X-100 and 1% sodium deoxycholate) containing PI and phosphatase inhibitor cocktail (Roche, 04906845001) on ice for 20 minutes, then sonicated briefly in a Diagenode Bioruptor® for 2.5 minutes (5 cycles with 30 seconds on and 30 seconds off per cycle on the high setting). The lysates were then

centrifuged at 21000g for 10 minutes to clear insoluble debris. The supernatants were WCL and transferred to fresh tubes for further analysis.

Nuclear extracts (NE) were prepared following the Dignam and Roeder method ([70](#)) modified for ESCs. Briefly, cell pellets were resuspended in 5 pellet volumes of ice-cold buffer A and incubated on ice for 15 minutes. The swollen cells were pelleted at 1000rpm for 10 min at 4°C on soft brake. Pellets were resuspended again in 3 pellet volumes of buffer A, and then homogenized in a glass homogenizer (1 mL Wheaton) with 20 strokes by a tight pestle. The homogenized cell suspension was collected and nuclei were pelleted by centrifugation at 21000g on soft brake for 20 minutes at 4°C. The supernatant (cytoplasmic fraction) was carefully removed and nuclei were then resuspended in 2 pellet volumes of buffer C and incubated on a vibrator at 4°C for 45 min. The mixtures were then centrifuged at 21000g for at least 30 min at 4°C on soft brake. The supernatants were nuclear extracts and were carefully transferred to fresh tubes for further analysis.

Protein concentration was determined by Bradford assays (Bio-Rad, 500-0006).

Immunoprecipitation (IP)

0.5 or 1mg of protein from WCL or NE were incubated with anti-HA-agarose (Roche cat. #11815016001, pre-equilibrated with wash buffer containing 10mM HEPES pH 7.9, 1.5mM MgCl₂, 300mM NaCl, 10mM KCl, 0.2% Triton X-100 and PI) overnight at 4 °C on a rotator. For each IP, 5-10% input was set aside and 20µl HA-beads (50% slurry) were used. Beads were then collected by centrifugation at 2000rpm for 2 min, followed by 3 washes for a total of 30 min in wash buffer at 4°C. Washed beads were collected, and the immunoprecipitates were eluted using HA peptide (Roche cat. #11666975001) (200 µg/mL in elution buffer containing 10mM HEPES pH 7.9, 1.5mM MgCl₂, 100mM NaCl, 0.05% Triton X-100 and PI) for 1-2 hours on a vibrator at RT. ¼ eluate volume of 5x SDS sample buffer was added to the eluted immunoprecipitates and inputs, then the mixtures were heated at 95°C for 10 min.

Immunoblotting

10-20µg of protein from WCLs or ½ volume of NE/IP products were resolved on 4-12% Bis-Tris protein gels (Invitrogen™ WG1402BOX). Proteins were transferred to nitrocellulose membranes (Invitrogen™, IB23001) using the iBlot2™ gel transfer device (Life Technology, IB21001). Membranes were blocked and incubated with primary antibodies following standard procedures. Primary antibodies were detected using peroxidase-conjugated secondary antibodies (1:8000). Amersham ECL prime western blotting detection reagent

(GE Healthcare, RPN2232) was used according to the manufacturer's instructions. Antibodies used for Immunoblotting are listed in Table 2.

Creation of J1ESCs expressing FHGCN5

Generation of FHGCN5 expressing J1ESCs by CRISPR/CAS9 targeting

The GCN5 guide RNA construct (gBlock-GCN5) targeting exon 1 of the mouse GCN5 gene were designed and generated as described in the MIT CRISPR tool ([71](#)). The cDNA (5'_TGTACAAAAAAGCAGGCTTTAAAGGAACCAATTCAGTCGACTGGATC CGGTACCAAGGTCGGGCAGGAAGAGGGCCTATTTCCCATGATTCCTTCA TATTTGCATATACGATACAAGGCTGTTAGAGAGATAATTAGAATTAATTTG ACTGTAAACACAAAGATATTAGTACAAAATACGTGACGTAGAAAGTAATA ATTTCTTGGGTAGTTTGCAGTTTTAAATTATGTTTTAAATGGACTATCA TATGCTTACCGTAACTTGAAAGTATTTGATTTCTTGGCTTTATATATCTT GTGGAAGGACGAAACACCGTGCGCTGCCGGGACCGGGTTGTTTTAGA GCTAGAAATAGCAAGTTAAAATAAGGCTAGTCCGTTATCAACTTGAAAAA GTGGCACCGAGTCGGTGCTTTTTTTCTAGACCCAGCTTTCTTGTACAAAG TTGGCATTAA) was synthesized by IDT and was subcloned into TOPO-TA cloning vectors (Invitrogen™ K452040) following the manufacturer's instructions, and then verified by DNA sequencing at the MB Core at UT-MD Anderson Cancer Center (UTMDACC) Science Park before being used for ESC nucleofection.

A single stranded oligo template for homologous recombination/repair (ssDNA-N-FHGCN5-ex1) was synthesized by BioSynthesis. The sequence (5'_GTTGCCCATGCGGCCCTAGGGCTGGGAGCGCGGCCGCTCCGCTGCGGGGGAGGCCATGGACTACAAGGACGACGATGACAAGTCGGCCGC TGGAGGATATCCCTACGACGTGCCCCGACTACGCCGCGGAACCTTCCCA GGCCCCAAATCCGGTGCCGGCCGCGCAGCCCCGGCCCCCTTCACTCCCC AGCCCCTGCCCCAACTTCG) contains a FLAG-HA tag sequence (a silent mutation within to create a EcoRV site unique from the wild type sequence) placed in frame immediately after the ATG of *Kat2a*, and a silent mutation in the 3' sequence to prevent targeting by the gBlock-GCN5/CAS9.

J1 ESCs were electroporated with the gBlock-GCN5 and CAS9-GFP plasmids (a kind gift by the Chen Laboratory at UTMDACC Science Park) and ssDNA-N-FHGCN5-ex1 template using a Lonza Nucleofector™ following the manufacturer instructions. 48 hours after nucleofection, the GFP⁺ cells were sorted and seeded by FACS in 96-well plates. Single clones were expanded and genomic DNA extracted and screened by PCR using primers 5'_GGCCCGTGACGCCTGCGC (forward) and 5'_CTTCTTGGCACGCGGCAGACC (reverse). The targeted loci of positive clones were verified for correct, in-frame insertion by DNA sequencing at Molecular Biology Core Facility (MB Core) at UT-MD Anderson Science Park.

Southern blotting was performed to determine the correct homologous recombination using a DIG High Prime DNA Labeling and Detection Kit (Roche, 11585614910) following the manufacturer's instructions. 6µg of genomic DNA was used for each reaction. Primers 5'_CTCCTGGGTTTCTGGGACTG (forward) and 5'_ACAGCGACTTGAGTGTTTTTGC (reverse) were used to generate 5'-probe, and 5'_GCAAGTGTAATGGCTGGAAAAAC (forward) and 5'_GGGCTGGGAAGAACAGAAGAG (reverse) were used to generate 3'-probe by standard PCR. The PCR products (4µL for each reaction) were subcloned into TOPO-TA cloning vectors (Invitrogen™ K452040) following the manufacturer's instructions, and then verified by DNA sequencing at the MB Core.

Ectopic expression of Flag-HA-GCN5 (FHGCN5) in J1 ESCs

cDNA of mouse *Kat2a* from our lab ([36](#)) was subcloned into pCDH-EF1a-FH-IRES-puro vectors that were kindly provided by Dr. Junya Tomida from the Wood Laboratory. The plasmids (FH-vector or FHGCN5 construct) were introduced to J1ESCs by lenti-viral infection and FHGCN5 expressing cells selected following the previously described procedures ([72](#)), with modifications in the following: 1) the infection time was reduced to 48 hours to meet the ESC media refreshment schedule (every two days), and 2) the puromycin concentration was reduced to 1µg/mL to allow speed selection

(50% killing in 2 days) without affecting normal growth of puromycin resistant ESCs .

Table 1 Antibodies used in this study

Antibodies	Manufacturers	Catalog No.	Applications
Anti-GCN5	Cell Signaling Technology	3305	Westerns, 1:500 ChIP, various amounts
Anti-phospho-ERK	Cell Signaling Technology	4370	Westerns, 1:1000
Anti-ERK	Cell Signaling Technology	4695	Westerns, 1:2000
Anti-phospho-AKT	Cell Signaling Technology	4060	Westerns, 1:1000
Anti-AKT	Cell Signaling Technology	4691	Westerns, 1:2000
Anti-phospho-p38	Cell Signaling Technology	4511	Westerns, 1:1000
Anti-p38	Cell Signaling Technology	9212	Westerns, 1:2000
Anti-phospho-c-RAF (S259)	Cell Signaling Technology	9421	Westerns, 1:1000
Anti-c-RAF	Cell Signaling Technology	53745	Westerns, 1:2000

Anti-FGFR1	Cell Signaling Technology	9740	Westerns, 1:500
Anti-TRRAP	Cell Signaling Technology	3967	Westerns, 1:300
Anti-ADA2B	Abcam	ab57953	Westerns, 1:500
Anti-H3	Abcam	ab1791	ChIP, 1µg/30µg Chromatin
Anti-H3K9ac	Millipore	07-352	ChIP, 3µg/30µg Chromatin
Anti-SOX1	BD Biosciences	560749	IF, 1:100 Mass Cytometry, 10µL
Anti-GATA4	Abcam	ab84593	IF, 1:100
Anti-Laminin	Millipore	AB2034	IF, 1:100
Anti-Vimentin	Abcam	ab92547	IF, 1:300
Alexa Fluor 568 Phalloidin	ThermoFisher Scientific	A12380	IF, 1:300
Donkey anti-rabbit IgG Alexa Fluor® 488	ThermoFisher Scientific	A21206	IF, 1:500

Donkey anti-rabbit IgG Alexa Fluor® 555	ThermoFisher Scientific	A31572	IF, 1:500
Donkey anti-rabbit IgG Alexa Fluor® 647	ThermoFisher Scientific	A31573	IF, 1:500
Donkey anti-mouse IgG Alexa Fluor® 488	ThermoFisher Scientific	A21202	IF, 1:500
Goat Anti-mouse IgG Alexa Fluor® 568	ThermoFisher Scientific	A11004	IF, 1:500
Donkey anti-mouse IgG Alexa Fluor® 647	ThermoFisher Scientific	A31571	IF, 1:500
Anti-NANOG	Cell Signaling Technology	3580	Mass Cytometry, 5µL
Anti-OCT4	Santa Cruz	sc-5279	Mass Cytometry, 10µL
Anti-SOX2	R&D Systems	MAB2018	Mass Cytometry, 10µL
Anti-GATA6	R&D Systems	AF1700	Mass Cytometry, 10µL
Anti-PAX3	R&D Systems	MAB2457	Mass Cytometry, 10µL
Anti-PAX6	R&D Systems	AF8510	Mass Cytometry,

			10µL
Anti-BRACHYURY	R&D Systems	AF2085	Mass Cytometry, 10µL
Anti-HAND1	R&D Systems	AF3168	Mass Cytometry, 10µL
Anti-FOXA2	BD Biosciences	561580	Mass Cytometry, 10µL
Anti-GATA4	BD Biosciences	560327	Mass Cytometry, 10µL
Anti-SOX17	BD Biosciences	561590	Mass Cytometry, 10µL

Table 2 Primers used for PCR analyses

qRT-PCR Primers for expression analysis		
Oligo name	Sequences (5'-3')	Source
Cdh2 fwd	CAGGGTGGACGTCATTGTAG	(73)
Cdh2 rev	AGGGTCTCCACCACTGATTC	
Fgf3 fwd	ACAGGCGGGAAGCATATGTA	Originally designed
Fgf3 rev	GGCCATGAACAAGAGAGGAC	
Fgf4 fwd	CGTTGTAGTTGTTGGGCAGA	Originally designed
Fgf4 rev	TTCTTCGTGGCTATGAGCAG	
Fgf5 fwd	GCGATCCACAGAACTGAAAA	(73)
Fgf5 rev	ACTGCTTGAACCTGGGTAGG	
Foxa2 fwd	GAGCAGCAACATCACCACAG	Originally designed
Foxa2 rev	CGTAGGCCTTGAGGTCCAT	
Gata6 fwd	CAAAAGCTTGCTCCGGTAAC	(73)
Gata6 rev	TGAGGTGGTCGCTTGTGTAG	
Grb10 fwd	ATCTTCCGTTTCCCATTTC	Originally designed
Grb10 rev	CTCCTTACCTCCTCCTCCGA	
Otx2 fwd	CTTCATGAGGGAAGAGGTGG	Originally designed
Otx2 rev	GGCCTCACTTTGTTCTGACC	
Pbgd fwd	CAGGGTACAAGGCTTTCAGC	Originally designed
Pbgd rev	CGGAGTCATGTCCGGTAAC	

Prcka fwd	AACGAACTCATGGCACCTCT	Originally designed
Prcka rev	CACTGCACCGACTTCATCTG	
Sox1 fwd	CCTCGGATCTCTGGTCAAGT	(73)
Sox1 rev	GCAGGTACATGCTGATCATCTC	
Spry4 fwd	AGGTCCTGAACTGCACCAAG	Originally designed
Spry4 rev	GGGGATTTACACAGACGTGG	
Stat3 fwd	CTGCTCCAGGTAGCGTGTGT	Originally designed
Stat3 rev	CTCAGCCCCGGAGACAGT	
T fwd	CTGGGAGCTCAGTTCTTTTCG	(73)
T rev	CCCCTTCATACATCGGAGAA	
qPCR primers for ChIP analysis		
Oligo name	Sequences (5'-3')	Source
Asf1b fwd	CAGCCTTCTTTCTGCCTTTC	Dr. Calley Hirsch
Asf1b rev	GGGAGGTGTATGAGATCGACA	
Alcam fwd	AACGAGTGTCCAAAGCCAAG	Dr. Calley Hirsch
Alcam rev	GAGGATGCGGAGAGCCTAT	
Havcr2 fwd	CCTGACCTGACCAAGAAACC	Dr. Calley Hirsch
Havcr2 rev	GGCTACCAAGGCTGTCCTAT	
Meg3 fwd	AGGGAAGGGCTGCATTATTT	Dr. Calley Hirsch
Meg3 rev	CTTACTCGCGTGATCCCATT	
Tbx3 fwd	TTGGATGGCTGAGGCCTTTCA	Dr. Calley Hirsch

Tbx3 rev	AAAGTCGCCTCTAGGTGGCTGAT	
Dicer fwd	CGAGTTCCCACTTCAACAATGC	Dr. Calley Hirsch
Dicer rev	TTAGCCTCTCTGACACCACA	
Usp10 fwd	TGGAAGAGCAGTCAGTGCTCTT	Dr. Calley Hirsch
Usp10 rev	TTCTCTTTGTAGCCCTGGCT	
Intergenic fwd	AAGGGGCCTCTGCTTAAAAA	Dr. Calley Hirsch
Intergenic rev	AGAGCTCCATGGCAGGTAGA	
Grb10_2 fwd	CCCAACTCCTACCTGACGTG	Originally designed
Grb10_2 rev	TTTCTCCGTTGTGACTCGTG	
Grb10_3 fwd	GAAGACCGACCGGACCTG	Originally designed
Grb10_3 rev	CAGCCCAGGAAGAGTTTGAA	
Spry4_1 fwd	AGCTTAACCCGTGATTGCTG	Originally designed
Spry4_1 rev	AACAACCTCCACCCCTCTTT	
Spry4_2 fwd	ATGAATGGGTGGGCACAAGT	Originally designed
Spry4_2 rev	AGCAATCACGGGTTAAGCTC	
Fmn2 fwd	CCTACTTGTTGCAGGAGGA	Originally designed
Fmn2 rev	ATGGCTGCACAGGACTCAG	
Etv5 fwd	AGCACACACGTCCCCATT	Originally designed
Etv5 rev	AGCTGGATTTGCCTGAAGAC	
Pcna fwd	CGGAGTTGTGGCGACTAGAT	Originally designed
Pcna rev	GCTTCTGCATCGTGAATCG	

Neg. Chr1 fwd	ATTCAGGCCATCAAGAGGAC	Originally designed
Neg. Chr1 rev	GGGGGCTTTGTAAAAAGTTAATG	

**Chapter 3. *Gcn5* loss leads to defective morphogenesis of EBs at
epiblast stage**

3.1 Embryoid body (EB) assay models embryogenesis leading to gastrulation

As aforementioned, ES cells form distinct 3-D structures (EBs) in suspension culture upon LIF and 2i removal. In a day or two into the differentiation course, ES cells readily aggregate, followed by the first lineage segregation that gives rise to the visceral endoderm (VE), a single layer of cuboidal epithelial like cells surrounding the ICM like inner cells. The basement membrane (BM) is then deposited in between the VE and the inner cells around day 3. During day 4-6, the inner cells undergo morphogenesis to become a columnar epithelial layer termed epiblast, lining up along the interior side of the BM, and the center cells that do not contact the BM are cleared by apoptosis to form a cystic cavity. The epiblast cells then further differentiate into lineages expressing marker genes for germ layers parallel to those that arise from embryonic gastrulation ([51](#)). This differentiation course progresses in a manner that recapitulates embryonic transitions from formation of the ICM through gastrulation, allowing us to define the molecular events that might contribute to the death of *Gcn5*^{-/-} embryos shortly after gastrulation *in vitro*.

3.2 *Gcn5*^{-/-} EBs do not exhibit defective proliferation or apoptosis at day5

We used isogenic ES cells (*Gcn5*^{fx/fx} and *Gcn5*^{-/-}) for EB differentiation, and observed that *Gcn5*^{-/-} EBs were much smaller than *Gcn5*^{fx/fx} control EBs at

day 9, when all three germ layer cells should be formed. To define the time of onset of abnormalities in the null EBs, we examined earlier time points. At day 3, *Gcn5*^{-/-} EBs were not obviously different from control EBs. They appeared to be in similar size as the controls, and to have similar density under the bright field lighting, indicating the aggregate structures were not different from those of the controls at day 3. However, by day 5, *Gcn5*^{-/-} EBs appeared to suffer more breakage than control EBs (Figure 4), as indicated by the increased smaller, irregularly shaped pieces evident in the *Gcn5*^{-/-} EB culture. Either or both of the following possibilities may contribute to these morphological defects observed in the *Gcn5*^{-/-} EBs. One is that the null EBs were more structurally fragile, which leads to increased collapse of EB populations. Alternatively these defects could reflect increased cell death and/or proliferation arrest.

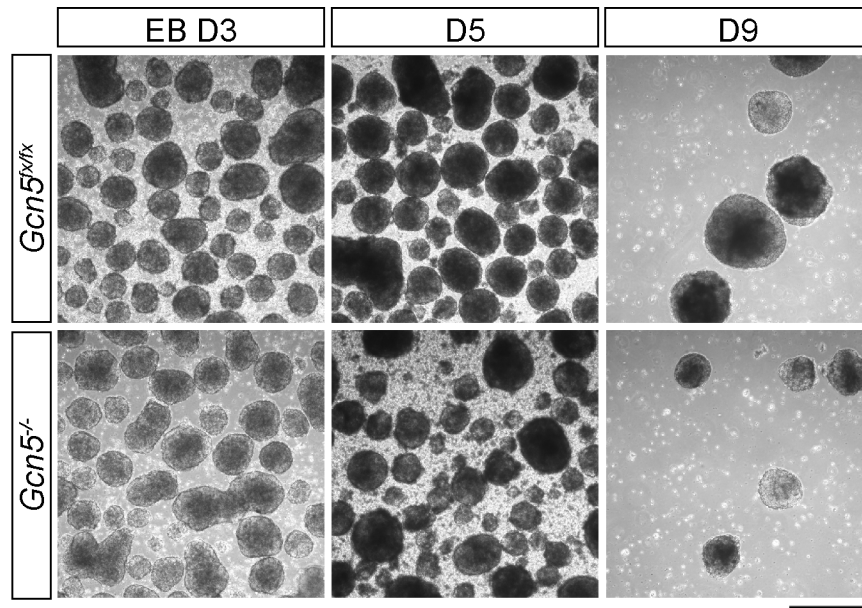


Figure 4 *Gcn5^{-/-}* EBs have abnormal morphology during early stages of differentiation

Bright field images showing differentiating EBs at days 3, 5, and 9, comparing EB morphology between *Gcn5^{fx/fx}* and *Gcn5^{-/-}* EBs. Scale bar, 200μM.

To better define the origin of the defects, we first examined expression of markers for proliferation and apoptosis by immunostaining and immunoblots. No increase was observed in the number of cleaved Caspase-3 (CC3) positive cells at day 5 in *Gcn5*^{-/-} EBs, nor was the expression of active Lamin A (C-LMNA) increased, as determined by immunostaining (CC3) and immunoblots (C-LMNA), indicating that *Gcn5* loss does not lead to increased apoptosis during early EB differentiation. Levels of H3S10p, a marker for mitotic cells, also did not change in the *Gcn5*^{-/-} EBs at day 5 compared to the control EBs, indicating that deletion of *Gcn5* does not lead to decreased cell proliferation in day 5 EBs (Figure 5, A and B).

We also examined the levels of H3K9ac in day5 EBs by immunoblotting, as it is one of the primary substrates of GCN5, but observed no decrease (Figure 5C) in *Gcn5*^{-/-} EBs. This observation is consistent with the presence of other HATs in the EBs, for example, PCAF, which is a highly similar homolog of GCN5 in mammals.

Altogether these data indicate that *Gcn5* is required for normal morphology, but not proliferation or survival, of EBs during the early stages of differentiation. In addition, loss of *Gcn5* alone does not cause decreases in global levels of H3K9ac much likely due to presence of other HATs.

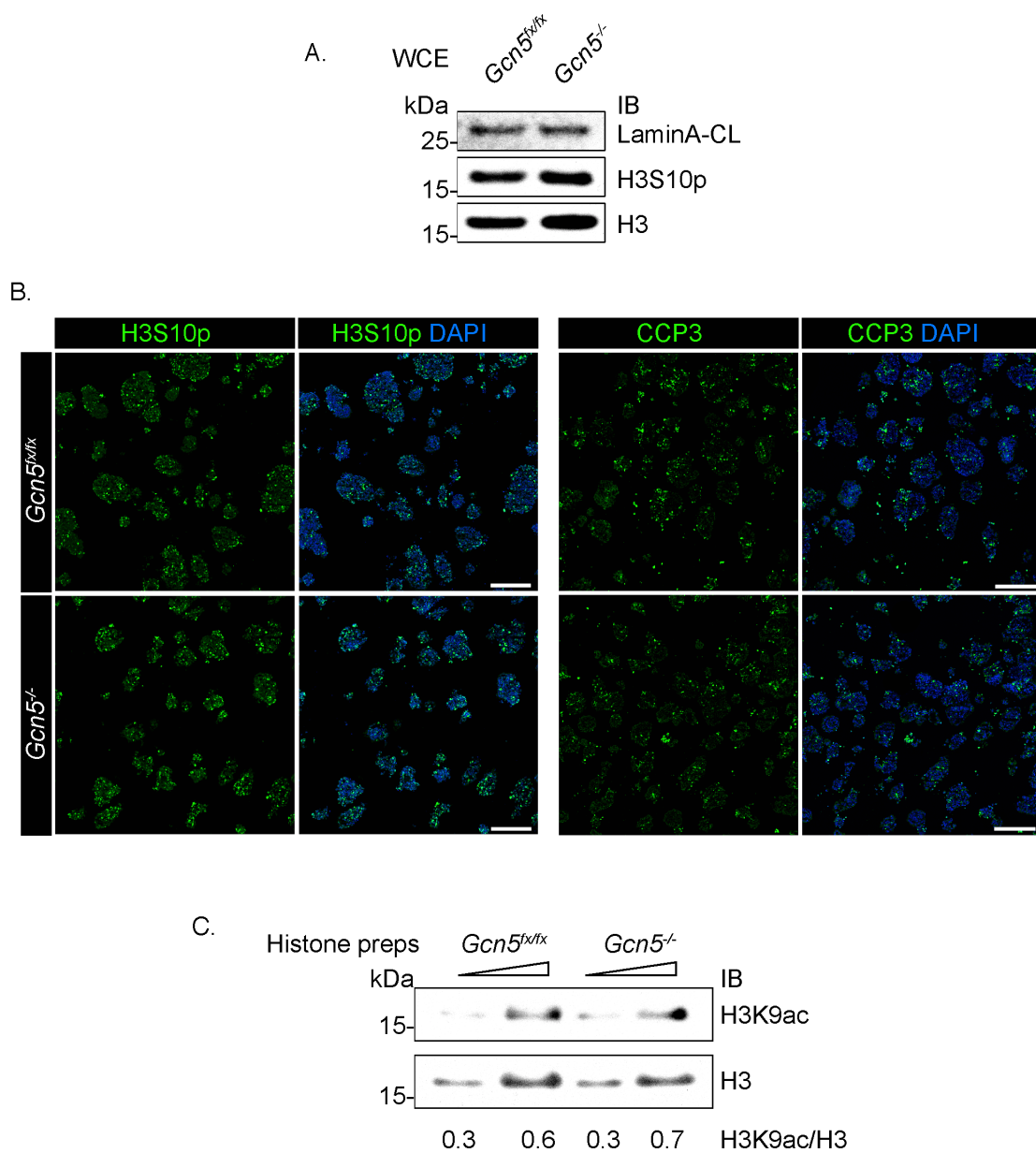


Figure 5 Loss of *Gcn5* does not inhibit proliferation or promote apoptosis at an early differentiation stage

(A and B) Immunoblots and immunostaining of mitotic marker (H3S10p) and apoptosis markers (cleaved-Caspase3, CCP3; cleaved-Lamin A) showed no differences between *Gcn5^{fx/fx}* and *Gcn5^{-/-}* EBs at day 5. Scale bars, 200mM.

(C) Immunoblots of H3K9ac and H3 in day 5 EBs demonstrated no global changes upon loss of *Gcn5* at early stage of differentiation.

3.3 *Gcn5*^{-/-} epiblast is severely disorganized at day 5

The unaffected proliferation or apoptosis observed in the *Gcn5*^{-/-} EBs at day 5 pointed to the possible defective structures in the null EBs. By day 5, the VE and the BM are already formed, while inner cells undergo morphogenesis to give rise to epiblast with a distinct columnar epithelial like organization. To investigate whether the abnormal morphology of *Gcn5*^{-/-} EBs observed under the bright field microscope reflects defective formation of these structures, we performed immunostaining with markers well characterized in the literature.

GATA4 is a transcription factor that marks the endodermal populations during early development (74) and was used as a marker for the VE. Laminin was used as a marker for the BM, as it is an integral component of basement membrane (75). Since a majority of the inner cells express early neuroectodermal markers by day 5, we used immunostaining for SOX1 to visualize the organization of epiblast cells. All sections were counterstained with DAPI to visualize the nuclei. Laminin staining of the BM showed little difference between the null and control EBs (Figure 6A). GATA4 staining was also very similar in *Gcn5*^{fx/fx} and *Gcn5*^{-/-} EBs. These observations indicated normal formation and organization of the BM and VE in *Gcn5*^{-/-} EBs. In sharp contrast, SOX1 staining revealed severe disorganization of the columnar epithelial morphology of the epiblast in *Gcn5*^{-/-} EBs (Figure 6B). Altogether,

these data clearly indicate that *Gcn5* is required for normal formation and organization of the epiblast during early differentiation.

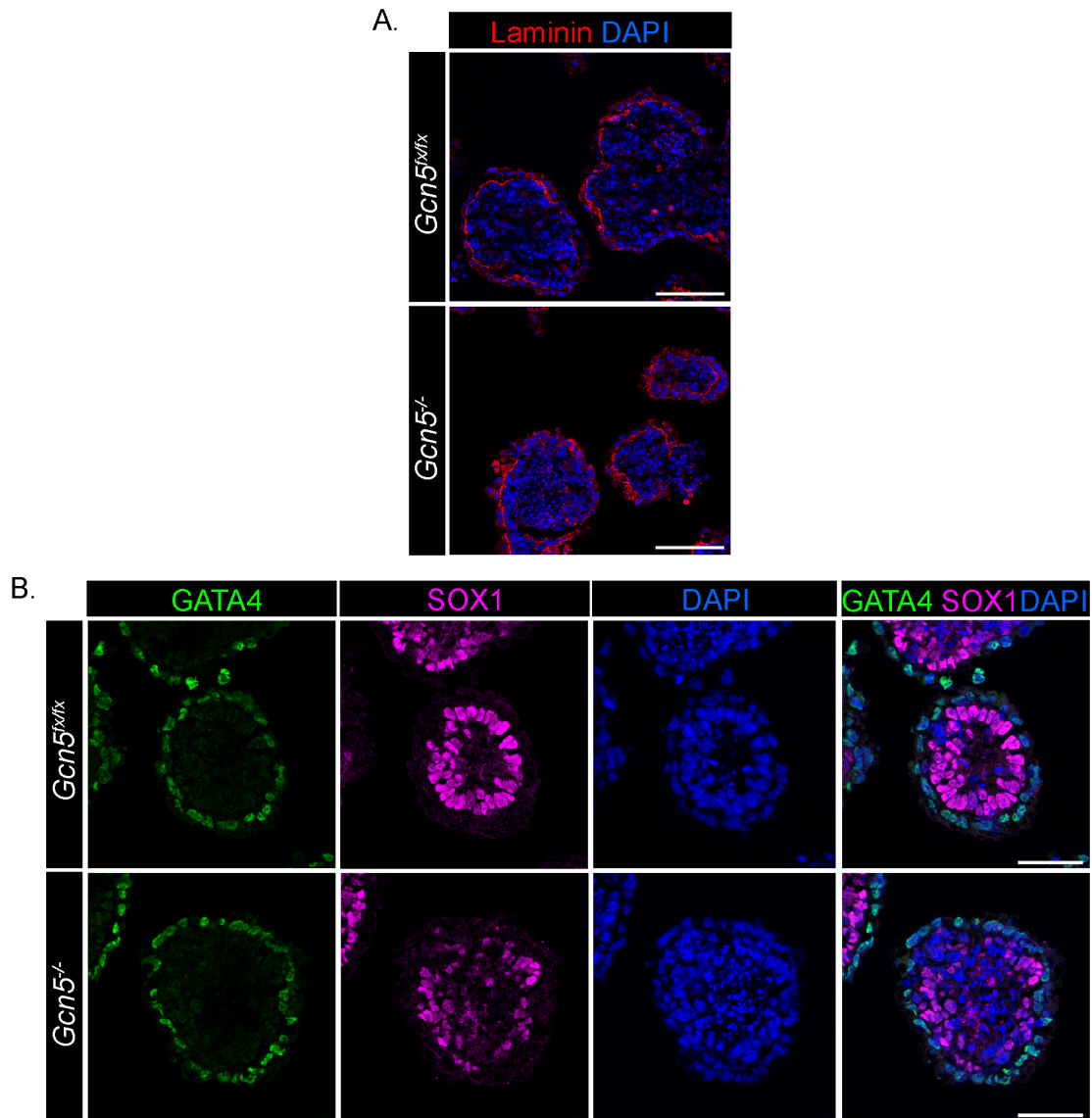


Figure 6 Severely disorganized epiblast of *Gcn5^{-/-}* EBs at day 5

Representative immunofluorescence (IF)/confocal images of EB architecture in day 5 *Gcn5^{flx/flx}* and *Gcn5^{-/-}* EBs, with Laminin (red) staining for BM (A), GATA4 (green) staining for VE, and SOX1 (magenta) and DAPI (blue) staining for nuclei of the epiblast (B). Scale bars, 100μM in (A) and 50μM in (B).

Chapter 4. *Gcn5*^{-/-} EBs have impaired capacities in differentiation

4.1 *Gcn5*^{-/-} expresses lower levels of epiblast-specific marker genes at day 5

The epiblast expresses specific genes, including *Fgf5* and *Otx2*, and expression levels of these genes usually peaks around day 5 in EBs or the equivalent embryonic stage ([46](#), [73](#), [76](#), [77](#)). The severe disorganization of the epiblast cells in the *Gcn5*^{-/-} EBs indicated that they might express these markers abnormally. To test this possibility, we used qRT-PCR to measure expression levels of *Fgf5* and *Otx2* in the *Gcn5*^{-/-} EBs at day 5, compared to the *Gcn5*^{fx/fx} EBs, and observed lower expression of both genes (Figure 7). These results suggested that the *Gcn5*^{-/-} epiblasts may have impaired functions, which might compromise subsequent formation of the three germ layers ([34](#), [78](#)).

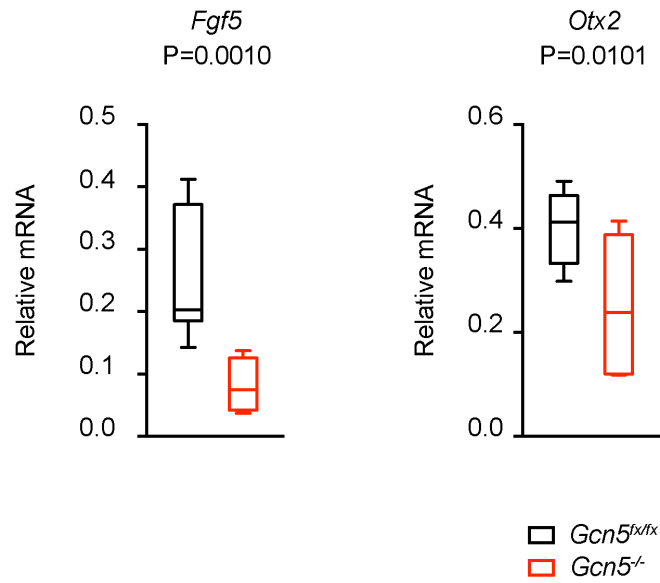


Figure 7 Epiblast marker genes are expressed at lower levels in *Gcn5^{-/-}* EBs

Gene expression analysis by qRT-PCR for epiblast marker genes, *Fgf5* and *Otx2*, normalized to a house-keeping gene *Pbgd*.

Data are presented as Mean \pm SD from 3 independent experiments.

4.2 Delineating heterogenic populations in day5 *Gcn5*^{-/-} EBs by mass cytometry

To more fully assess the composition of cell populations within the control and null EBs at day 5, when the epiblast cells have begun to adopt fates toward germ layers, we utilized state-of-the-art mass cytometry. Mass cytometry fuses two advanced technologies, flow cytometry and mass spectrometry, to provide measurement of over 40 simultaneous cellular parameters at single-cell resolution, significantly augmenting the ability of cytometry to evaluate complex cellular systems and processes that, at the same time, leverages precision from mass spectrometry ([79](#)). As such, mass cytometry offers unique and powerful abilities to investigate the cellular identities at the level of proteins and properties of proteins (e.g. posttranslational modifications of proteins), and monitor behavior of cells in response to intrinsic or environmental cues, such as differentiation of ESCs. The high dimensionality of mass cytometry is afforded by antibodies labeled with non-radioactive isotopes of rare earth metals with distinct atomic masses, which can be distinguished by mass cytometry and serve as reporters for the labeled cells ([79](#)). This approach allowed us to delineate and compare the compositions of heterogeneous populations in day 5 EBs. Application of SPADE analytic tool ([80](#)) then allowed us to visualize, delineate and quantify each lineage population in EBs and assess how loss of *Gcn5* affects a given population during differentiation.

We first tested an array of antibodies against each germ layer and pluripotent cells using differentiated and undifferentiated wild type ESCs, and selected those that specifically identify their intended cell populations (Table 3 and Figure 8) for day 5 EBs. Subsequent mass cytometry data from *Gcn5^{fx/fx}* and *Gcn5^{-/-}* EBs were analyzed with SPADE and represented as a comparative graphical tree plot (Figure 9A, *Gcn5^{fx/fx}* vs. *Gcn5^{-/-}*, blue represents subpopulations decreased in the nulls, and red represents subpopulations increased in the nulls), allowing us to visualize the cell populations impacted by *Gcn5* loss. Each population of *Gcn5^{-/-}* EBs was also quantified using SPADE in fold change relative to that of *Gcn5^{fx/fx}* EBs (Figure 9B). The results indicated that the *Gcn5^{-/-}* EBs contained significantly lower numbers of endodermal and mesodermal cells relative to the control EBs, as shown by the blue nodes in the endoderm and mesoderm regions in Figure 9A and the P-Value (<0.05) in Figure 9B. However, only one or two blue nodes were evident in the mesoderm region of the tree plot (Figure 9A), in contrast to the significant decreased population in *Gcn5* null EBs as shown by the quantification (Figure 9B). This discrepancy may be explained by the small size of the mesodermal population relative to the other lineage populations at day 5, which may make this population more sensitive to expression changes of the markers (Brachyury and HAND1) in the statistical test for significance. For the ectoderm population, although there was no difference between

Gcn5^{fx/fx} and *Gcn5*^{-/-} EBs for the entire lineages population (Figure 9B), there were indeed decreased SOX1⁺ (Figure 9A, blue nodes in ectoderm region) and increased SOX1⁻ subpopulations (Figure 9A, red nodes in ectoderm region) in the null EBs. However, because the overall percentile of the ectodermal cells (labeled by SOX1, PAX3 and PAX6, Table 3) was quantified altogether in SPADE, the changes in SOX1 subpopulations of the null EBs were not reflected in the comparison of the overall ectodermal populations (Figure 9B).

Table 3 Lineage markers used for mass cytometry

Antibodies	Expression	Isotope Label
Anti-NANOG	Pluripotency	¹⁶³ Dy
Anti-OCT4	Pluripotency	¹⁴⁶ Nd
Anti-SOX2	Pluripotency	¹⁴⁷ Sm
Anti-SOX1	Ectoderm	¹⁷⁶ Yb
Anti-PAX3	Ectoderm	¹⁷⁰ Er
Anti-PAX6	Ectoderm	¹⁵³ Eu
Anti-FOXA2	Endoderm	¹⁵⁰ Nd
Anti-GATA6	Endoderm	¹⁴² Nd
Anti-GATA4	Endoderm	¹⁷¹ Yb
Anti-SOX17	Endoderm	¹⁷⁵ Lu
Anti-Brachyury (T)	Mesoderm	¹⁵⁶ Gd
Anti-HAND1	Mesoderm	¹⁵⁸ Gd

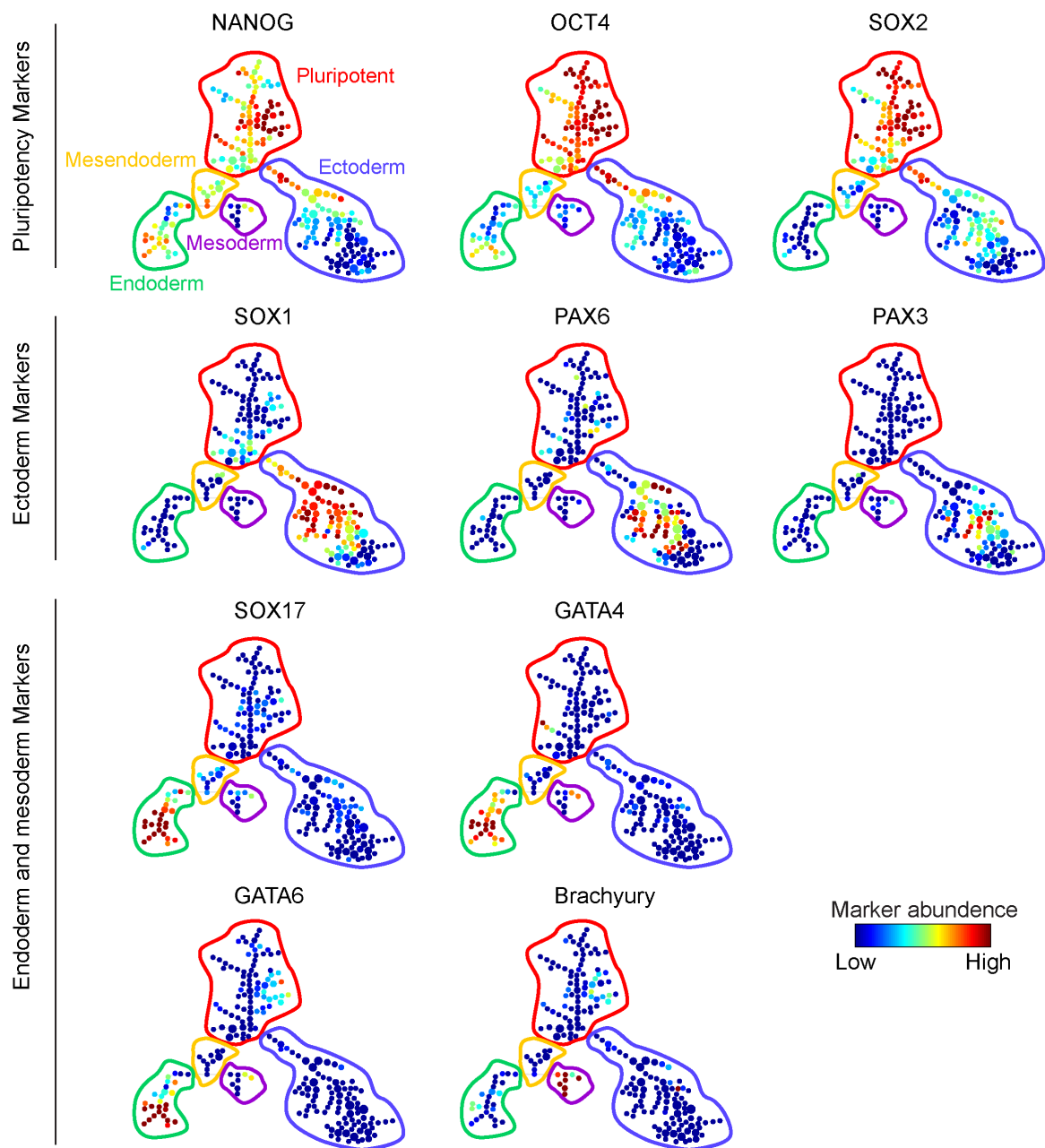


Figure 8 Using mass cytometry to delineate heterogeneous cell populations in differentiating ESCs

Proof-of-principle experiment showing lineage markers are enriched for corresponding cell populations.

Upper panels: ES cells, NANOG, OCT4, and SOX2 enriched in pluripotent region defined in red.

Middle panels: differentiated EBs, SOX1, PAX6 and PAX3 enriched in ectoderm region (blue).

Lower panels: differentiated EBs, SOX17, GATA4, GATA6 enriched for endoderm region (green) and Brachyury enriched in mesoderm region (purple).

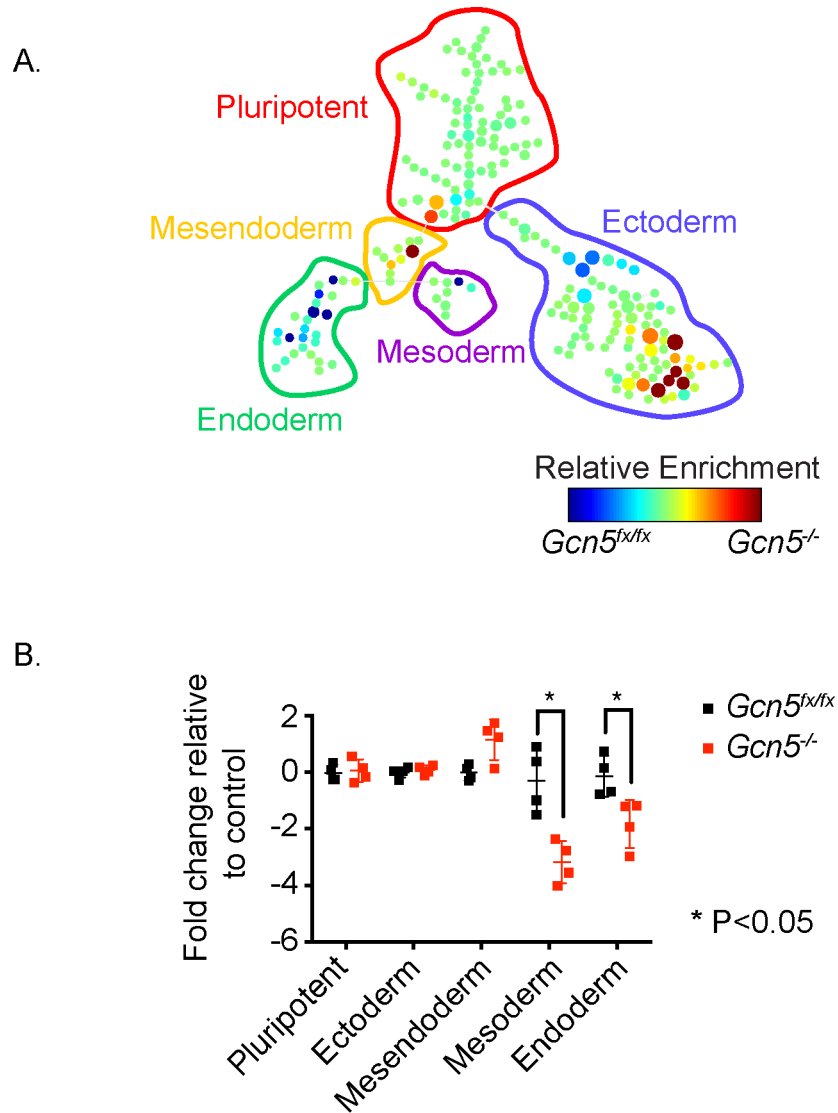


Figure 9 Changes in cell population composition in $Gcn5^{-/-}$ EBs at the epiblast stage

(A) SPADE plot showing decreased endoderm and mesoderm populations in the $Gcn5^{-/-}$ EBs at day 5; (B) Quantitation of fold changes in cell numbers of a given population in $Gcn5^{-/-}$ EBs relative to control.

Data are presented as Mean \pm SD from 4 independent experiments.

4.3 *Gcn5*^{-/-} EBs have impaired abilities to differentiate into germayers

Both the population analysis and the epiblast marker mRNA analysis indicated clearly that the *Gcn5*^{-/-} EBs likely have impaired ability to differentiate further into mature germayer cells. To test this idea, we analyzed expression of germayer marker genes in late-stage (days 9 and 12) EBs using qRT-PCR. We observed decreased expression of all germayer markers analyzed in null EBs in both day 9 and day 12, including ectoderm (*Sox1*, *Cdh2*), endoderm (*Gata6*, *Foxa2*) and mesoderm (*T*) (Figure 10). These findings validated our prediction that the *Gcn5*^{-/-} EBs have compromised potentials in differentiation, indicating that *Gcn5* is required for normal differentiation of the germayer lineages during EB formation.

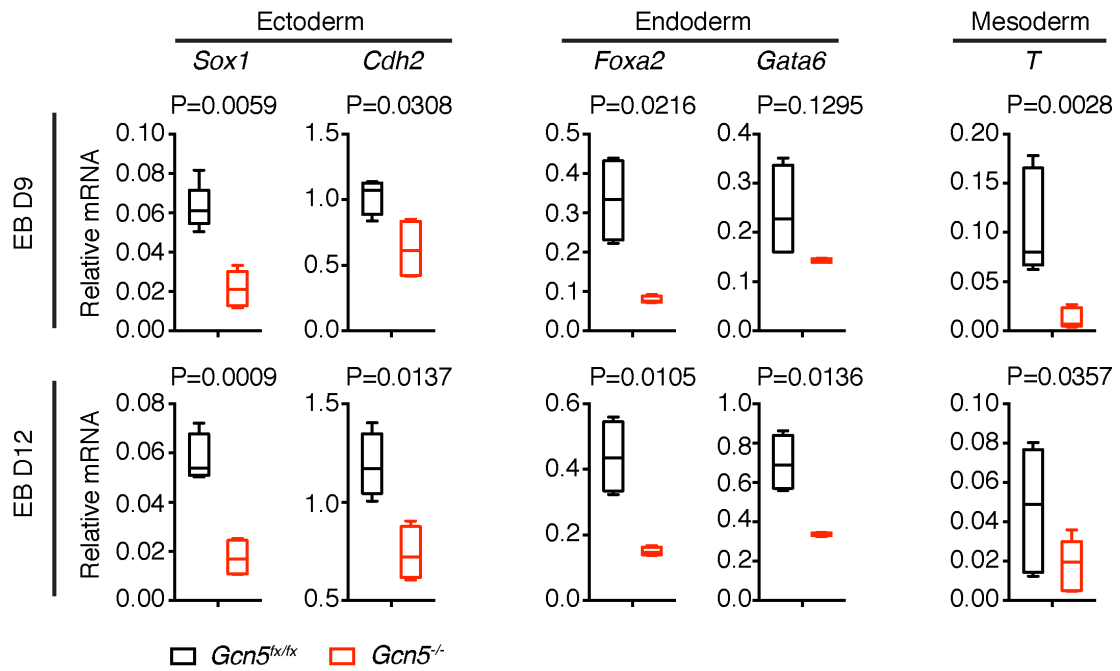


Figure 10 Impaired differentiation abilities of *Gcn5*^{-/-} EBs

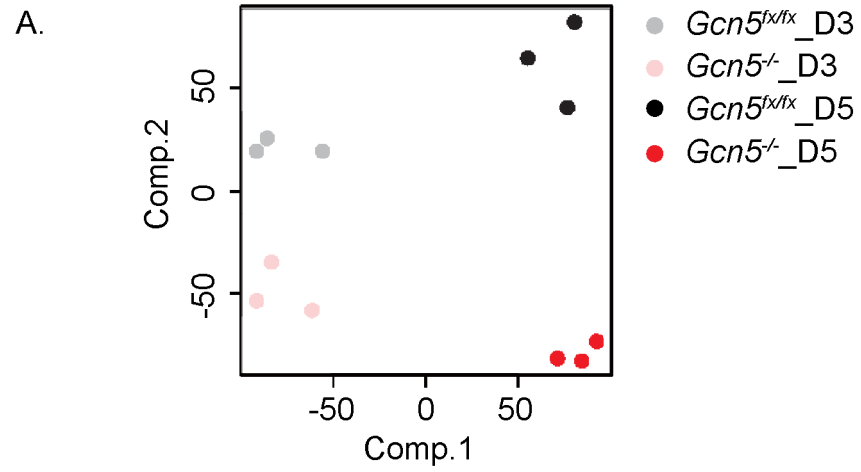
qRT-PCR plots showing decreased expression of marker genes for ectoderm (*Sox1*, *Cdh2*), endoderm (*Foxa2*, *Gata6*), and Mesoderm (*T*) in late stage EBs (days 9 and 12), normalized to *Pbgd*.

Data are presented as Mean \pm SD from 3 independent experiments.

**Chapter 5. Gene expression profiling points to a regulatory role of *Gcn5*
in FGF signaling pathway**

5.1 Overview of differentially expressed genes upon *Gcn5* loss at day 3 and day 5

GCN5 is characterized primarily as a transcriptional co-activator in the context of the SAGA and ATAC complexes ([14](#), [81](#), [82](#)), so to better understand the molecular basis underlying the defects in structures and differentiation capacity caused by *Gcn5* loss in early EBs, we compared gene expression profiles in day 3 and day 5 control and null EBs using RNA-seq. Total RNA was isolated from three technical replicates of *Gcn5*^{fx/fx} and *Gcn5*^{-/-} EBs, and key gene expression changes were confirmed using a second biological replicate by quantitative real-time polymerase chain reaction (qRT-PCR). These time points were chosen to define both early events (day 3) and events that coincide with the onset of the abnormal phenotype of *Gcn5*^{-/-} EBs (day 5). Principle-component analysis (PCA) revealed significant differences in gene expression profiles for all EBs between day 3 and day 5, consistent with developmental progression over time. However, gene expression profiles of null and control EBs were much more similar at day 3 than at day 5 (Figure 11A). Further, more genes (754 genes) exhibited altered expression at day 5 in mutant EBs than at day 3 (158 genes) (Figure 11, B and C). These data indicate that *Gcn5* loss impacts more significantly on gene expression at day 5, consistent with the timing of the onset of null morphological phenotype. Therefore, we focused further detailed analyses on differences in gene expression observed at day 5.



B.

Samples \ DE gene No.	DE gene No.		
	Total	DN	UP
D3	158	46	112
D5	754	240	514
Overlap of D3^D5	104	20	72

C.

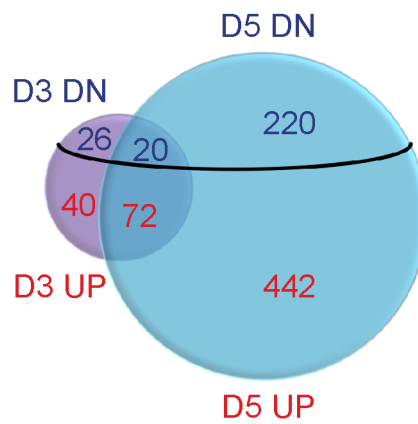


Figure 11 Overview of altered gene expression profiles in early stage *Gcn5*^{-/-} EBs

(A) Principle component analysis (PCA) plots showing variance of expression profiles among replicative samples, and increased differences in profiles between *Gcn5*^{fx/fx} and *Gcn5*^{-/-} EBs at day 5 (D5, Appendix 1) compared to day 3 (D3, Appendix 2), (n=3).

(B) Break down of the numbers of down or up regulated genes upon *Gcn5* loss at days 3 and 5.

(C) A Venn diagram view of (B).

5.2 Gene ontology and pathway analysis reveal deregulated FGF signaling in *Gcn5*^{-/-} EBs at day5

Gene set enrichment analysis (GSEA) revealed significant down regulation of several biological processes in the null EBs at day 5, with multicellular organismal development (MOD) and cell surface receptor linked signal transduction (CSRLST) among the most affected (Figure 12). In the MOD category, 15 out of 50 genes were among the core enrichment group in the mutant EBs, including *Pax5*, *Msx2*, *Gli1*, *Spry2* and *Mest*, which are all important for early development ([83-87](#)) (Figure 12 A and B, and Table 4). In the CSRLST category, 7 out of 30 genes are in the core enrichment group, including *Grb10*, the most down regulated gene in the null EBs (Figure 12 C and D, and Table 5). Consistent with these results, Ingenuity Pathway Analysis (IPA) identified a number of signaling pathways to be significantly altered in the *Gcn5* null EBs. Interestingly, 4 of the 7 top ranked affected pathways were intimately linked to FGF signaling, including Regulation of epithelial-to-mesenchymal transition (EMT), STAT3, FGF and Growth Hormone Signaling pathways (Figure 13A).

5.3 Validating Changes in Expression of FGF pathway genes by qRT-PCR

FGF ligands and their receptor tyrosine kinases (RTKs) exert control of multiple developmental processes including proliferation, survival,

differentiation and migration ([88](#)). Expression of key genes in these pathways was markedly altered in the *Gcn5*^{-/-} EBs as identified by the RNAseq. Using qRT-PCR with a second pair of isogenic cells, we validated several key genes of the FGF pathway from the RNAseq. For example, expression of *Fgf3* and *Fgf4* was significantly downregulated in the *Gcn5*^{-/-} EBs, as was expression of a negative regulator of these pathways, *Spry4* ([89](#)). *Grb10*, which is a negative regulator of insulin-AKT signaling ([90](#), [91](#)), was also downregulated in the *Gcn5*^{-/-} EBs. Conversely, effector genes such as *Stat3* and *Prkca* were markedly up regulated (Figure 13B). Together, these data strongly indicate that FGF signaling is abnormal in the *Gcn5*^{-/-} EBs at day 5.

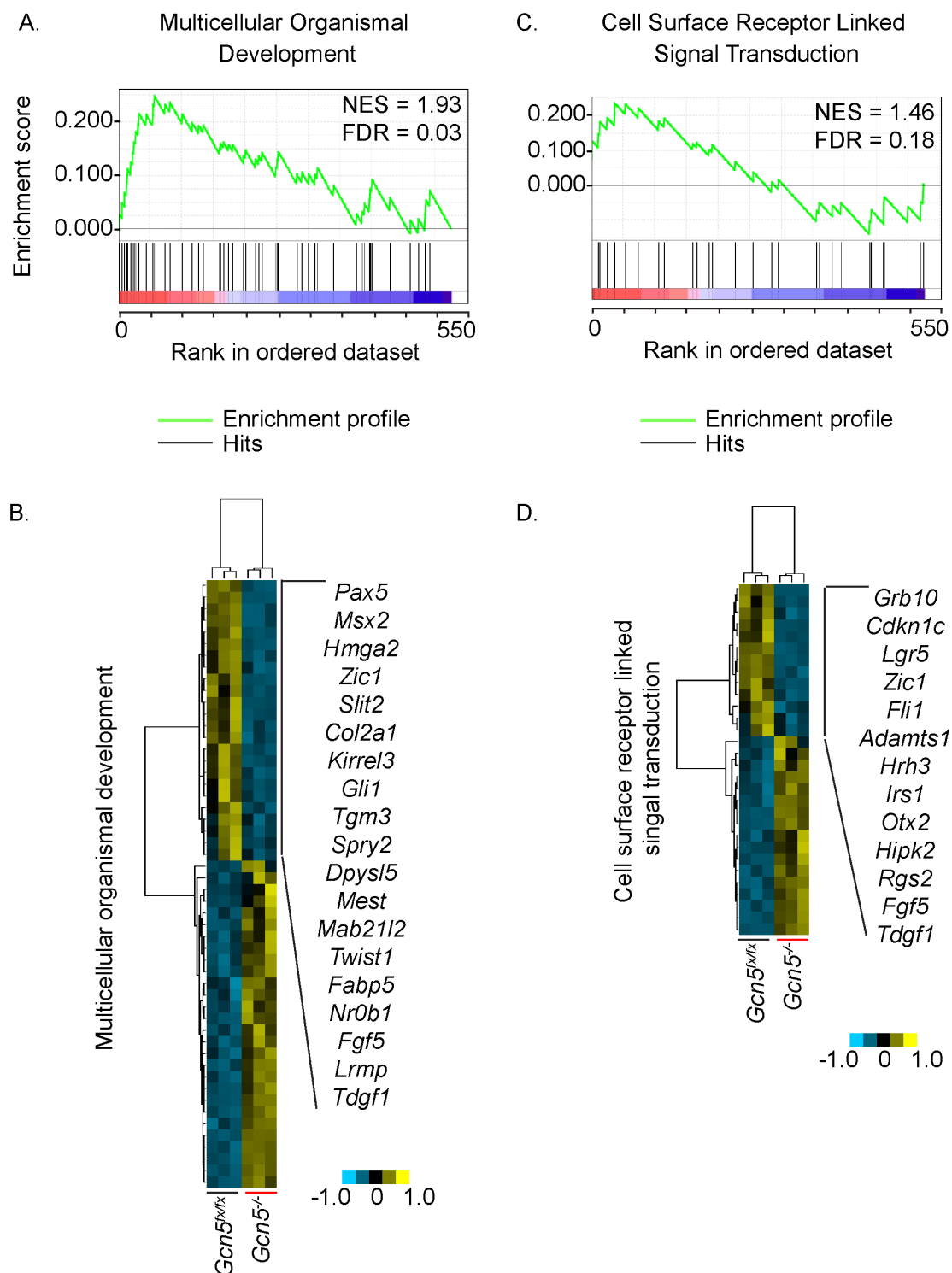


Figure 12 Top enriched processes identified by GSEA in the control EBs compared to *Gcn5*^{-/-} EBs at day 5

(A and B) GSEA enrichment profile (A) and heatmap (B) showing the multicellular organismal development gene set is enriched in the control EBs comparing to *Gcn5*^{-/-} EBs at day 5.

(C and D) GSEA enrichment profile (A) and heatmap (B) showing the cell surface receptor linked signal transduction gene set is enriched in the control EBs comparing to *Gcn5*^{-/-} EBs at day 5.

Color code: Red, positively correlated with *Gcn5*^{fx/fx}, Blue, negatively correlated with *Gcn5*^{-/-}.

Table 4 Gene list of GSEA set Multicellular Organismal Development

GENE SYMBOL	RANK IN GENE LIST	RANK METRIC SCORE	RUNNING ES	CORE ENRICHMENT
PAX5	2	3.143970966	0.026952207	Yes
MSX2	6	2.793720722	0.048327506	Yes
HMGA2	10	2.60679245	0.067849986	Yes
ZIC1	13	2.445233583	0.08787638	Yes
SLIT2	14	2.438150406	0.11204308	Yes
COL2A1	20	2.313369513	0.12444666	Yes
KIRREL3	23	2.268698215	0.14272325	Yes
GLI1	25	2.187872887	0.16230397	Yes
TGM3	27	2.169377327	0.18170136	Yes
SPRY2	31	2.100628138	0.1962068	Yes
DPYSL5	33	2.077706337	0.21469556	Yes
MEST	44	1.956736565	0.21303791	Yes
MAB21L2	54	1.908952236	0.21301188	Yes
TWIST1	55	1.892674208	0.23177189	Yes
FABP5	57	1.876633048	0.24826762	Yes
OTX2	74	1.794868827	0.23237398	No

PTCH2	81	1.774591208	0.23733197	No
NDP	101	1.670649171	0.21389128	No
FGF17	117	1.568956375	0.19786368	No
EPHA2	127	1.409094691	0.19288312	No
NR0B1	134	1.361806631	0.19374964	No
FGF5	160	1.005194783	0.15108146	No
LRMP	162	1.003890395	0.15892665	No
TDGF1	166	0.946586847	0.16199334	No
ALOX12B	174	-1.041075826	0.15757555	No
TRIM14	181	-1.18687892	0.1567082	No
ANXA2	198	-1.373691678	0.13663988	No
SGCD	201	-1.397668123	0.1462829	No
ETS1	217	-1.476131439	0.12933522	No
ERG	222	-1.50989151	0.13588007	No
RAPGEFL1	227	-1.535297155	0.14267674	No
IGFBP3	249	-1.666120291	0.11498063	No
SGCE	251	-1.675953865	0.12948726	No
JAG2	253	-1.683297992	0.14406668	No
SGCG	282	-1.763670683	0.10260065	No
MYH3	290	-1.779546738	0.10550249	No
IGFBP4	301	-1.796701074	0.10225859	No

CACNA1H	311	-1.824573159	0.10139622	No
SHOX2	315	-1.830768824	0.11322682	No
AEBP1	340	-1.907915235	0.08161158	No
RASGRP4	376	-2.075456142	0.028499093	No
NEUROG3	385	-2.098732948	0.032459423	No
FGF11	389	-2.107631922	0.04703428	No
ALDH3A2	397	-2.13826108	0.05349167	No
MEF2C	398	-2.148215771	0.07478458	No
STAT3	401	-2.162971735	0.09201321	No
CRIM1	429	-2.307478189	0.05804261	No
NMUR2	462	-2.529047012	0.015741859	No
DMRT1	474	-2.65857625	0.01893551	No
EVPL	485	-2.816974878	0.02580446	No
GFRA3	486	-2.819857836	0.053754613	No
SNAI2	492	-2.860271454	0.07157903	No

Table 5 Gene list of GSEA set Cell Surface Receptor Linked Signal Transduction

GENE SYMBOL	RANK IN GENE LIST	RANK METRIC SCORE	RUNNING ES	CORE ENRICHMENT
GRB10	0	4.903269768	0.07419716	Yes
CDKN1C	1	3.456902027	0.12650761	Yes
LGR5	11	2.555413246	0.14706793	Yes
ZIC1	13	2.445233583	0.18205757	Yes
GLI1	25	2.187872887	0.19303207	Yes
ADAMTS1	36	2.065867424	0.20417242	Yes
HRH3	37	2.059562922	0.23533809	Yes
IRS1	53	1.913015485	0.2341051	No
OTX2	74	1.794868827	0.22102393	No
HIPK2	106	1.659950376	0.18376835	No
RGS2	115	1.601378202	0.19190411	No
FGF5	160	1.005194783	0.11858372	No
TDGF1	166	0.946586847	0.12284728	No
STC1	186	-1.224491358	0.10314713	No
FLT4	191	-1.312462449	0.114959255	No

RAPGEFL1	227	-1.535297155	0.06776911	No
TBXA2R	256	-1.689142942	0.0369915	No
RAMP1	285	-1.764481425	0.007353922	No
GPR20	295	-1.789713264	0.016327534	No
IL13RA1	356	-1.987249494	-0.07432539	No
BDKRB2	360	-2.004709721	-0.050025985	No
SOCS1	381	-2.084973097	-0.058717243	No
OPRD1	394	-2.121104479	-0.05076518	No
RASD1	439	-2.354247332	-0.10367147	No
GABRA4	442	-2.365311384	-0.071903296	No
NMUR2	462	-2.529047012	-0.07186268	No
CD274	463	-2.539172888	-0.03343946	No
LAT	500	-2.93972373	-0.06138964	No
IL12RB1	521	-3.552495718	-0.04787409	No
CLEC1A	524	-3.695590973	0.004024112	No

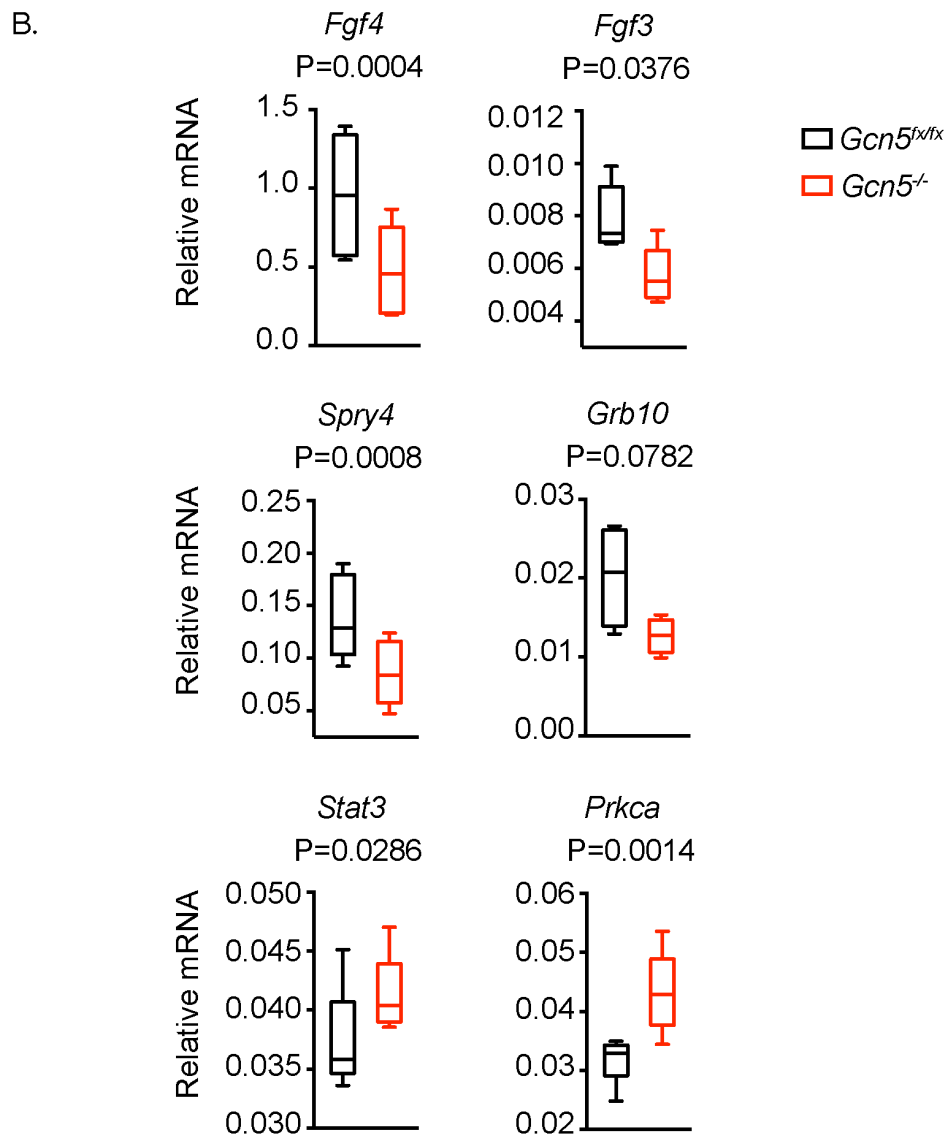
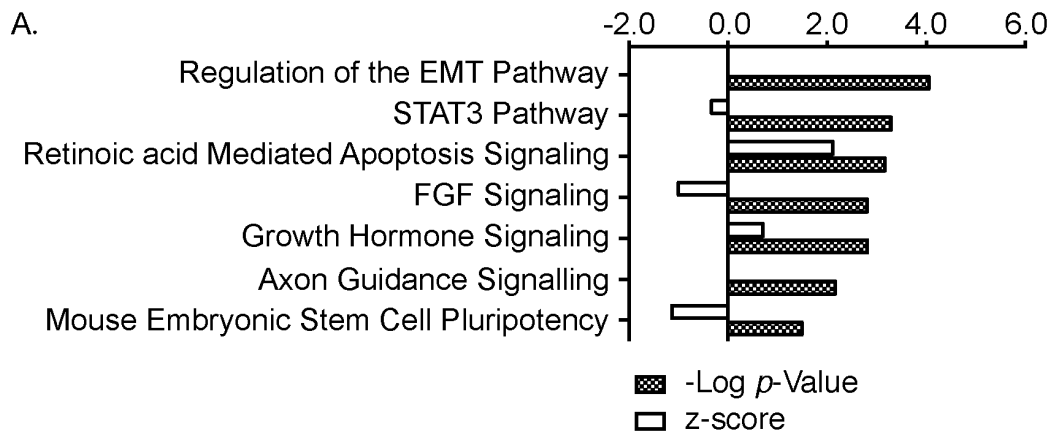


Figure 13 Altered gene expression profiles of FGF signaling pathway components in *Gcn5*^{-/-} EBs at day 5

(A) Significantly altered pathways in day 5 *Gcn5*^{-/-} EBs identified by IPA canonical pathway analysis.

(B) qRT-PCR validating expression changes of key genes encoding FGF signaling pathway components identified by RNAseq, using a second biological sample, normalized to *Pbgd*. Data are presented as Mean \pm SD from 3 independent experiments.

Chapter 6. Deregulation of FGF signaling in *Gcn5*^{-/-} EBs

6.1 Abnormal FGF signaling in day5 *Gcn5*^{-/-} EBs

Mammalian FGF signaling involves several secreted FGF ligands that interact with four types of tyrosine receptor kinases (FGFRs). Upon binding of the ligands, FGF receptors are activated and phosphorylated at specific tyrosine residues that mediate interactions with cytosolic adaptor proteins and intracellular signaling pathways including RAS-MAPK, PI3K-AKT, PLC- γ and STAT pathways ([92](#)). To further define the status of FGF signaling intermediates in *Gcn5*^{-/-} EBs, we examined expression of FGFR1 and phosphorylation of downstream signaling intermediates, including ERK, p38, c-RAF, and AKT, by immunoblotting (Figure 14, A and B). FGFR1 protein levels were notably decreased in the null EBs, as were the activated, phosphorylated forms of both ERK and p38 (P-ERK and P-p38, respectively), indicating deficient activation of the RAS/MAPK pathway. In contrast, levels of activated AKT (P-AKT) and P-c-RAF-Ser259 were not decreased, and might even be slightly increased, suggesting the AKT pathway downstream of FGF signaling is affected to a lesser degree. Levels of PLC- γ did not change (Figure 14C), even though *Prkca* mRNA was up regulated in the null EBs. We also attempted to examine phosphorylated STAT3 levels by immunoblotting to determine if STAT pathway activities were altered in the null EBs, as the *Stat3* gene was significantly upregulated. However we could not assess the status of STAT3 activation because the antibody did not work in our hands.

6.2 Deficient activation of ERK and p38 is associated with crippled cytoskeletal networks in *Gcn5*^{-/-} EBs at day 5

To relate these molecular changes back to the morphological phenotypes of the *Gcn5*^{-/-} EBs, we examined organization of cytoskeletal networks regulated by ERK and p38 signaling ([93](#)) using Airyscan confocal microscopy. Airyscan uses a revolutionary area detector that enables light-efficient imaging with super-resolution and significantly improved signal-to-noise ratio ([94](#)), which allows us to visualize and examine detailed intracellular structures.

We first assessed the actin cytoskeletons of day 5 EBs using phalloidin, which specifically stains filamentous actin (F-actin). In the epiblast of EBs or in early embryonic epithelial structures, F-actin localizes to the periphery of epithelial cells and is particularly enriched at apical sites of columnar epithelial cells ([95](#), [96](#)). This staining pattern was observed as expected in the Airyscan images of phalloidin staining of *Gcn5*^{fx/fx} EBs. In contrast, *Gcn5*^{-/-} EBs displayed disarrayed F-actin, primarily in the inner cells (epiblast) with reduced apical distribution (Figure 14E, left panels). Airyscan images of an intermediate filament protein, vimentin, also showed disrupted staining patterns in the null EBs with notable reduction in fluorescent intensity (Figure 14E, right panels). Decreased vimentin expression was confirmed by immunoblotting (Figure 14D). Conversely, E-cadherin staining showed little difference in localization or expression levels between *Gcn5*^{fx/fx} and *Gcn5*^{-/-}

EBs (Figure 14F). These observations suggest that insufficient activation of ERK and p38 upon *Gcn5* loss affects primarily the F-actin and vimentin networks during early differentiation, in concordance with disorganized epithelial architectures observed in the null epiblasts (Figure 6B), whereas E-cadherin mediated cellular adhesion is not affected by *Gcn5* loss.

Of note, defective ERK signaling is also consistent with decreased mesoderm differentiation (97) in the null EBs (Figure 9 and Figure 10), as well as mesodermal defects previously observed in *Gcn5*^{-/-} embryos (24).

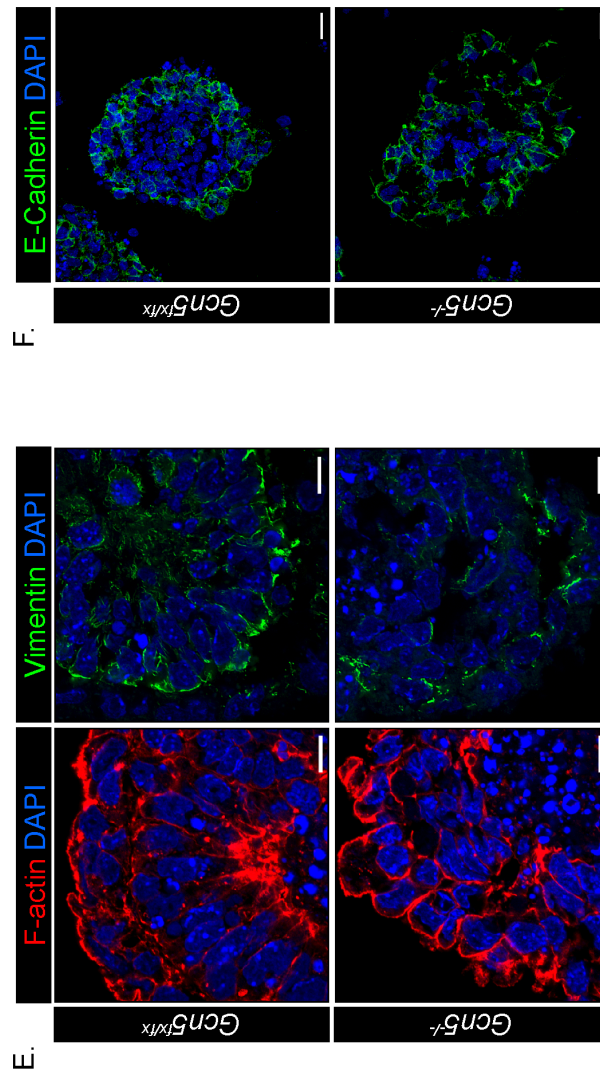
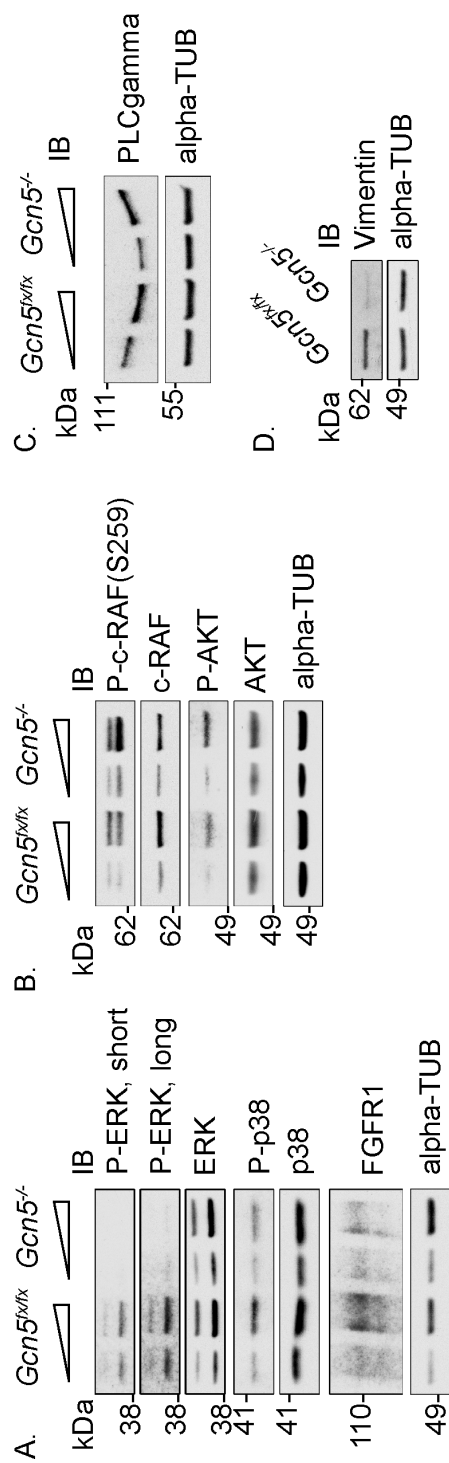


Figure 14 Deficient activation of the FGF pathway in the day 5 *Gcn5*^{-/-} EBs

(A) Representative immunoblots showing decreased phosphorylated forms of ERK and p38 in the *Gcn5*^{-/-} EBs at day 5.

(B) Representative immunoblots showing AKT pathway is affected to a lesser degree in the *Gcn5*^{-/-} EBs at day 5.

(C) Representative immunoblots showing PLC γ is not changed in the *Gcn5*^{-/-} EBs at day 5.

(D) Representative immunoblots showing vimentin expression is decreased in the *Gcn5*^{-/-} EBs at day 5.

(E) Confocal Airyscan (Zeiss LSM880) image showing disarray of F-actin (red) and vimentin (green) cytoskeleton networks in day 5 null EBs. Scale bars, 10 μ M.

(F) Confocal images showing E-cadherin is not overtly affected in the day 5 null EBs. Scale bars, 20 μ M.

**Chapter 7. GCN5 regulates selective c-MYC target genes in early
differentiation**

7.1 Attempts of ChIPs for GCN5 in differentiating EBs not successful

To identify the gene targets directly regulated by GCN5 at the epiblast stage, I attempted ChIP-Seq for GCN5 in the control EBs, but was not successful using either a commercially available antibody or tagging systems in differentiating cells.

I first attempted ChIP using a GCN5 antibody (Cell Signaling #3305), which works well for immunoprecipitation (IP), in the *Gcn5^{fx/fx}* and *Gcn5^{-/-}* ES cells. However there were non-specific ChIP-qPCR signals in the *Gcn5^{-/-}* cells when using *Asf1b* gene promoter (36) for GCN5 antibody titration ChIPs (Figure 15A). The enrichment of GCN5 at *Asf1b* in the *Gcn5^{fx/fx}* ESCs was also very low (<0.001%) and was not augmented as the antibody amount increased (Figure 15A). As *Asf1b* gene promoter is a validated binding region for bioGCN5 (36), these observations suggested the GCN5 antibody is likely not suitable for ChIPs. However, qPCRs results of additional validated GCN5 binding genes/loci are needed to confirm this conclusion and rule out this Cell Signaling GCN5 antibody for ChIPs.

I then tried streptavidin ChIP in day 5 EBs differentiated from bioGCN5 ES cells and vector control cells. Although I was able to see enrichment of bioGCN5 at promoter regions of few target genes (e.g. *Asf1b*, *Alcam*) identified by the ESC-ChIPseq (36) in bioGCN5 ESCs, I was unsuccessful in

optimizing the streptavidin ChIP conditions (*Asf1b*, *Usp10*, *Tbx3*, *Dicer*) for EBs (Figure 15, B and C).

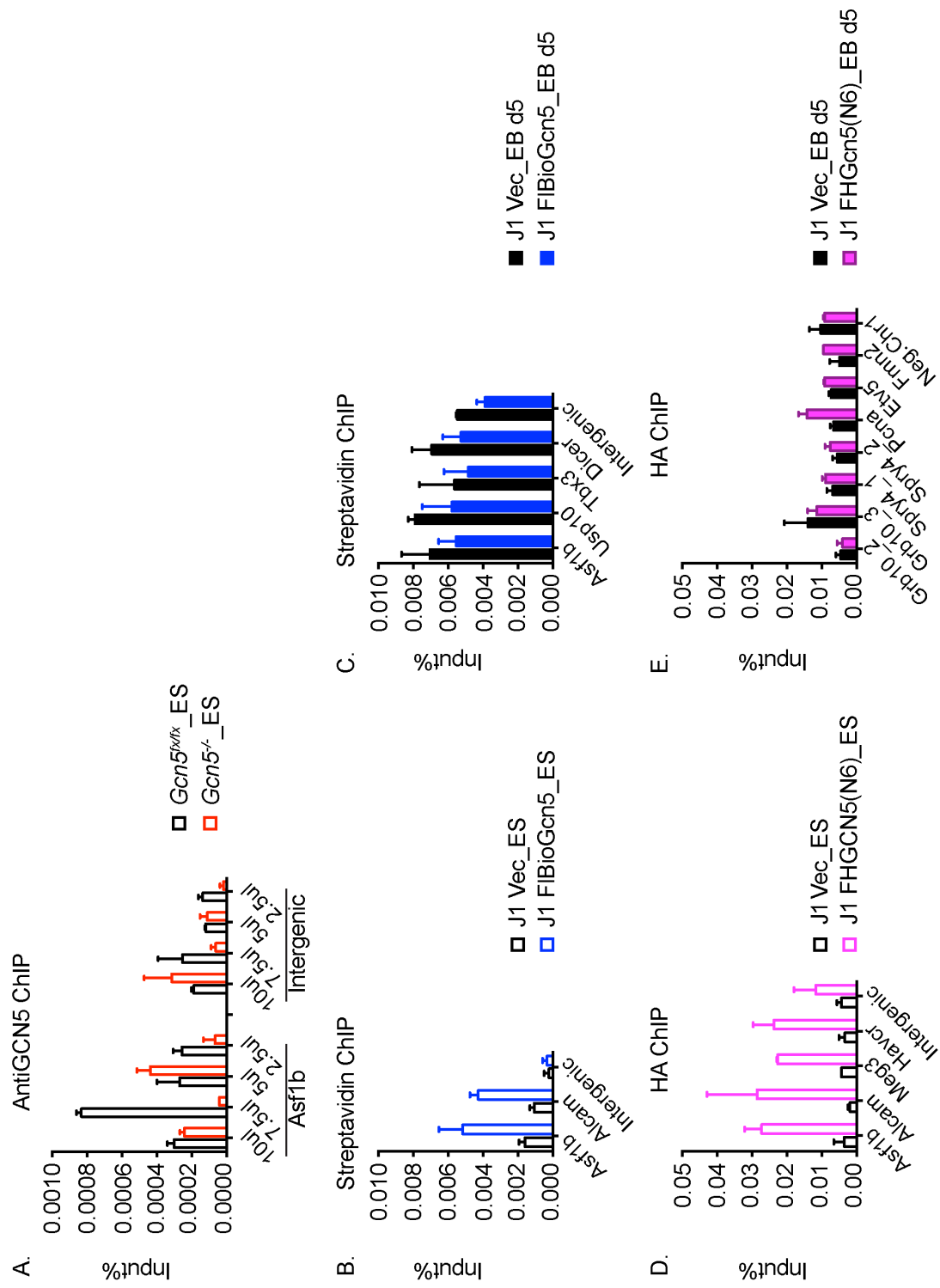


Figure 15 Attempts of GCN5 ChIPs for EBs are not successful

(A) Anti-GCN5 (Cell Signaling 3305) ChIPs with *Gcn5*^{fx/fx} and *Gcn5*^{-/-} ESCs. For each IP, 25ug of sheared chromatin was incubated with increasing amounts of anti-GCN5 (2.5, 5, 7.5 and 10μL) in order to determine the appropriate antibody/chromatin ratio. *Asf1b* gene promoter and an intergenic region were used as positive and negative controls (36).

(B) Streptavidin ChIPs in FIBioGCN5 ESCs. IP was performed as previously reported, *Asf1b* and *Alcam* promoter regions were used as positive loci or qPCR and the intergenic region was used as negative (non-binding) locus (36).

(C) Streptavidin ChIPs in day 5 EBs differentiated from FIBioGCN5 ESCs. IPs were performed as previously reported with adjusted chromatin/streptavidin-beads ratio (2 x chromatin) as *Gcn5* level in ESCs is higher than in differentiated cells (36). Since direct target genes of GCN5 in EBs were not defined at the time, we selected genes strongly bound by bioGCN5 in ESCs (36) that are known to be important for development or essential cellular functions (98-100) for qPCR tests.

(D) HA ChIPs in FHGCN5 (N6 clone) ESCs. For each IP, 25μg of sheared chromatin were incubated with 3μg of HA antibody per manufacturer's instructions. Bound HA-DNA mixtures were eluted by HA peptide following standard procedures. qPCR results showed strong enrichment of FHGCN5 over Vec at gene promoters (36) tested, compared to the intergenic region.

(E) HA ChIPs in day 5 EBs differentiated from FHGCN5 ESCs. IPs were performed with adjusted chromatin amount similar to (C). At that time, the H3K9ac ChIPseq results were obtained, and genomic loci with decreased K9ac peaks in *Gcn5*^{-/-} EBs were selected for qPCR tests; genes associated with these loci (promoters) were also downregulated upon *Gcn5* loss as indicated by our RNAseq data.

Next I sought to create ES cells expressing GCN5 that contains a different tag. To do so, I employed two strategies. One was to introduce a Flag-HA dual tag to the N-terminus of the endogenous GCN5 allele using CRISPR/CAS9 mediated targeting, and the other method was to ectopically express FLAG-HA tagged GCN5 using a lenti-viral vector. For CRISPR/CAS9 targeting strategy (Figure 16A), small guide RNA (sgRNA) and a template single strand oligo were introduced to the J1 ESCs together with the CAS9-EGFP expression vector using nucleoporation. The GFP positive cells were sorted after 48 hours, and seeded one cell per well in a 96-well plate. The ES clones that survived were screened for targeted insertion of the tags by junction PCRs, and positive clones were sequenced to verify the insertion. A total of 666 such clones were analyzed and 3 were confirmed by to have only HA targeted to the intended locus (clones 140, 616, and 666). The flag tag was lost for reasons unknown, and the HA tag inserted in the clone 666 caused a frame shift. The homology arms were examined by Southern blotting, and clone 140 was confirmed to have one allele targeted correctly. For clone 616, one allele was correctly targeted, but the other was abnormal (Figure 16, B and C). Westerns using an anti-GCN5 antibody could not detect GCN5 in the HA-IP products from clones 140 and 616, suggesting that either the HA-GCN5 is not expressed or the HA tag might be hidden due to protein folding, which could render it undetectable (Figure 16D).

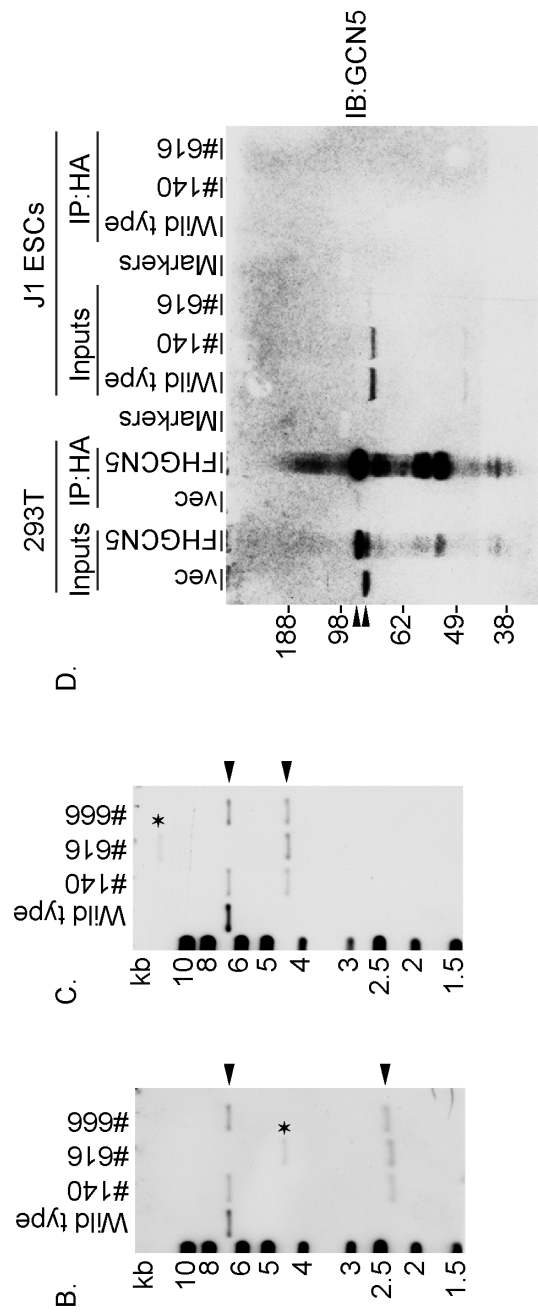
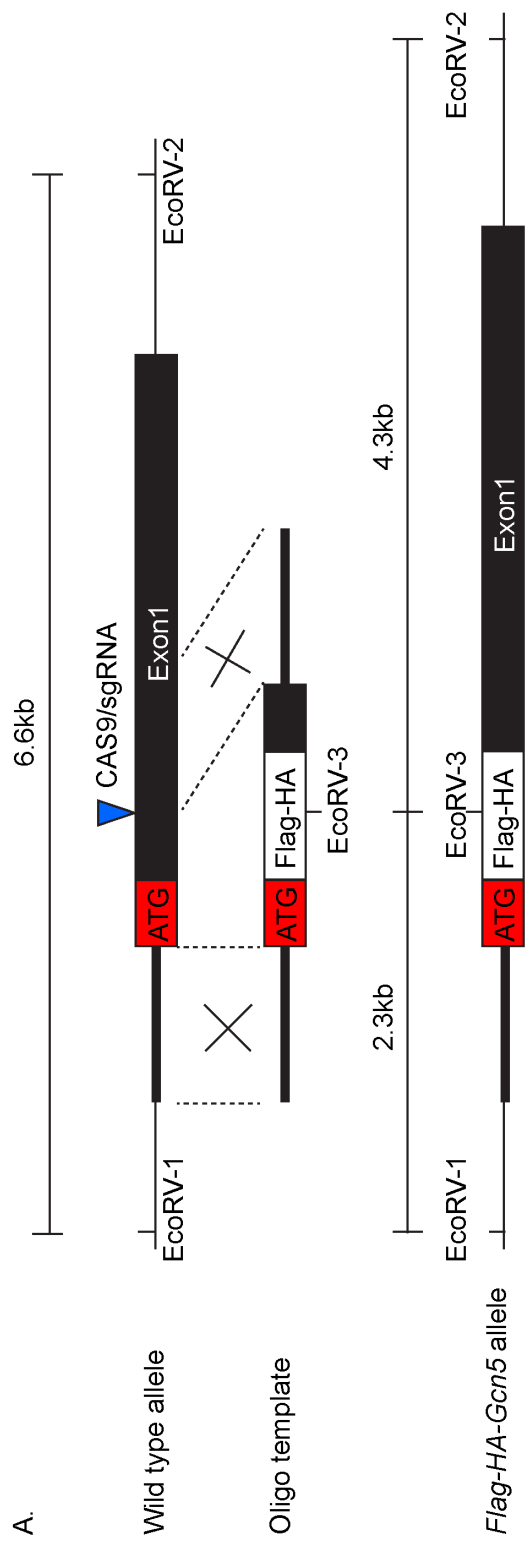


Figure 16 Creation of Flag-HA-GCN5 expressing J1 ESCs using targeted insertion mediated by CRISPR/CAS9

(A) Targeting strategy to create Flag-HA-GCN5 allele. The excision site (blue triangle) was recognized and targeted by the small guide RNA (sgRNA) bound CAS9-GFP. A single strand oligo containing a dual Flag-HA tag placed directly downstream of ATG in frame is used as the template for homologues recombination (HR).

(B) and (C) Southern blots of clones 140, 616, and 666 using probes upstream (B) or downstream (C) of the targeted site. Clone 140 had a correctly targeted allele (2.3kb bands in B, 4.3kb bands in C) and an intact wild type allele (6.6kb bands). Clone 616 had a correctly targeted allele, but the other allele showed abnormal recombination (starred bands). Clone 666 appeared to have similar targeting pattern as 140, however the DNA sequencing showed frame-shift downstream of the tag.

(D) Immunoblots showing HA-IP products from clones 140 and 616 blotted with antiGCN5. The J1 wild-type ESCs were used as a negative control. The Flag-HA-GCN5 expressing 293T cells and their control cells (vec) were used as a positive control for HA-IP/GCN5 western. The positions of FHGCN5 (upper band) and endogenous GCN5 (lower band) are indicated.

In parallel, I also created the Flag-HA-GCN5 (FHGCN5) expressing J1 ESCs, and control cells that express only the dual tag (FH), by lenti-viral infection. This work was done in collaboration with a talented scientist, Dr. Junya Tomida, who is an instructor in the laboratory of Dr. Rick Wood. We verified that the FHGCN5 is expressed and interacts with the SAGA subunits TRRAP and ADA2B, indicating that addition of the tags did not interfere with incorporation of the FHGCN5 into SAGA complex (Figure 17). Next, I used these FHGCN5 ESCs (N6 clone) and their vector control cells for HA-ChIP/qPCR at several ES target genes (e.g. *Asf1b*, *Alcam*, *Meg3*, *Havcr*) (36), and I was able to see enrichment of FHGCN5 at these targets (Figure 15D). However I could not detect enrichment of FHGCN5 at selective promoters when using the EBs generated from these ESCs for HA-ChIPs (Figure 15E), even though these regions are likely to be bound by GCN5 as indicated by our H3K9ac ChIPseq and RNAseq data.

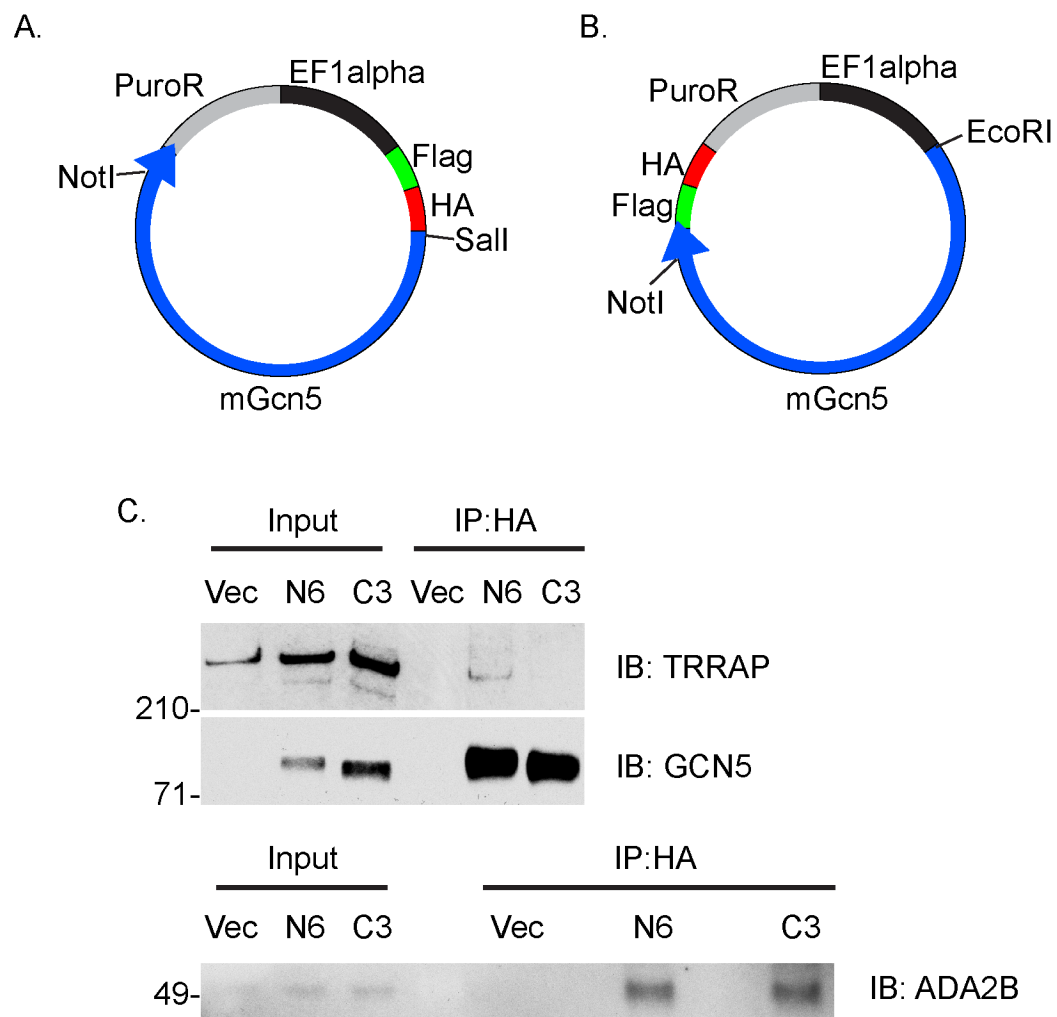


Figure 17 FLAG-HA-GCN5 interacts with subunits of SAGA complex in ESCs

(A) Illustration of the vector of pCDH-EF1alpha-FH-GCN5 (N-terminus tag, N6).

(B) Illustration of the vector of pCDH-EF1alpha-GCN5-FH (C-terminus tag, C3). The original empty pCDH-EF1alpha-FH vector used to generate (A) and (B) was a kind gift from the Wood laboratory at UTMDACC Science Park.

(C) HA immunoprecipitation of the J1 FHGCN5 ESC nuclear extracts immunoblotted with TRRAP, GCN5 and ADA2B. Vec: J1 FH vector, N6: J1 ESCs expressing GCN5 tagged with FH at N-terminus, C3: J1 ESCs expressing GCN5 tagged with FH at C-terminus.

7.2 H3K9ac ChIPs in *Gcn5^{fx/fx}* and *Gcn5^{-/-}* EBs at day5

Since histone H3 lysine 9 (H3K9) is a well-characterized substrate for GCN5 ([101](#)), we performed H3K9ac ChIP, using the same control and *Gcn5^{-/-}* EBs as used for RNAseq. We reasoned that localized decreases in H3K9ac in the *Gcn5^{-/-}* EBs might identify genes that uniquely require the presence of this HAT for proper regulation. As global levels of H3K9ac were not affected by *Gcn5* loss (Figure 5C), regions identified by this approach will likely provide an underestimate of GCN5 targets due to redundancies with PCAF and possibly other HATs.

7.3 GCN5 is required for activating c-MYC target genes in day 5 EBs

Coupled with deep sequencing, we identified 12000 – 21000 peaks in each sample with good mapping rates (Table 6 and Table 7). Peaks were called at P value of 1e-5 and merged for replicative samples of a given genotype. A total of 26031 peaks were used for differential analysis between the control and null samples (Table 7).

Table 6 Mapping rates of the tags from the H3K9ac ChIPseq to mouse genome assembly mm10

	<i>Gcn5^{ΔHX}</i> 4_CHIP_K9ac_1	<i>Gcn5^{ΔHX}</i> 4_CHIP_K9ac_2	<i>Gcn5^{Δ-}</i> 4_CHIP_K9ac_1	<i>Gcn5^{Δ-}</i> 4_CHIP_K9ac_2	<i>Gcn5^{ΔHX}</i> 6_CHIP_K9ac_1	<i>Gcn5^{ΔHX}</i> 6_CHIP_K9ac_2	<i>Gcn5^{Δ-}</i> 6_CHIP_K9ac_1	<i>Gcn5^{Δ-}</i> 6_CHIP_K9ac_2
Mapping rates to mm10 (K9ac)								
total number of tags	39276080	38437831	39472163	33998465	37965900	46478023	46601462	36129352
tags that are not mappable	2698060	2859912	2412469	2378186	2423013	3650349	4294602	2560223
tags that are mapped to multiple locations	3968799	4415225	3867316	3631436	3970451	4864448	4819255	3681526
(% to total)	10.10%	11.49%	9.80%	10.68%	10.46%	10.47%	10.34%	10.19%
tags that are mapped to unique location (usable tags)	32611221	31162694	33192378	27988843	31572436	37963226	37487605	29887603
(% to total)	83.03%	81.07%	84.09%	82.32%	83.16%	81.68%	80.44%	82.72%
usable tags in chr1-22 X,Y	32607572	31160378	33189624	27985339	31569585	37958931	37483920	29885363
unique usable tags	25647982	23983542	25507804	22514314	24949587	29399397	28313414	23831056
non-redundancy fraction (NRF)	79%	77%	77%	80%	79%	77%	76%	80%

	<i>Gcn5^{ΔHX}</i> 4_CHIP_H3_1	<i>Gcn5^{ΔHX}</i> 4_CHIP_H3_2	<i>Gcn5^{Δ-}</i> 4_CHIP_H3_1	<i>Gcn5^{Δ-}</i> 4_CHIP_H3_2	<i>Gcn5^{ΔHX}</i> 6_CHIP_H3_1	<i>Gcn5^{ΔHX}</i> 6_CHIP_H3_2	<i>Gcn5^{Δ-}</i> 6_CHIP_H3_1	<i>Gcn5^{Δ-}</i> 6_CHIP_H3_2
Mapping rates to mm10 (H3)								
total number of tags	36220470	39667819	45442073	33866362	39449367	40565993	43205502	37591292
tags that are not mappable	2815084	3224924	2974289	2577698	2664815	3385678	4353158	2774732
tags that are mapped to multiple locations	6369823	6987762	7775250	5930437	6665012	7037902	7204340	6714952
(% to total)	17.59%	17.62%	17.11%	17.51%	16.90%	17.35%	16.67%	17.86%
tags that are mapped to unique location (usable tags)	27035563	29455133	34692534	25358227	30119540	30142413	31648004	28101608
(% to total)	74.64%	74.25%	76.34%	74.88%	76.35%	74.30%	73.25%	74.76%
usable tags in chr1-22 X,Y	27034685	29453842	34658124	25356906	30118763	30141611	31646814	28100532
unique usable tags	20000290	21268790	25025986	19228627	22515834	22124875	22524566	21109421
non-redundancy fraction (NRF)	74%	72%	72%	76%	75%	73%	71%	75%

Table 7 Peak calling for differential test between *Gcn5*^{fx/fx} and *Gcn5*^{-/-} samples

peak calling	#original peaks called by comparing to H3	#peaks that overlap ENCODE blacklist regions	#peaks that were not called by comparing to Input	#final peaks	UPSTREAM	PROMOTER	EXON	INTRON	TES	DOWNS TREAM	DISTANT
<i>Gcn5^{Δix}</i> _4_CHIP_K9ac_1	16029	8	706	15315	2.4%	76.7%	4.3%	5.8%	1.6%	1.4%	7.7%
<i>Gcn5^{Δix}</i> _4_CHIP_K9ac_2	13795	6	529	13260	2.1%	82.5%	2.8%	4.3%	1.0%	1.2%	6.1%
<i>Gcn5^{Δ-}</i> _4_CHIP_K9ac_1	16514	6	1561	14947	2.4%	75.1%	4.6%	6.9%	1.9%	1.6%	7.5%
<i>Gcn5^{Δ-}</i> _4_CHIP_K9ac_2	12866	6	819	12041	2.0%	83.4%	2.8%	4.2%	1.2%	1.0%	5.4%
<i>Gcn5^{Δix}</i> _6_CHIP_K9ac_1	22689	11	1869	20809	3.8%	60.2%	7.3%	12.4%	2.6%	2.3%	11.4%
<i>Gcn5^{Δix}</i> _6_CHIP_K9ac_2	19938	7	1454	18477	3.4%	65.7%	6.1%	10.1%	2.3%	2.0%	10.4%
<i>Gcn5^{Δ-}</i> _6_CHIP_K9ac_1	19893	9	952	18932	3.4%	63.9%	6.7%	11.4%	2.4%	2.2%	10.0%
<i>Gcn5^{Δ-}</i> _6_CHIP_K9ac_2	18553	5	699	17849	3.2%	67.1%	6.0%	10.4%	2.2%	2.1%	9.1%
#merged_peaks_used_for_differential_test				26031	4.5%	50.3%	9.9%	16.7%	3.1%	2.9%	12.7%

Differential peak analysis identified 173 peaks that were decreased in the *Gcn5*^{-/-} EBs, the majority (154) of which were located near gene promoters (Table 8). Gene annotation identified 238 genes likely driven by these promoters, with occasions where an H3K9ac peak falls in a putative promoter region driving more than one gene. We also uncovered 144 H3K9ac peaks that increased upon *Gcn5* loss, yet only 30 of those peaks were near promoters, associated with 31 genes. These data are consistent with the co-activator role of GCN5 in gene transcription (Table 8).

Comparison of genes identified in our analyses as having decreased H3K9ac peaks in their promoters with ENCODE ChIPseq data identified candidate transcription factors that might recruit GCN5 to these regions (Table 9). Top TFs identified by this approach include HCFC1, a nuclear protein known to associate with GCN5 containing complexes ([102](#)), as well as TBP and CTCF. Strikingly, a number of MYC family members, including MAX, MXI1 and c-MYC, were also identified by this approach, consistent with our previous work connecting GCN5 to MYC functions in both ESCs and during somatic cell reprogramming ([36](#)).

Table 8 Comparison of H3K9ac peaks and associated genes in *Gcn5^{fx/fx}* and *Gcn5^{-/-}* EBs at day 5

<i>Gcn5^{-/-}</i> vs <i>Gcn5^{fx/fx}</i>	Decreased	Increased
Number of peaks	173	144
Number of peaks in promoters	154	30
Genes associated	238	31

Table 9 Top ranked transcription factors or regulators reported to bind genes with decreased H3K9ac identified in *Gcn5* null EBs at day 5

Rank	TFs or regulators	Number of genes with H3K9ac decrease	Q-value
1	HCFC1	205	1.25E-77
2	MAX	204	4.43E-72
3	MXI1	199	4.25E-66
4	GCN5	172	2.65E-61
5	NELFE	192	2.65E-61
6	TBP	192	1.69E-59
7	CTCF	210	3.77E-59
8	SIN3A	192	9.08E-59
9	P300	188	1.14E-58
10	C-MYC	164	2.44E-57
11	E2F4	99	1.40E-48
12	ZNF	145	1.69E-43
13	POL2	218	4.62E-43
14	FLI1	103	1.48E-42
15	CHD2	143	5.48E-35

To better determine which of these regions might reflect genes directly activated by GCN5, we compared genes with decreased H3K9ac at their promoters (Appendix 3) with genes identified as down regulated more than 2 fold by RNAseq. Only 7 genes ($P=0.0096$, one-sided hyper geometric test) were both downregulated and decreased in H3K9ac, and 4 of these genes are reported to be regulated by c-MYC in different cellular systems ([103-106](#)). *Myc* is induced by most mitogenic factors including FGFs to exert the immediate early cellular responses through its transcriptional targets ([107](#)). Specifically, *Rps6ka2* encodes RSK3 that belongs to the 90kDa ribosomal S6 kinase (RSK) family. RSK kinases are directly activated by ERK and p38 cascades downstream of mitogen and stress mediated stimuli, by which regulate diverse cellular processes including cell growth and migration. Transcriptional regulation of *RSK* genes is much less defined compared to RSK activation mechanisms mediated by protein phosphorylation. Our findings here suggested that GCN5 is required for normal transcription of *Rps6ka2* during early differentiation (Figure 18A, and Figure 18B, middle panels). *Mthfd2*, also a c-MYC target, regulates vimentin expression in breast cancer cells ([108](#)). As it is markedly downregulated upon *Gcn5* loss in the developing EBs (Figure 18A and Figure 18B lower panels), downregulation of this gene might contribute to the vimentin loss observed in the *Gcn5* null EBs. Additional experiments are needed to explore this possibility. The other two c-

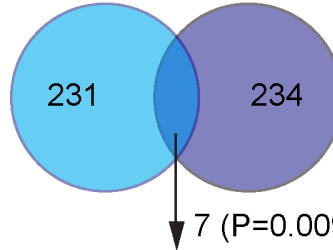
MYC targets, *Bcat1* and *Srm* (Figure 18A) both promote cancerous growth in a *c-Myc* dependent manner ([103](#), [109](#)). Whether such connection holds true in the developing EBs or early embryonic development is an interesting area for further investigation.

The most significantly downregulated gene, *Grb10* (Figure 18A and Figure 18 B upper panels), as well as *Nmnat2* (Figure 18A), are also involved in regulation of insulin/AKT signaling and MAPK signaling, respectively, as implicated in studies done in different cellular contexts ([90](#), [110-112](#)). These implications reinforce the potential roles of GCN5 in regulation of signaling events during early differentiation.

Collectively, these data suggest that GCN5 directly activates selective genes, including several MYC targets, during early differentiation of EBs. The literature-implicated involvement of these genes in signaling events, particularly related to MAPK and AKT pathways, supported the link between GCN5 and FGF signaling identified in gene expression analysis in early EB differentiation.

A.

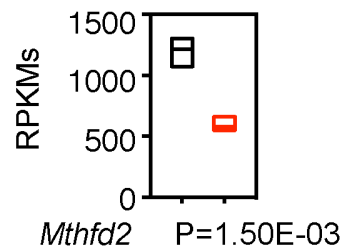
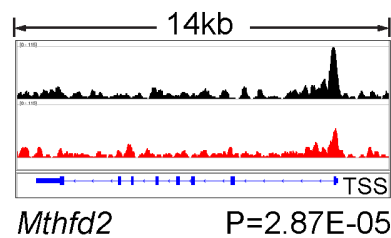
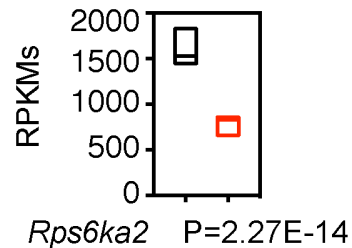
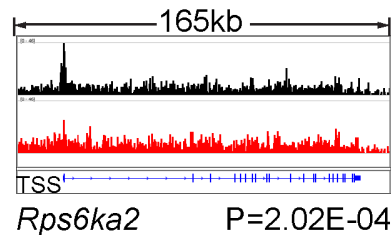
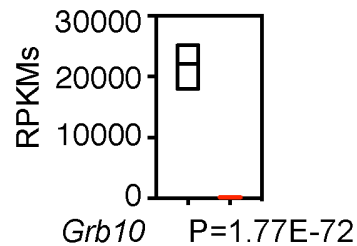
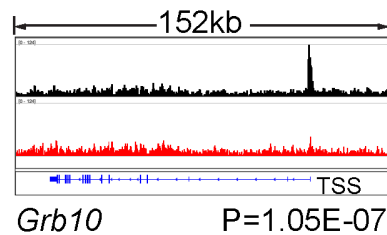
Genes with decreased
H3K9ac at promoter
(FDR0.05)



RNAseq down
regulated genes
(FDR0.05, FC2)

Putative direct targets	Functions
<i>Grb10</i>	AKT/mTOR substrate, insuling/IGF signaling
<i>Nmnat2</i>	Metabolism, Signaling
<i>Bcat1</i>	c-MYC target, metabolism/growth, signaling
<i>Gldc</i>	Folate metabolism
<i>Rps6ka2</i>	c-MYC target, signaling
<i>Mthfd2</i>	c-MYC target, metabolism/proliferation, Vim network
<i>Srm</i>	c-MYC target, metabolism

B.



■ *Gcn5^{fx/fx}* ■ *Gcn5^{-/-}*

□ *Gcn5^{fx/fx}* □ *Gcn5^{-/-}*

Figure 18 Putative target genes of GCN5 during early EB differentiation

(A) Putative target genes directly regulated by GCN5. Venn diagram showing overlap between H3K9ac decreased genes and GCN5 induced genes. Overlapping genes are listed in the table with a general description of the reported functions.

(B) Examples of H3K9ac peak profiles (n=4) and RNA transcripts (n=3) for top targets of GCN5 in day 5 EBs.

Chapter 8. Conclusions, Discussion and Future Directions

8.1 Conclusions

Previous studies showed that *Gcn5* is essential for embryo development and survival, but the functions of this HAT in regulating differentiation are not well defined ([24](#), [25](#)). Our findings reveal a new role of *Gcn5* in regulation of FGF signaling during early differentiation (Figure 19). FGF signaling regulates both migration and patterning of mesoderm during gastrulation ([88](#)). We report here that *Gcn5* is required for proper expression of *Fgf3*, *Fgf4*, and *Fgfr1*, as well as for activation of downstream pathway effectors including ERK and p38. Failures in the execution of these pathways result in defective mesoderm differentiation and cytoskeletal networks ([93](#), [97](#), [113](#)) as reported by others using mouse models and cellular systems. Consistently, we show that *Gcn5*^{-/-} EBs have abnormal cytoskeletal organization and defective mesoderm and endoderm formation during early differentiation. Loss of *Gcn5* also leads to significant downregulation of *Grb10*, which is characterized as a negative regulator for insulin/IGF mediated AKT signaling ([90](#), [91](#), [110](#)), indicating that *Gcn5* may be also required for normal insulin signaling during early differentiation.

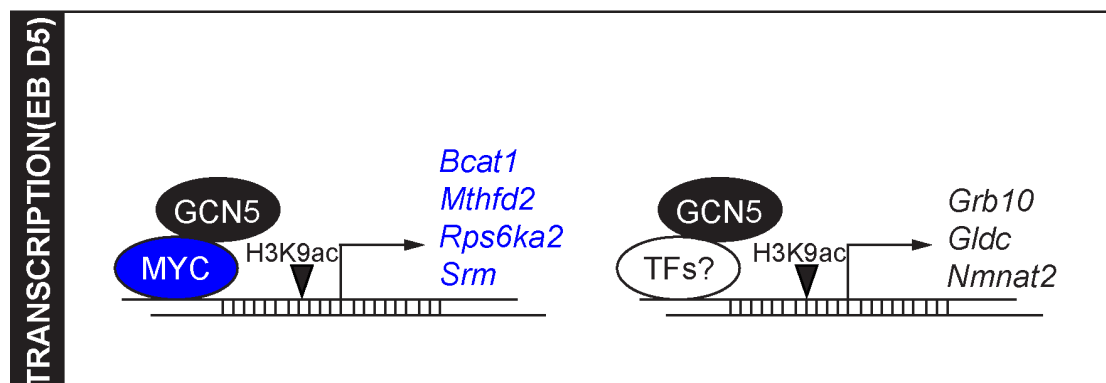
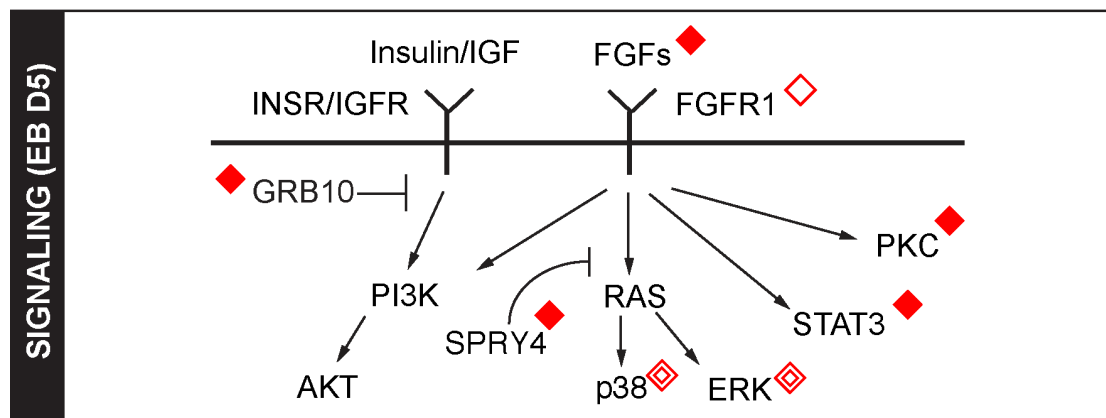
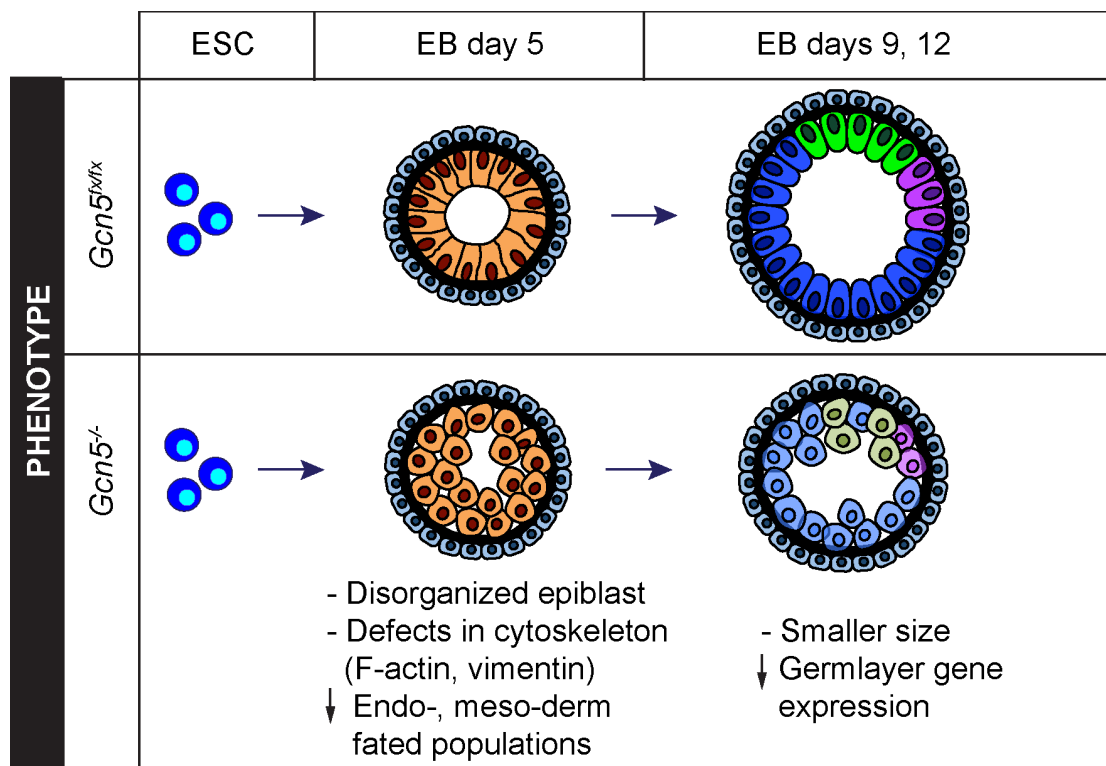


Figure 19 GCN5 impacts multiple components of the FGF signaling pathway and activates MYC targets during early differentiation

Upper illustration:

The abnormal phenotype of *Gcn5*^{-/-} EBs becomes evident early during EB differentiation (day 5). Loss of *Gcn5* leads to disorganization of the epiblast architecture that is associated with defective cytoskeleton, including F-actin and vimentin networks, and decrease in progenitors fated for endoderm and mesoderm.

At later stages of differentiation (days 9 and 12), *Gcn5* null EBs are smaller in size and express lower levels of germlayer marker genes, compared to the controls. Color codes: Blue represents ectoderm, green represents endoderm, and magenta represents mesoderm. Lighter shades in the *Gcn5*^{-/-} EBs indicate decreased expression levels of marker genes for each population.

Middle illustration:

At day 5 of differentiation, GCN5 impacts expression of multiple genes encoding critical components in FGF signaling pathway and for proper activation of ERK and p38 pathways.

Solid diamond: altered level of transcripts

Open diamond: altered level of protein expression

Double open diamond: altered level of protein phosphorylation

Bottom illustration:

At day 5 of differentiation, GCN5 is required for activating genes important for signaling through promoter associated H3K9ac, including 4 c-MYC targets (blue).

Further, we identified *Grb10*, *Nmnat2*, *Gldc*, *Bcat1*, *Rps6ka2*, *Mthfd2*, and *Srm* as likely direct targets of GCN5, which exhibit both decreased acetylation at H3K9 and decreased expression upon *Gcn5* loss. Four of these genes (*Bcat1*, *Rps6ka2*, *Mthfd2*, and *Srm*) are reportedly MYC targets ([103](#), [104](#), [106](#), [109](#)) in various tumorous cell lines. These findings point to a co-activator role of GCN5 for these MYC targets during early differentiation. Such partnership between GCN5 and MYC in gene regulation is also consistent with previous observations in ESCs, during somatic cell reprogramming and during neural development ([29](#), [36](#)), once again, highlighting the significant relationship of GCN5-MYC in gene regulation in diverse physiological and pathological contexts.

Myc itself is targeted by RAS/ERK and AKT pathways through both transcription dependent and independent mechanisms, as shown by studies using cellular models ([114](#)), and its induction is an immediate early response to most mitogenic factors including FGFs ([107](#)). *Myc* deletion in ESCs induces a dormant pluripotent state that mimics embryonic diapause, and promotes primitive endoderm formation *in vitro* ([115](#), [116](#)). *C-Myc*^{-/-} mice die by E10.5 with growth retardation, defective cardiac and neural development, and defects in vasculogenesis, angiogenesis, and primitive erythropoiesis in the yolk sac and in the embryo proper ([117](#), [118](#)). Whereas *n-Myc*^{-/-} mice die by E12.5, exhibiting developmental delay and a decrease in size/cellularity of

certain organs, for instance, nervous system, lung, and heart ([119-121](#)). These phenotypes are different from what we observed here in *Gcn5*^{-/-} ESCs and previously reported in *Gcn5* null mice ([24](#), [36](#)), indicating *Myc* independent requirement for *Gcn5* during early development or differentiation, or that GCN5 may be required for selective genes targeted by MYC, as supported by our data.

We previously reported that in mouse ESCs, GCN5 also has shared transcriptional targets with E2F1, as GCN5 binding sites are highly enriched of E2F1 motif and GCN5 induced genes significantly overlap with E2F1 targets in the ESCs ([36](#)). Our study in differentiating ESCs identified E2F4 as a TF likely to recruit GCN5/SAGA to a subset of its target genes to acetylate H3K9 (Table 9). However we did not observe changes in expression of direct E2F4 gene targets in *Gcn5*^{-/-} EBs. The best-characterized function of E2F family TFs is cell cycle regulation ([122](#)). Individual E2F family members are dispensable in mouse development, but compound deletions of *E2F3* in combination with *E2F1* and/or *E2F2* lead to embryonic lethality after E9.5, with evident growth retardation largely attributed by proliferation arrest ([123](#)). Our EB studies probe for differentiation events that parallel embryonic stages prior to gastrulation, much earlier than E9.5 when E2F1-3 become essential for embryonic survival, and we did not observe overt proliferation defect at such early stage of differentiation in the absence of *Gcn5*. This timing

difference could explain the absence of E2F targets affected by loss of *Gcn5* in our data set. Further, roles of E2F family TFs in ESC differentiation remain an understudied area. Of interest, *E2F4* has been implicated in cell lineage differentiation during mouse development by regulating cell-cycle exit ([122](#)), which is essential for controlling differentiation dynamics. Knowledge of GCN5 genomic locations during differentiation will help us gain insights on coinciding TFs that are specifically required for GCN5 target gene expression in such developmental context. A GCN5-ChIP or tag-mediated GCN5 ChIP in differentiating ESCs will help to achieve this goal.

In addition, some of the putative gene targets of GCN5 identified in this study have been shown to function in specific lineages or cell migration, though in different cellular systems. For example, the paternally expressed *Grb10* isoform is specifically important for neuronal tissue development in mice, while the maternal, major isoform of *Grb10* is required for growth inhibition involving insulin/AKT pathway regulation ([124](#)). NMNAT2 is required for MAPK signaling mediated axon degeneration in response to injury as a survival mechanism, as shown in a mouse dorsal root ganglia culture based study ([112](#)). *Mthfd2* is a regulator of vimentin expression in breast cancer cells and might promote migration and invasion of these cells ([108](#)). These findings provide clues for us to further clarify if these genes may indeed contribute to the phenotypes in *Gcn5*^{-/-} EBs, with additional experiments to

assess if lineage specific *Grb10* expression is associated with defective germlayer differentiation, or if decreased expression of *Nmnat2* or *Mthfd2* may be directly related to the cytoskeletal defects upon *Gcn5* loss.

Another notable common function of GCN5 targets identified here is that they regulate metabolism and growth, either positively (*Nmnat2*, *Bcat1*, *Gldc*, *Mthfd2* and *Srm*) or negatively (*Grb10*, *Bcat1* and *Rps6ka2*) ([90](#), [91](#), [103](#), [105](#), [111](#), [125-127](#)). Altered carbon metabolism induced by these gene expression changes could further derail differentiation ([128](#)). Some of these genes are also directly regulated by ERK/MAPK pathway (*Rps6ka2*, *Nmnat2*) ([111](#), [112](#), [129](#)) or AKT pathway (*Grb10*) ([90](#)), indicating their metabolic impacts could be part of the signaling outputs and may lead to the phenotypes observed in the *Gcn5* null EBs. However, additional studies are needed to establish such direct links.

Finally, some of the FGF pathway components did not appear to be directly regulated by GCN5 at the level of transcription. For instance, transcripts of *Fgf3* and *Fgf4* are downregulated in *Gcn5*^{-/-} EBs at day 5, but H3K9ac levels were not altered in their promoters. Phosphorylation of ERK and p38 is decreased in the day 5 *Gcn5*^{-/-} EBs without overt alterations in their transcript levels. Perhaps the best-characterized mechanism by which FGF signaling is regulated involves protein-protein interactions and the resulting post-

translational modifications (phosphorylation) of these proteins. However, transcriptional regulation of FGF pathway genes themselves seems a much less investigated area. It has been suggested that microRNAs can target multiple FGF signaling genes including *Fgfr2*, *Stat3* and *Mapk14* to influence cellular differentiation during development (92). In addition, SOX2 and OCT4 regulate *Fgf4* transcription in early development by binding to a downstream enhancer of the *Fgf4* gene in a cooperative manner. Interestingly, *Oct4* mRNA is decreased 2 fold in *Gcn5*^{-/-} EBs, suggesting this event might contribute to the downregulation of *Fgf4* observed in the null EBs. How loss of *Gcn5* leads to deregulation of the other FGF signaling genes observed remains an open question. Future work will address these questions, and the answers will enrich our understandings in regulatory mechanisms controlling FGF signaling pathway and the biological consequences it confers.

8.2 Possible contributions to the observed EB phenotypes by non-transcriptional targets of GCN5

Our study primarily focused on transcriptional changes caused by *Gcn5* loss at the epiblast stage of EB differentiation, as abnormal phenotypes were first observed in day 5 EBs. However, among 240 genes downregulated upon *Gcn5* loss, only 7 genes were identified as likely to be directly regulated by GCN5 transcriptionally, as they have decreased H3K9ac peaks in the promoter region. Such small proportion pointed to alternative mechanisms by

which loss of *Gcn5* contributes to altered gene expression and/or the cellular phenotypes observed in day 5 *Gcn5*^{-/-} EBs. One possible explanation is that PCAF, the highly related homolog of GCN5, largely compensates for transcriptional activation of GCN5 target genes in absence of *Gcn5*, and we will discuss this possibility in the next section. Another possibility might be that *Gcn5* loss impacts gene expression by its ability to modify non-histone proteins ([26](#), [30](#), [130](#)). For example, GCN5 pairs with MYC-nick, a CALPAIN-cleaved cytoplasmic derivative of MYC, to acetylate alpha-tubulin (ac-alpha-TUB) and regulate cytoskeleton organization and differentiation of myoblasts. We examined the ac-alpha-TUB using immunostaining and immunoblotting in the day 5 EBs. The levels of alpha-tubulin appeared to be similar between *Gcn5*^{fx/fx} and *Gcn5*^{-/-} EBs, as indicated by both confocal images and the immunoblot (Figure 20A, upper panels and Figure 20B). However, the acetylate alpha-tubulin showed cytoplasmic diffusion in the null EBs, compared to the distinctive apical distribution in the controls, as in the confocal images, even though the changes in ac-alpha-TUB protein level were minimum as indicated by the immunoblot (Figure 20A, lower panels and Figure 20B). These findings suggested that loss of *Gcn5* indeed affected subcellular localization of the acetylated alpha-tubulin, even though the level of this modification appeared to be maintained by other HATs. The altered staining pattern of acetylated alpha-tubulin is also consistent with the disorganized epiblast architecture observed in the absence of *Gcn5*.

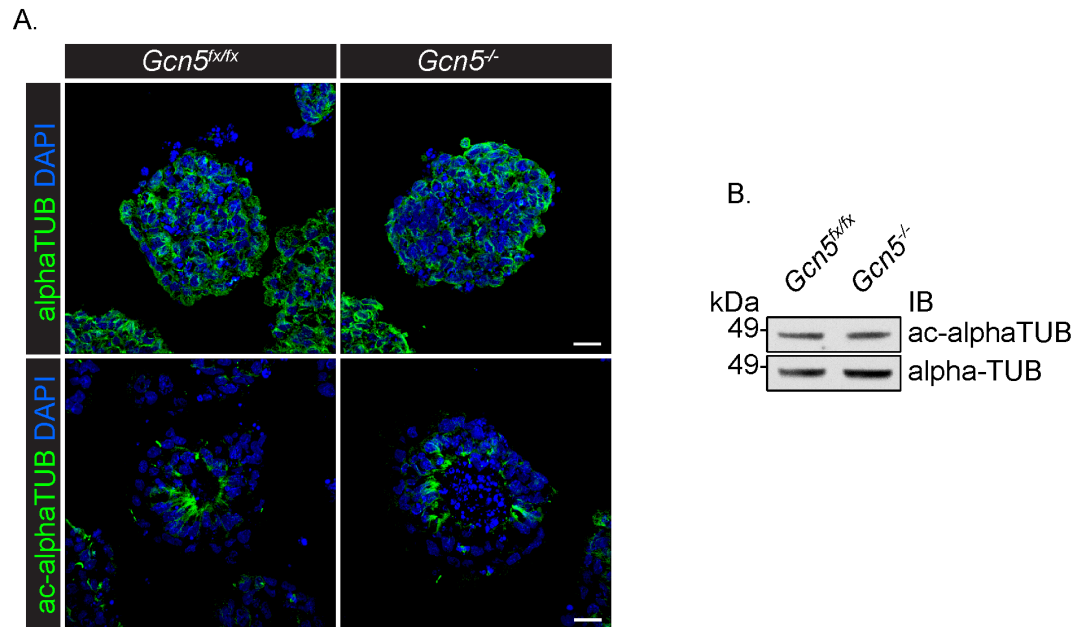


Figure 20 Acetylation of tubulin is not overtly affected by *Gcn5* loss in day 5 EBs

(A) Confocal images of alpha-tubulin (green, cytoplasmic) and acetylated-alpha tubulin (green, apical distribution in control epiblast cells, but cytoplasmic diffusion and less well organized fibers in the null epiblast cells) in day 5 EBs. Scale bar, 20 μ M.

(B) Representative immunoblots for acetylated-alpha tubulin levels in day 5 EBs.

GCN5 can also acetylate transcription factors, such as E2F, c-MYC and p53 ([25](#), [131](#), [132](#)). Such acetylation event can increase DNA-binding ability, facilitate activation or prolong half-life of these TFs, thereby modulate their abilities in gene regulation and in carrying out cellular functions. IPA analysis can predict upstream regulators based on the overall gene expression changes in a given gene set. In the day 5 *Gcn5*^{-/-} EBs, we did identify c-MYC (z= -1.613, P=1.11E-06) and p53 (z=0.917, P=5.66E-07) as potential regulators for genes changed in absence of *Gcn5*, but not E2F family factors. A positive z score indicates upregulation of the predicted regulator, and a negative z score indicates downregulation. So these results suggested downregulation of c-MYC, consistent with decreased c-MYC targets transcription observed earlier, and slight upregulation of p53. We did not observe direct targets of p53 with altered promoter H3K9ac levels in the absence of *Gcn5* by our genomic sequencing data, so it is possible that *Gcn5* loss may alter p53 acetylation levels to affect the transcription of p53 target genes. More interestingly, the most downregulated upstream transcriptional regulators in the absence of *Gcn5* predicted by IPA include TRIM24 (z=-5.255, P=2.07E-20), NKX2-3 (z=-3.539, P=7.60E-12), IRF4 (z=-2.360, P=3.63E-04) and CTNNB1 (z=-2.346, P=2.90E-07). GCN5 interacts with beta-catenin (CTNNB1) in colon cancer cell lines ([133](#), [134](#)), yet it is unclear whether such interaction occurs during early differentiation, nor is known if the interaction leads to acetylation and functional consequences in early

differentiation. Little is known about relations of GCN5 with the other TFs identified here and about other non-histone targets of GCN5 during early differentiation, and we cannot exclude the contributions of such targets to developmental processes that require GCN5.

The FHGCN5 expressing ES cells created during this project, together with the previously generated bioGCN5 expressing ES cells will be useful tools for identifying new substrates of GCN5 in both ES cells and lineages generated thereof. However, successfully tagging endogenous GCN5 remains the best strategy in studying GCN5 binding partners and genomic distribution *in vivo* and during various developmental stages. My attempts to use exogenously tagged GCN5 for ChIP experiments proved to be fruitless. One explanation is that GCN5 expression level is regulated during differentiation, with lower expression in day 5 EB compared to day 0 (ESC) ([36](#)) (Figure 21). Also our data from this study suggest that GCN5 regulates specific sets of genes that may not be large in number. All of these factors could increase the difficulty in optimizing ChIP conditions in differentiating cells, even for tag proteins/beads proven to be efficient for ChIP in ESCs. In addition, a tagged GCN5 expressed from its own promoter, is most likely to be regulated as the wild type protein. If such tagged GCN5 is normally expressed and functions as the wild type protein, for instance, to acetylate H3K9/14, to be incorporated into SAGA or ATAC complexes and to be loaded onto the chromatin at reported

GCN5 target genes, then the biochemical or functional analysis performed through the tag will give reliable information as to what GCN5 interacts with, where in the genome it binds, and how these interactions may confer cellular consequences.

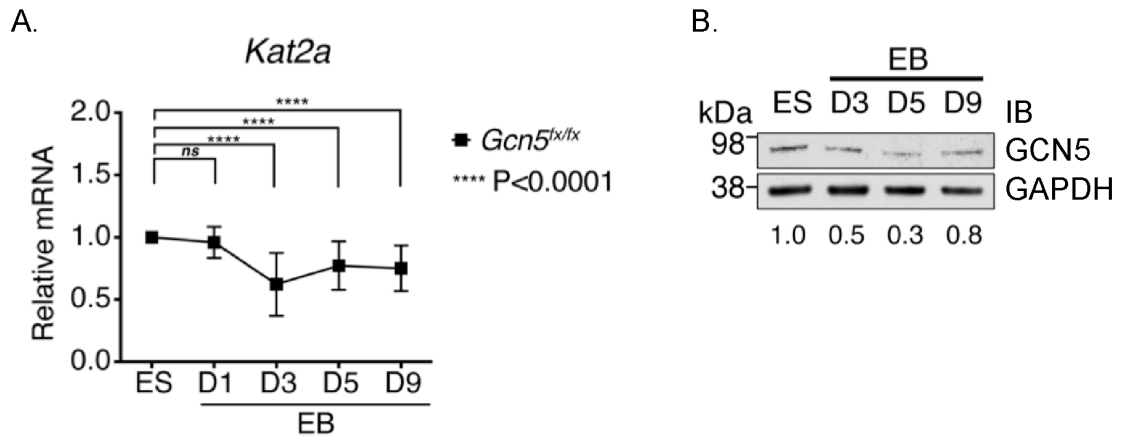


Figure 21 GCN5 expression is regulated during early differentiation

(A) qRT-PCR plot showing *Gcn5* mRNA levels in *Gcn5^{fx/fx}* cells during differentiation, normalized to *Pbgd* gene. Data from 4 independent experiments represented as Mean \pm SD. 2-way ANOVA was used to test the statistical difference in *Gcn5* mRNA level between EBs and ES.

(B) Representative immunoblots showing GCN5 protein levels in *Gcn5^{fx/fx}* WCLs during differentiation.

8.3 Potential compensatory effects from GCN5/ATAC or PCAF

GCN5 is most active *in vivo* when incorporated into modular complexes, including SAGA and ATAC in mammals ([14](#)). Our studies do not differentiate the functions of the two complexes, and the phenotypes we observe may reflect loss of activity of both. However, knockout of *Atac2*, a component of ATAC but not SAGA, did not cause defects in lineage differentiation ([135](#)), as was observed in *Gcn5*^{-/-} embryos, suggesting SAGA may be more important for these early developmental events. Nonetheless, future studies disrupting subunits specific to SAGA or ATAC will aid in differentiating the overlapping or distinct gene sets regulated by these two GCN5 containing complexes during early differentiation stage or embryogenesis.

Our previous genetic studies showed *Gcn5*^{-/-};*Pcaf*^{-/-} embryos die earlier than do *Gcn5*^{-/-} embryos, even though *Pcaf* deletion on its own exhibits no overt abnormal phenotype ([24](#), [136](#)). These findings indicate that *Gcn5* and *Pcaf* have shared functions during early development. The phenotypes of *Gcn5*^{-/-} EBs at day 5 despite the presence of PCAF suggested non-redundant function of GCN5 during early differentiation. However, generation of ES cells lacking *Gcn5* in different *Pcaf* allelic background will provide opportunities to identify common or unique gene targets regulated by these two sister proteins in stem cell state or during differentiation processes.

8.4 Potential novel roles of GCN5 during early differentiation

Interestingly, more genes were up regulated upon loss of *Gcn5* (at both day 3 and day 5) than were down regulated, in contrast to the role of GCN5 as a co-activator of transcription. Many of these events are likely indirect effects upon *Gcn5* loss, although we cannot exclude the possibility that GCN5 may be involved in gene repression during early differentiation. Indeed, a recent study revealed that another HAT, TIP60, acts as a transcriptional repressor in ES cells by a HAT independent mechanism ([137](#)). Notably, many of the genes up regulated upon *Gcn5* loss are involved in acute phase response and interferon signaling, as indicated by both IPA and GSEA (Figure 22).

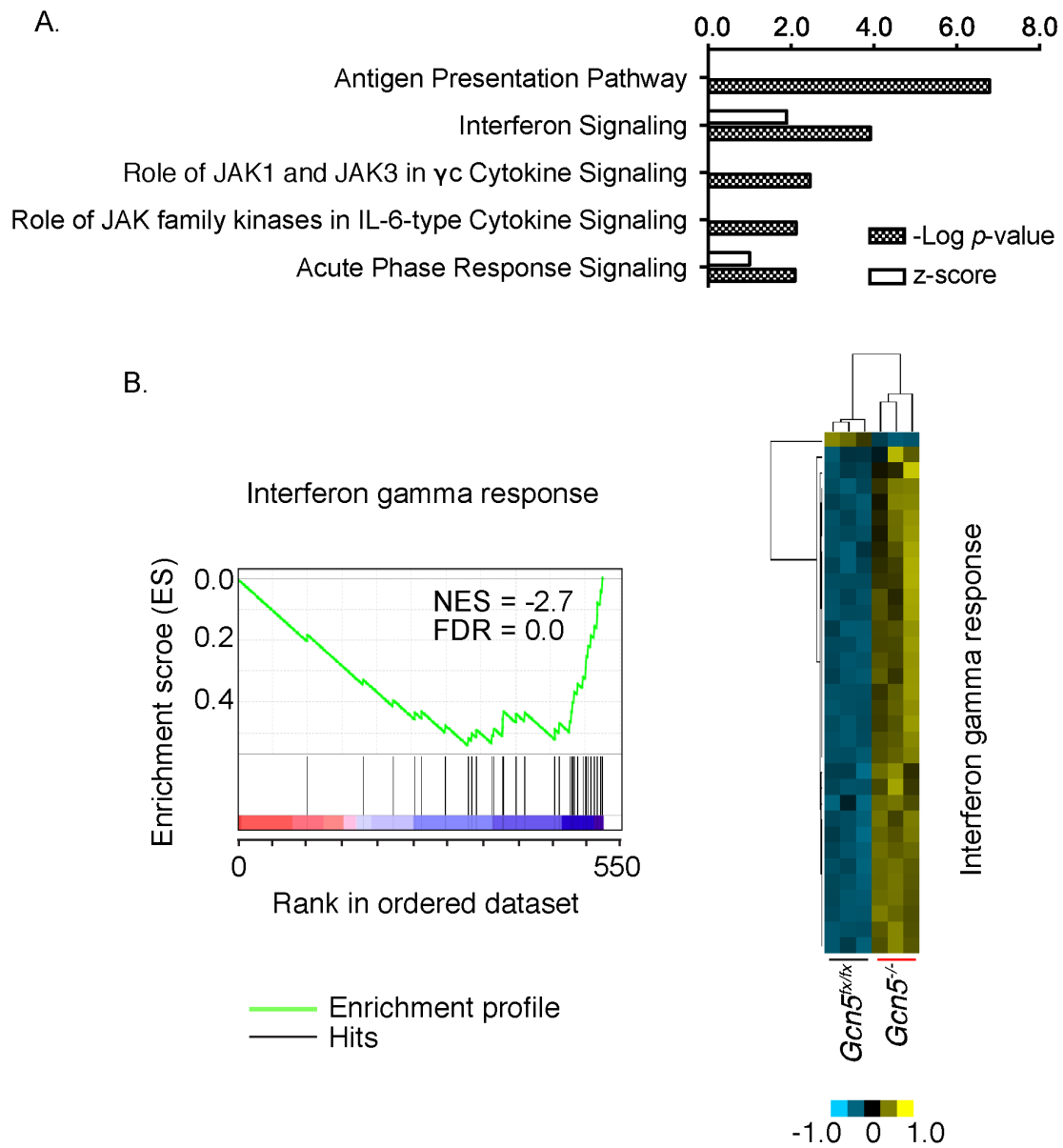


Figure 22 Increased immune response in day 5 *Gcn5*^{-/-} EBs

(A) Top ranked immune response related pathways (IPA) in the *Gcn5*^{-/-} EBs at day 5.

(B) Top one gene set enriched in the null EBs at day 5 identified by GSEA.

Red: positively correlated to *Gcn5*^{fx/fx}. Blue: positively correlated to *Gcn5*^{-/-}.

These findings are in line with our previous work in fibroblasts that indicated GCN5 and PCAF repress IFN β expression by targeting a non-histone substrate, TBK1 ([138](#)). The links between interferon signaling and early embryonic development or ESCs remain an understudied area. Apart from its important roles in immune response, this pathway may be also involved in cell adhesion, proliferation and early development. A recent report shows Interferon-induced trans-membrane protein 3 (IFITM3) is expressed at relatively high levels at primitive streak region, and marks the stem/progenitor cell pool for the allantois ([139](#)). Future work will help determine how GCN5 regulates the interferon-signaling pathway during early development.

8.5 Concluding remarks and perspectives

In summary, our study identified a novel role of an epigenetic factor, GCN5, in regulating FGF signaling pathways, particularly through ERK and p38 activation, in early differentiating embryoid bodies that are equivalent to the embryonic stage leading to gastrulation *in vivo*. This work built up on our previous discovery of an essential requirement of *Gcn5* for embryonic survival shortly after gastrulation, presented multiple points of action of GCN5 within the FGF signaling pathway, that are accomplished through transcription dependent and independent mechanisms.

This work also brings forth new areas to be investigated as discussed in the above chapter. For instance, how is FGF signaling pathway modulated by GCN5, if GCN5-mediated H3K9ac is not a major regulatory event in the expression of multiple genes within the pathway? What genes are directly bound by GCN5 at early differentiation stage, and what TFs recruit GCN5 to its targets, other than MYC family TFs? Another important area that needs more investigation is that how GCN5 is distributed between SAGA and ATAC in gene regulation during early differentiation, and further, how are GCN5 and PCAF differentially required for the early differentiation processes? And finally, in addition to its co-activator role in gene regulation, does GCN5 repress gene transcription during early differentiation, and if yes, is such repressive role unique to the developmental context or also applicable to terminally differentiated somatic cells? Answers to these questions will expand the roles of GCN5 in more specific, intercalated developmental processes. As the full functions of GCN5 unveil, they will inspire in-depth research to add more epigenetic regulators to the blueprint of developmental pathways.

Since many human diseases thrive on deregulation of signaling pathways essential for development, understanding fully how these pathways function in physiological contexts will allow us to identify and alleviate or correct

deregulated components/processes in pathological conditions, eventually equip us to win the battles against those diseases.

APPENDIXES

Appendix 1 List of genes with altered expression levels upon *Gcn5* loss in day 5 EBs identified by RNAseq (FDR 0.05, FC2)

Gene name	Normalized expression		Log2ratio	P-value	FDR
	<i>Gcn5</i> ^{fx/fx}	<i>Gcn5</i> ^{-/-}			
<i>Grb10</i>	22128.0674	216.1360	-6.6778	1.77E-72	3.23E-68
<i>Gm26709</i>	26.4121	0.6739	-5.2926	8.81E-05	1.81E-03
<i>Nccrp1</i>	33.3149	1.0622	-4.9710	2.00E-09	2.33E-07
<i>Zic4</i>	37.2170	2.2623	-4.0401	1.85E-03	1.91E-02
<i>Mirg</i>	97.1816	6.0881	-3.9966	6.05E-14	1.94E-11
<i>Gm26945</i>	14.4247	1.0622	-3.7634	9.73E-05	1.97E-03
<i>Rian</i>	1190.6757	87.9964	-3.7582	1.10E-07	7.26E-06
<i>Meg3</i>	155.5578	13.3514	-3.5424	4.09E-08	3.14E-06
<i>Tfap2e</i>	9.9507	0.8914	-3.4807	6.04E-03	4.48E-02
<i>Gm37899</i>	33.6802	3.1751	-3.4070	3.54E-05	8.64E-04
<i>Zic1</i>	990.8949	97.3476	-3.3475	5.60E-05	1.25E-03
<i>Accsl</i>	26.6962	2.6275	-3.3449	2.65E-05	6.79E-04
<i>Krt42</i>	22.5114	2.3420	-3.2649	5.96E-04	8.00E-03
<i>Nlrc4</i>	38.9378	4.0763	-3.2558	1.70E-04	3.06E-03
<i>Cdkn1c</i>	2457.2057	283.9797	-3.1132	5.97E-54	5.45E-50
<i>Tgm3</i>	16.4238	1.9420	-3.0802	6.42E-03	4.66E-02

<i>Chrna9</i>	19.4325	2.3420	-3.0527	7.85E-04	9.86E-03
<i>Aox3</i>	19.6486	2.5479	-2.9471	5.94E-03	4.42E-02
<i>H19</i>	4233.7052	568.4079	-2.8969	3.26E-04	5.10E-03
<i>Gm26793</i>	31.2848	4.2373	-2.8842	2.28E-04	3.85E-03
<i>Tril</i>	399.3314	54.8963	-2.8628	5.33E-03	4.10E-02
<i>Hrh3</i>	18.8222	2.8099	-2.7438	9.07E-05	1.85E-03
<i>Fgf15</i>	1205.6433	180.9974	-2.7358	4.89E-07	2.53E-05
<i>Pax5</i>	198.2041	31.2130	-2.6668	1.26E-14	4.91E-12
<i>Timp4</i>	60.6949	9.7428	-2.6392	4.56E-06	1.63E-04
<i>Crisp1</i>	26.9425	4.3520	-2.6301	1.15E-03	1.33E-02
<i>Irs4</i>	460.6010	74.7667	-2.6230	1.16E-04	2.27E-03
<i>Vtn</i>	71.7713	11.7078	-2.6159	1.54E-03	1.66E-02
<i>1700097N02Rik</i>	64.4900	10.6577	-2.5972	1.03E-05	3.14E-04
<i>A730089K16Rik</i>	48.3558	8.0765	-2.5819	1.47E-05	4.18E-04
<i>Gli1</i>	139.7209	24.0668	-2.5374	2.36E-07	1.36E-05
<i>Rspo3</i>	67.4786	12.1410	-2.4745	1.37E-06	5.90E-05
<i>Aoah</i>	68.1841	12.8017	-2.4131	2.47E-05	6.40E-04
<i>Cp</i>	220.3961	42.9131	-2.3606	2.57E-04	4.20E-03
<i>Nr0b1</i>	329.1974	64.8138	-2.3446	8.58E-04	1.06E-02
<i>Lonrf2</i>	314.2172	63.4280	-2.3086	4.72E-07	2.47E-05
<i>Pcdh8</i>	898.8077	182.0427	-2.3037	3.67E-03	3.12E-02

<i>Foxd3</i>	108.3497	23.0282	-2.2342	1.21E-03	1.38E-02
<i>Ndp</i>	48.6021	10.6105	-2.1955	1.49E-03	1.62E-02
<i>Ism1</i>	103.6340	23.2081	-2.1588	3.16E-08	2.52E-06
<i>4930519F16Rik</i>	28.4236	6.3969	-2.1517	6.59E-04	8.69E-03
<i>Etv4</i>	287.3084	66.9886	-2.1006	1.85E-07	1.12E-05
<i>Sytl2</i>	157.4214	37.1883	-2.0817	4.70E-03	3.73E-02
<i>Car14</i>	552.6317	132.7884	-2.0572	2.89E-07	1.63E-05
<i>Rassf9</i>	31.1592	7.7078	-2.0153	2.27E-03	2.19E-02
<i>Tdh</i>	2292.4677	567.6737	-2.0138	1.17E-05	3.46E-04
<i>Grrp1</i>	49.1450	12.6906	-1.9533	3.77E-04	5.68E-03
<i>Plip</i>	17.3060	4.5461	-1.9286	1.51E-03	1.64E-02
<i>Wfikkn1</i>	113.2081	30.5876	-1.8880	5.11E-07	2.60E-05
<i>Klhl14</i>	26.7804	7.3114	-1.8730	6.17E-03	4.55E-02
<i>Sfrp2</i>	6661.6870	1818.9214	-1.8728	1.65E-04	2.99E-03
<i>Gm7325</i>	120.9587	33.0427	-1.8721	6.93E-09	7.04E-07
<i>A730017C20Rik</i>	65.5780	18.0253	-1.8632	4.94E-04	6.95E-03
<i>Gm6792</i>	47.9732	13.2501	-1.8562	1.93E-04	3.37E-03
<i>Ajap1</i>	188.1074	52.2570	-1.8479	5.19E-09	5.51E-07
<i>Scube3</i>	852.2563	238.6717	-1.8363	2.81E-04	4.50E-03
<i>Msx2</i>	162.7654	46.0763	-1.8207	7.13E-08	4.97E-06
<i>Nkx1-2</i>	145.2421	41.2793	-1.8150	1.80E-03	1.87E-02

<i>Lgr5</i>	67.3983	19.6001	-1.7819	2.74E-04	4.42E-03
<i>Cyp26b1</i>	1217.3294	357.7910	-1.7665	1.37E-03	1.52E-02
<i>Enox1</i>	390.1685	114.7678	-1.7654	3.18E-03	2.80E-02
<i>Slc8a1</i>	393.8127	116.7655	-1.7539	8.98E-05	1.84E-03
<i>Myc</i>	375.7351	111.8573	-1.7481	4.47E-06	1.60E-04
<i>Tcerg1l</i>	40.1714	12.0497	-1.7372	1.17E-04	2.29E-03
<i>Tdgf1</i>	2619.9410	788.2355	-1.7328	1.54E-03	1.66E-02
<i>Dkk1</i>	165.1393	49.7782	-1.7301	2.11E-06	8.56E-05
<i>Tcl1</i>	120.4452	36.6087	-1.7181	2.36E-04	3.92E-03
<i>Tmem132c</i>	1185.8459	363.6488	-1.7053	1.41E-13	4.16E-11
<i>Slc44a5</i>	559.7664	172.0509	-1.7020	2.14E-08	1.82E-06
<i>Mab21l2</i>	73.1490	22.6736	-1.6898	4.56E-04	6.52E-03
<i>Spred3</i>	449.0330	139.5566	-1.6860	1.04E-06	4.65E-05
<i>Pdzd4</i>	1000.2840	310.9493	-1.6857	2.33E-06	9.22E-05
<i>Hmga2</i>	3485.0433	1096.4454	-1.6683	1.36E-34	4.15E-31
<i>Platr10</i>	394.8537	124.5546	-1.6645	2.83E-03	2.58E-02
<i>Phlda2</i>	267.5180	84.6624	-1.6598	2.63E-12	6.09E-10
<i>Cdh11</i>	843.0047	267.8497	-1.6541	3.28E-03	2.87E-02
<i>Rprm</i>	609.4064	198.1424	-1.6209	2.32E-03	2.23E-02
<i>Wnt3a</i>	366.1002	119.3479	-1.6171	2.51E-03	2.37E-02
<i>Kirrel3</i>	122.9077	40.3085	-1.6084	2.44E-05	6.36E-04

<i>Sdc3</i>	413.7918	135.8707	-1.6067	2.21E-05	5.87E-04
<i>Nsg1</i>	742.2702	245.6103	-1.5956	9.00E-04	1.10E-02
<i>Mylk</i>	994.7025	331.8835	-1.5836	4.81E-04	6.80E-03
<i>Tspan7</i>	710.8583	241.4018	-1.5581	8.37E-04	1.04E-02
<i>Fam184b</i>	26.7121	9.1037	-1.5530	4.49E-03	3.60E-02
<i>Nr4a3</i>	121.8141	41.5743	-1.5509	2.76E-03	2.54E-02
<i>Dpysl5</i>	1903.2606	650.2402	-1.5494	1.70E-06	7.16E-05
<i>Ckb</i>	3284.3390	1124.9350	-1.5458	4.06E-03	3.35E-02
<i>Epha2</i>	1322.7012	453.0738	-1.5457	4.56E-07	2.40E-05
<i>Frem1</i>	399.3119	136.9355	-1.5440	2.46E-05	6.39E-04
<i>Slit2</i>	725.9245	250.0231	-1.5378	5.35E-07	2.69E-05
<i>Mfsd2a</i>	129.9173	44.9747	-1.5304	3.94E-04	5.86E-03
<i>Trh</i>	4207.8256	1458.4873	-1.5286	6.75E-10	9.28E-08
<i>Lypd1</i>	36.8998	12.7932	-1.5282	3.28E-03	2.87E-02
<i>Adamts20</i>	61.6139	21.6681	-1.5077	4.66E-04	6.63E-03
<i>Fgf3</i>	146.6152	51.7094	-1.5035	3.58E-06	1.34E-04
<i>Fgf4</i>	781.2407	276.4722	-1.4986	6.19E-03	4.55E-02
<i>Mfsd7b</i>	638.1105	226.4205	-1.4948	1.69E-18	1.24E-15
<i>Vcan</i>	2020.1769	717.4804	-1.4935	1.61E-20	1.40E-17
<i>Mcf2</i>	486.4079	172.9397	-1.4919	1.61E-05	4.51E-04
<i>Ptch2</i>	150.0112	54.3304	-1.4652	2.34E-09	2.69E-07

<i>Zfp819</i>	137.8092	49.9740	-1.4634	3.17E-06	1.20E-04
<i>Fndc3c1</i>	2829.4600	1027.3070	-1.4617	5.93E-22	5.70E-19
<i>Spry4</i>	339.6938	124.0294	-1.4536	2.66E-04	4.31E-03
<i>Calcoco2</i>	166.7671	60.9530	-1.4521	1.77E-04	3.15E-03
<i>Tmem40</i>	51.5239	18.8721	-1.4490	6.05E-04	8.08E-03
<i>Col2a1</i>	6973.2614	2555.8359	-1.4480	8.02E-10	1.07E-07
<i>Fgf17</i>	111.8676	41.0625	-1.4459	1.21E-04	2.34E-03
<i>Gareml</i>	188.4349	69.2764	-1.4436	1.63E-03	1.73E-02
<i>Kirrel2</i>	25.2922	9.3194	-1.4404	3.57E-03	3.06E-02
<i>Kat2a</i>	2207.4250	817.0114	-1.4339	1.42E-25	2.35E-22
<i>Foxa2</i>	228.7116	84.9930	-1.4281	3.70E-04	5.62E-03
<i>Etv5</i>	3291.7605	1226.4589	-1.4244	8.09E-06	2.60E-04
<i>Hsd17b14</i>	45.4036	17.2019	-1.4002	3.02E-03	2.71E-02
<i>Pde8b</i>	40.7985	15.5820	-1.3886	2.20E-03	2.15E-02
<i>Klf15</i>	167.0599	64.3376	-1.3766	2.00E-07	1.18E-05
<i>Fgd3</i>	63.3471	24.4427	-1.3739	5.44E-03	4.15E-02
<i>Nedd9</i>	783.3409	304.5100	-1.3632	2.72E-04	4.39E-03
<i>Plch1</i>	3921.6363	1532.1270	-1.3559	1.47E-10	2.33E-08
<i>Ccdc96</i>	89.2425	35.2148	-1.3415	6.57E-04	8.67E-03
<i>Sep1</i>	244.8066	96.8499	-1.3378	1.83E-03	1.89E-02
<i>Stmn2</i>	1208.6429	480.9150	-1.3295	7.69E-15	3.12E-12

<i>Rarb</i>	134.1129	53.3687	-1.3294	5.59E-04	7.61E-03
<i>Plxnc1</i>	315.5200	125.7499	-1.3272	2.87E-05	7.23E-04
<i>Trim67</i>	98.6861	39.4710	-1.3221	6.19E-03	4.55E-02
<i>A830082K12Rik</i>	97.9611	39.3184	-1.3170	1.49E-03	1.62E-02
<i>Scube1</i>	830.8794	334.3613	-1.3132	5.66E-04	7.68E-03
<i>Esrrb</i>	1188.7064	479.3134	-1.3104	1.42E-05	4.08E-04
<i>Ctnnd2</i>	491.2564	198.6209	-1.3065	1.25E-04	2.41E-03
<i>Nodal</i>	562.6321	227.4994	-1.3063	2.93E-07	1.64E-05
<i>Ncald</i>	480.5016	194.3429	-1.3059	1.73E-03	1.82E-02
<i>Emilin2</i>	1133.1554	459.8020	-1.3013	1.99E-03	2.01E-02
<i>Dppa2</i>	330.0419	134.3557	-1.2966	8.71E-06	2.74E-04
<i>Lrp3</i>	951.1686	387.2976	-1.2963	4.28E-08	3.27E-06
<i>Spry2</i>	2668.9097	1089.7856	-1.2922	4.51E-14	1.47E-11
<i>C77370</i>	290.6548	119.6264	-1.2808	2.05E-03	2.04E-02
<i>Hsd11b2</i>	142.9096	59.2543	-1.2701	4.26E-05	1.00E-03
<i>Adamts1</i>	384.3574	159.6061	-1.2679	3.61E-10	5.35E-08
<i>Nmnat2</i>	264.8970	110.5387	-1.2609	1.87E-03	1.93E-02
<i>Trabd2b</i>	99.0198	41.7142	-1.2472	4.37E-04	6.32E-03
<i>Ccno</i>	34.3156	14.4731	-1.2455	2.18E-03	2.13E-02
<i>Adgrv1</i>	2773.3252	1173.3112	-1.2410	3.07E-05	7.67E-04
<i>Plxna2</i>	1815.4866	768.4387	-1.2404	4.55E-04	6.52E-03

<i>Il17rd</i>	4567.8114	1937.7115	-1.2371	3.15E-03	2.79E-02
<i>Megf6</i>	1655.8588	702.7732	-1.2364	1.51E-08	1.40E-06
<i>Mapk11</i>	466.1863	198.0744	-1.2349	1.14E-04	2.25E-03
<i>Slc6a15</i>	264.1292	112.3220	-1.2336	4.10E-06	1.49E-04
<i>Dppa5a</i>	3806.0278	1622.5131	-1.2301	3.77E-08	2.92E-06
<i>Ass1</i>	1103.2782	476.0740	-1.2125	6.61E-06	2.17E-04
<i>Rpl34-ps2</i>	43.5779	18.8813	-1.2066	4.98E-03	3.90E-02
<i>Slc4a5</i>	128.7386	55.9204	-1.2030	2.18E-04	3.73E-03
<i>Slc28a1</i>	105.6846	45.9183	-1.2026	9.56E-04	1.16E-02
<i>Cdh2</i>	4676.2733	2033.2732	-1.2016	6.10E-04	8.13E-03
<i>Gm4430</i>	97.6676	42.4873	-1.2008	2.21E-04	3.78E-03
<i>Sema3d</i>	86.1518	37.5429	-1.1983	1.47E-03	1.60E-02
<i>Vegfc</i>	205.8726	90.0057	-1.1937	6.10E-06	2.03E-04
<i>Mest</i>	29226.9679	12785.5010	-1.1928	4.70E-05	1.09E-03
<i>Zik1</i>	960.5538	420.8368	-1.1906	3.19E-06	1.20E-04
<i>Nr2f1</i>	1213.0883	532.0365	-1.1891	7.60E-05	1.61E-03
<i>Cbs</i>	89.5502	39.3006	-1.1881	1.53E-03	1.66E-02
<i>Snora26</i>	66.4027	29.1506	-1.1877	5.96E-04	8.00E-03
<i>Scube2</i>	309.7533	136.2751	-1.1846	2.38E-03	2.27E-02
<i>Agpat3</i>	1116.3188	491.3896	-1.1838	1.44E-07	9.09E-06
<i>Fam78b</i>	139.7806	61.6117	-1.1819	1.86E-04	3.29E-03

<i>H13</i>	1428.7179	629.8178	-1.1817	1.19E-16	6.21E-14
<i>Gm3531</i>	82.7837	36.6229	-1.1766	4.11E-04	6.07E-03
<i>Bcl2</i>	394.6888	174.7148	-1.1757	5.66E-07	2.81E-05
<i>Crb2</i>	1217.8694	540.1290	-1.1730	3.25E-14	1.12E-11
<i>Cdh6</i>	800.8449	356.6617	-1.1670	1.02E-03	1.21E-02
<i>Rex2</i>	447.0485	199.1438	-1.1666	9.84E-04	1.18E-02
<i>Irs1</i>	1693.7849	756.3541	-1.1631	6.50E-16	3.04E-13
<i>Slco3a1</i>	180.5684	80.6976	-1.1619	1.57E-04	2.88E-03
<i>Zfp459</i>	357.6479	160.2568	-1.1582	5.47E-04	7.47E-03
<i>Fabp5</i>	1746.0709	785.5523	-1.1523	1.87E-08	1.63E-06
<i>Exoc3l</i>	63.4773	28.6108	-1.1497	1.27E-03	1.43E-02
<i>Twist1</i>	76.3181	34.4054	-1.1494	7.62E-04	9.68E-03
<i>Etv1</i>	407.1285	183.6976	-1.1482	3.11E-08	2.50E-06
<i>P3h2</i>	337.6349	153.2041	-1.1400	1.34E-07	8.56E-06
<i>Gm37065</i>	75.2258	34.1552	-1.1391	2.78E-04	4.47E-03
<i>Zfp600</i>	403.0853	183.2855	-1.1370	7.81E-04	9.82E-03
<i>Zfp296</i>	115.6875	52.6626	-1.1354	2.12E-03	2.09E-02
<i>Adamts6</i>	160.7424	73.2262	-1.1343	3.57E-05	8.67E-04
<i>Aldh1l2</i>	136.0960	62.1846	-1.1300	4.23E-04	6.19E-03
<i>Gm13461</i>	81.9653	37.4674	-1.1294	6.37E-04	8.44E-03
<i>Igf2r</i>	9292.7014	4260.7296	-1.1250	8.24E-20	6.27E-17

<i>Lrmp</i>	59.1559	27.1290	-1.1247	2.13E-03	2.10E-02
<i>Tshz3</i>	228.6931	105.1169	-1.1214	2.22E-03	2.16E-02
<i>Megf9</i>	906.7817	416.8409	-1.1213	3.50E-04	5.39E-03
<i>Amer2</i>	103.7563	47.7130	-1.1207	2.41E-03	2.29E-02
<i>Gm13225</i>	238.3780	109.7908	-1.1185	1.02E-03	1.21E-02
<i>Sfxn2</i>	331.3617	152.8832	-1.1160	5.91E-09	6.17E-07
<i>Al504432</i>	72.4162	33.5019	-1.1121	1.89E-03	1.94E-02
<i>Lrrc17</i>	1079.8847	499.6516	-1.1119	2.66E-04	4.32E-03
<i>Siglec1</i>	84.4393	39.1476	-1.1090	2.39E-03	2.28E-02
<i>Cachd1</i>	2012.8475	937.0510	-1.1030	1.89E-16	9.59E-14
<i>Rab11fip5</i>	489.5926	227.9935	-1.1026	3.73E-03	3.16E-02
<i>Tst</i>	110.3775	51.6380	-1.0959	5.63E-05	1.26E-03
<i>Gpa33</i>	169.9918	79.6341	-1.0940	1.19E-04	2.31E-03
<i>Wnt3</i>	85.4388	40.0858	-1.0918	3.37E-04	5.23E-03
<i>Zhx2</i>	431.6440	202.7086	-1.0904	3.08E-08	2.49E-06
<i>Spry1</i>	887.9858	417.4841	-1.0888	1.48E-11	2.79E-09
<i>Slc7a3</i>	1334.5146	627.8050	-1.0879	1.12E-03	1.30E-02
<i>Dnajc6</i>	235.6596	111.0981	-1.0849	1.37E-03	1.52E-02
<i>Otx2</i>	624.1963	294.4326	-1.0841	1.27E-04	2.43E-03
<i>Bcat1</i>	3085.0929	1456.8619	-1.0824	2.45E-05	6.37E-04
<i>Apcdd1</i>	404.4224	191.3827	-1.0794	9.28E-08	6.28E-06

<i>Mppe1</i>	93.7328	44.4242	-1.0772	2.55E-03	2.40E-02
<i>Sp8</i>	1271.3243	602.7558	-1.0767	2.15E-03	2.11E-02
<i>Gldc</i>	5076.5395	2409.8249	-1.0749	1.95E-17	1.19E-14
<i>Tfcp2l1</i>	1532.2853	731.1865	-1.0674	2.94E-03	2.65E-02
<i>Ooep</i>	194.0437	92.8414	-1.0635	6.20E-04	8.24E-03
<i>Pcsk5</i>	146.5803	70.1366	-1.0635	4.16E-04	6.11E-03
<i>Fam167a</i>	175.8964	84.2116	-1.0626	1.72E-04	3.09E-03
<i>Hipk2</i>	1233.9159	591.0208	-1.0620	8.38E-06	2.67E-04
<i>Gm6180</i>	60.5278	29.0223	-1.0604	4.33E-03	3.51E-02
<i>Gm13154</i>	450.9449	216.4462	-1.0589	2.53E-03	2.38E-02
<i>Trim2</i>	1909.2769	916.4267	-1.0589	3.89E-14	1.32E-11
<i>Pou5f1</i>	3780.2337	1819.8995	-1.0546	1.53E-03	1.65E-02
<i>Cerk</i>	431.0249	207.6804	-1.0534	5.34E-04	7.35E-03
<i>Fut9</i>	568.2209	273.9605	-1.0525	1.61E-07	9.91E-06
<i>2610318N02Rik</i>	693.0175	334.5087	-1.0508	1.44E-10	2.30E-08
<i>Sep3</i>	1148.5513	555.8546	-1.0470	2.13E-03	2.10E-02
<i>Dgat2</i>	292.5788	141.7787	-1.0452	4.85E-07	2.51E-05
<i>Ppp4r4</i>	180.9182	87.6996	-1.0447	4.35E-04	6.30E-03
<i>Pkdcc</i>	1831.2646	888.8444	-1.0428	2.30E-06	9.14E-05
<i>Fgf5</i>	223.8867	108.7134	-1.0422	3.04E-03	2.72E-02
<i>Pkia</i>	690.2532	335.3060	-1.0416	1.94E-06	7.96E-05

<i>Rgs2</i>	488.7387	237.8183	-1.0392	1.48E-03	1.61E-02
<i>Sparcl1</i>	161.7817	78.8366	-1.0371	6.34E-04	8.41E-03
<i>Rps6ka2</i>	1601.7214	783.2298	-1.0321	2.27E-14	8.11E-12
<i>Phf2</i>	625.8573	306.3095	-1.0308	7.33E-04	9.42E-03
<i>Tmem229a</i>	97.5618	48.1562	-1.0186	1.44E-03	1.57E-02
<i>Lad1</i>	262.5589	129.7457	-1.0170	4.34E-05	1.02E-03
<i>Map6</i>	366.1999	181.9378	-1.0092	1.32E-03	1.48E-02
<i>Myb</i>	232.8799	115.8400	-1.0075	2.84E-03	2.59E-02
<i>BC064078</i>	149.5282	74.4598	-1.0059	4.14E-03	3.40E-02
<i>Adgrl3</i>	380.9406	189.7584	-1.0054	3.51E-03	3.02E-02
<i>Adamts7</i>	462.6814	230.5014	-1.0052	9.37E-05	1.91E-03
<i>Mthfd2</i>	1197.3426	597.1456	-1.0037	1.50E-03	1.63E-02
<i>Vash2</i>	811.2325	405.2200	-1.0014	5.41E-10	7.72E-08
<i>Prob1</i>	131.0078	262.2272	1.0012	1.36E-04	2.57E-03
<i>Hpn</i>	111.9873	224.2406	1.0017	1.68E-07	1.03E-05
<i>Pld6</i>	58.1154	116.5129	1.0035	3.47E-05	8.51E-04
<i>Shisa8</i>	68.5369	137.5728	1.0052	2.74E-06	1.06E-04
<i>Sgce</i>	583.6004	1172.0925	1.0060	1.12E-09	1.42E-07
<i>Fam161a</i>	43.4289	87.2430	1.0064	1.08E-03	1.27E-02
<i>Calr3</i>	46.3571	93.3138	1.0093	1.02E-03	1.21E-02
<i>Jag2</i>	320.7101	646.2447	1.0108	6.75E-10	9.28E-08

<i>Ypel2</i>	176.1140	355.2591	1.0124	1.71E-07	1.05E-05
<i>Trim21</i>	282.8989	571.2565	1.0139	1.42E-05	4.08E-04
<i>Ankrd37</i>	69.8897	141.2213	1.0148	6.06E-04	8.09E-03
<i>Tnik</i>	124.9679	253.0258	1.0177	1.36E-05	3.94E-04
<i>Gatm</i>	189.9437	384.8729	1.0188	5.10E-08	3.79E-06
<i>Fbxl8</i>	37.6645	76.5067	1.0224	4.42E-03	3.56E-02
<i>Gm43597</i>	74.1591	150.7637	1.0236	8.08E-05	1.70E-03
<i>Phldb3</i>	43.4643	88.3856	1.0240	2.01E-03	2.02E-02
<i>Psme1</i>	1561.8508	3176.3498	1.0241	1.33E-08	1.27E-06
<i>Tmem220</i>	31.4002	63.8606	1.0242	6.06E-03	4.49E-02
<i>Synpo</i>	75.1128	152.9660	1.0261	9.24E-04	1.12E-02
<i>Car12</i>	119.7580	243.9981	1.0267	8.26E-07	3.85E-05
<i>Cbx4</i>	163.3112	332.8440	1.0272	1.33E-05	3.85E-04
<i>Chpt1</i>	481.2397	982.2217	1.0293	7.64E-12	1.62E-09
<i>Hrc</i>	158.7639	324.5373	1.0315	4.14E-03	3.40E-02
<i>Parp9</i>	483.9018	989.7124	1.0323	2.05E-06	8.37E-05
<i>Rrad</i>	116.4774	238.5323	1.0341	5.19E-04	7.22E-03
<i>Zfp750</i>	33.2537	68.1665	1.0355	3.14E-03	2.78E-02
<i>Neur11b</i>	42.0078	86.1619	1.0364	4.88E-04	6.89E-03
<i>Ttc25</i>	49.3097	101.3803	1.0398	2.07E-03	2.06E-02
<i>Cyb5d2</i>	132.6106	272.8612	1.0410	8.01E-07	3.75E-05

<i>Ets1</i>	895.9082	1843.8147	1.0413	3.23E-07	1.77E-05
<i>Kat2b</i>	851.1111	1754.2415	1.0434	1.24E-14	4.91E-12
<i>Nab1</i>	440.1994	907.8816	1.0443	1.64E-04	2.99E-03
<i>Brdt</i>	44.8196	92.5631	1.0463	1.92E-03	1.96E-02
<i>D330045A20Rik</i>	104.5146	216.3352	1.0496	3.81E-04	5.73E-03
<i>Ampd3</i>	36.0659	74.7922	1.0523	2.38E-04	3.96E-03
<i>Slc13a4</i>	109.5769	227.5871	1.0545	5.09E-04	7.13E-03
<i>Egflam</i>	177.9292	369.5558	1.0545	5.92E-05	1.31E-03
<i>Mme11</i>	23.9390	49.8124	1.0571	3.12E-03	2.78E-02
<i>Kcnab3</i>	34.3806	71.7704	1.0618	1.17E-03	1.34E-02
<i>Pde11a</i>	32.8473	68.6360	1.0632	1.94E-03	1.97E-02
<i>Crym</i>	39.5045	82.5515	1.0633	3.91E-04	5.84E-03
<i>2810408A11Rik</i>	220.7593	462.0095	1.0654	1.23E-03	1.40E-02
<i>Gca</i>	104.0192	217.7193	1.0656	5.21E-07	2.63E-05
<i>Amigo2</i>	131.6653	275.6869	1.0662	5.57E-05	1.25E-03
<i>Taf7l</i>	29.8063	62.5464	1.0693	5.79E-03	4.35E-02
<i>Il33</i>	34.5568	72.5394	1.0698	2.78E-03	2.55E-02
<i>Efhc1</i>	41.5037	87.1288	1.0699	1.70E-03	1.79E-02
<i>Slc16a3</i>	2393.9230	5029.7354	1.0711	8.82E-18	6.19E-15
<i>Gm11423</i>	29.4688	61.9261	1.0714	6.79E-03	4.86E-02
<i>Slc16a4</i>	40.3450	84.8765	1.0730	5.61E-03	4.24E-02

<i>Atp2a3</i>	154.0728	324.4829	1.0745	9.73E-09	9.66E-07
<i>Flt4</i>	101.1528	213.2430	1.0760	3.94E-06	1.45E-04
<i>P4ha1</i>	1339.7264	2829.2422	1.0785	1.48E-04	2.77E-03
<i>Mtl5</i>	41.1533	86.9896	1.0798	3.27E-03	2.87E-02
<i>Gpr20</i>	36.3525	76.8850	1.0806	3.05E-04	4.82E-03
<i>P3h4</i>	432.3480	915.4230	1.0822	8.84E-08	6.00E-06
<i>Dkk3</i>	309.3824	655.4901	1.0832	8.46E-05	1.75E-03
<i>Slc50a1</i>	169.6146	359.4506	1.0835	2.45E-08	2.03E-06
<i>Cyb561</i>	235.0551	498.6183	1.0849	7.13E-11	1.19E-08
<i>Inf2</i>	228.5933	486.2688	1.0890	4.40E-04	6.35E-03
<i>Eps8l1</i>	132.4285	281.8443	1.0897	2.90E-04	4.63E-03
<i>Trap1a</i>	908.6037	1935.3587	1.0909	1.60E-08	1.45E-06
<i>Gngt2</i>	45.7121	97.5489	1.0935	1.25E-04	2.41E-03
<i>BC026585</i>	175.9901	376.5348	1.0973	1.46E-08	1.37E-06
<i>Nfatc2</i>	86.1391	184.4727	1.0987	2.06E-03	2.05E-02
<i>Lmntd2</i>	47.6173	102.1715	1.1014	3.02E-04	4.79E-03
<i>Gm12758</i>	36.9528	79.3143	1.1019	1.07E-03	1.26E-02
<i>Klhl10</i>	23.9768	51.5524	1.1044	5.28E-03	4.08E-02
<i>Myh3</i>	40.4427	86.9597	1.1045	1.65E-04	2.99E-03
<i>Sema3e</i>	962.8070	2070.4302	1.1046	1.32E-06	5.74E-05
<i>Chrnbl</i>	113.6280	244.6372	1.1063	7.48E-07	3.56E-05

<i>Nrg4</i>	23.9575	51.6091	1.1071	5.53E-04	7.54E-03
<i>Nr3c1</i>	231.0857	497.8996	1.1074	7.52E-12	1.62E-09
<i>Ezh1</i>	741.9629	1601.0540	1.1096	1.83E-09	2.18E-07
<i>4632428N05Rik</i>	59.3387	128.0653	1.1098	1.94E-03	1.97E-02
<i>Aifm2</i>	60.1259	130.0617	1.1131	1.71E-06	7.17E-05
<i>Adssl1</i>	241.7634	523.4435	1.1144	3.35E-04	5.21E-03
<i>Atg10</i>	96.2186	208.4947	1.1156	4.43E-06	1.59E-04
<i>Dmc1</i>	241.3049	523.7430	1.1180	4.23E-13	1.17E-10
<i>Pygl</i>	194.7303	422.8381	1.1186	3.13E-04	4.93E-03
<i>Adcy2</i>	84.0482	182.9711	1.1223	1.58E-05	4.44E-04
<i>Cox7a1</i>	55.9473	121.8228	1.1226	2.77E-05	7.07E-04
<i>Gstm6</i>	100.8593	219.6616	1.1229	1.98E-06	8.11E-05
<i>Des</i>	552.9723	1207.0696	1.1262	2.14E-04	3.68E-03
<i>Lgals9</i>	33.7515	73.6967	1.1266	2.98E-03	2.68E-02
<i>Syne1</i>	129.1445	283.1264	1.1325	1.25E-07	8.11E-06
<i>Padi3</i>	57.3445	125.8573	1.1341	5.10E-06	1.76E-04
<i>Rras</i>	201.3204	442.7093	1.1369	3.46E-08	2.73E-06
<i>Galnt12</i>	149.9222	329.7356	1.1371	1.62E-08	1.45E-06
<i>Cyp4f13</i>	173.5500	382.1771	1.1389	4.68E-09	5.03E-07
<i>Platr14</i>	233.5314	514.5256	1.1396	1.64E-09	1.98E-07
<i>Aifm3</i>	88.4641	194.9165	1.1397	1.11E-08	1.08E-06

<i>Rapgef5</i>	431.7828	951.6675	1.1402	1.36E-14	5.17E-12
<i>Igfbp4</i>	1712.9685	3783.8160	1.1433	8.13E-05	1.70E-03
<i>Neat1</i>	444.9396	983.4956	1.1443	4.06E-04	6.02E-03
<i>1810011O10Rik</i>	101.4409	224.4117	1.1455	5.40E-03	4.12E-02
<i>Nmi</i>	111.3087	246.4445	1.1467	1.25E-04	2.41E-03
<i>Oas1c</i>	53.3562	118.2923	1.1486	7.13E-05	1.53E-03
<i>Stat5a</i>	152.6822	338.5577	1.1489	5.50E-09	5.80E-07
<i>Shox2</i>	36.7677	81.5896	1.1499	4.81E-03	3.80E-02
<i>Psmb10</i>	537.7742	1193.9891	1.1507	2.12E-04	3.65E-03
<i>Rassf6</i>	36.5446	81.1553	1.1510	2.93E-04	4.68E-03
<i>Elmo3</i>	151.9440	338.2652	1.1546	6.77E-09	6.94E-07
<i>Rbm44</i>	292.7688	652.4125	1.1560	1.85E-09	2.18E-07
<i>Myo1h</i>	16.2671	36.2660	1.1567	4.33E-03	3.51E-02
<i>Susd2</i>	76.5772	170.8675	1.1579	1.02E-04	2.05E-03
<i>Adgre5</i>	124.5779	278.1937	1.1590	1.51E-08	1.40E-06
<i>Plekhd1</i>	30.0761	67.3210	1.1624	1.23E-04	2.37E-03
<i>Cep112</i>	82.4597	184.7758	1.1640	5.45E-04	7.46E-03
<i>Thra</i>	754.1833	1690.5729	1.1645	2.51E-16	1.24E-13
<i>Pde4b</i>	285.0702	639.5426	1.1657	1.10E-11	2.16E-09
<i>Carns1</i>	28.6357	64.3534	1.1682	4.06E-03	3.35E-02
<i>Anxa2</i>	1117.3788	2512.3936	1.1689	5.17E-07	2.62E-05

<i>Ybx2</i>	45.5383	102.4967	1.1704	8.75E-06	2.75E-04
<i>Cyp2j9</i>	20.9745	47.3032	1.1733	6.78E-03	4.86E-02
<i>Dhx58</i>	19.8504	44.8123	1.1747	2.80E-03	2.56E-02
<i>Zrsr1</i>	235.4355	532.1963	1.1766	1.17E-11	2.28E-09
<i>Sec11c</i>	180.1998	407.8163	1.1783	6.45E-10	9.04E-08
<i>Syne3</i>	83.4225	188.8382	1.1786	1.29E-03	1.45E-02
<i>Slc26a10</i>	44.6496	101.2329	1.1810	1.80E-04	3.20E-03
<i>Bik</i>	67.7784	153.9069	1.1832	2.66E-04	4.32E-03
<i>N4bp2l1</i>	37.9123	86.2993	1.1867	1.14E-04	2.24E-03
<i>Rbakdn</i>	13.6407	31.1952	1.1934	3.26E-03	2.86E-02
<i>Pde4a</i>	82.0765	187.8452	1.1945	1.93E-06	7.93E-05
<i>Plekhn1</i>	56.7969	130.2063	1.1969	1.57E-05	4.43E-04
<i>Faah</i>	46.7281	107.3610	1.2001	8.43E-07	3.92E-05
<i>Zcchc24</i>	267.6080	615.0488	1.2006	7.99E-07	3.75E-05
<i>Unc5a</i>	90.5073	208.0177	1.2006	1.01E-06	4.58E-05
<i>Sohlh2</i>	180.6396	415.3628	1.2013	3.75E-03	3.17E-02
<i>Dcxr</i>	307.2823	706.6574	1.2014	5.67E-13	1.48E-10
<i>Acsf2</i>	283.0399	651.7198	1.2032	3.92E-10	5.73E-08
<i>Igfbp3</i>	604.8068	1393.1117	1.2038	3.84E-05	9.20E-04
<i>C130074G19Rik</i>	85.8001	197.8819	1.2056	5.10E-04	7.14E-03
<i>Kank3</i>	355.0133	819.4889	1.2069	1.14E-06	5.05E-05

<i>Mr1</i>	42.7577	98.8170	1.2086	1.59E-03	1.70E-02
<i>Agbl2</i>	34.2427	79.2916	1.2114	4.28E-04	6.23E-03
<i>Bnip3</i>	1226.1206	2843.0872	1.2134	1.49E-04	2.77E-03
<i>Bcas1</i>	17.1401	39.7514	1.2136	3.42E-03	2.96E-02
<i>Cacna1h</i>	191.4933	444.8348	1.2160	7.39E-10	9.92E-08
<i>Gm2a</i>	553.6214	1286.5082	1.2165	3.07E-09	3.44E-07
<i>Klc3</i>	297.8823	693.6161	1.2194	1.57E-09	1.91E-07
<i>Ngfr</i>	252.3736	588.2520	1.2209	2.22E-03	2.16E-02
<i>Kif19a</i>	54.9329	128.5452	1.2265	5.31E-03	4.09E-02
<i>Slc7a4</i>	77.7602	181.9865	1.2267	3.81E-07	2.05E-05
<i>Gnat2</i>	27.2693	63.9204	1.2290	7.76E-04	9.79E-03
<i>Lrrn4cl</i>	40.3331	94.5541	1.2292	2.26E-04	3.84E-03
<i>Lrrc51</i>	51.1807	120.0955	1.2305	1.51E-03	1.64E-02
<i>Rnf135</i>	125.9822	295.9356	1.2321	6.27E-09	6.47E-07
<i>Rel1</i>	778.6661	1829.2434	1.2322	9.03E-10	1.18E-07
<i>Ugt8a</i>	51.1276	120.1421	1.2326	2.67E-08	2.20E-06
<i>Trim12a</i>	125.8894	296.3314	1.2351	2.41E-09	2.75E-07
<i>Il13ra1</i>	98.9678	233.5487	1.2387	6.44E-08	4.58E-06
<i>Dhdh</i>	216.0011	511.1760	1.2428	9.74E-14	2.92E-11
<i>Prkca</i>	160.4162	380.3879	1.2457	1.57E-04	2.88E-03
<i>Cmpk2</i>	82.9617	196.7794	1.2461	1.61E-06	6.81E-05

<i>Trf</i>	19.4986	46.2611	1.2464	6.35E-03	4.63E-02
<i>Alpk1</i>	70.8724	168.9188	1.2530	4.25E-06	1.53E-04
<i>BC022960</i>	45.2550	107.9692	1.2545	2.39E-05	6.26E-04
<i>Podn</i>	24.3385	58.0786	1.2548	6.79E-03	4.86E-02
<i>Susd5</i>	24.6694	58.8698	1.2548	2.22E-04	3.78E-03
<i>Fbxo47</i>	36.2580	86.5247	1.2548	2.79E-05	7.09E-04
<i>Fam83b</i>	83.2569	198.9160	1.2565	1.54E-07	9.57E-06
<i>Pla2g16</i>	220.9291	530.2184	1.2630	1.96E-13	5.60E-11
<i>Sh2d5</i>	32.4518	77.8947	1.2632	1.93E-03	1.97E-02
<i>Fetub</i>	67.8254	162.8652	1.2638	2.63E-03	2.45E-02
<i>Ptpn18</i>	36.2862	87.1345	1.2638	1.01E-04	2.04E-03
<i>Ly6a</i>	98.0719	235.7541	1.2654	2.26E-06	9.02E-05
<i>Sfi1</i>	477.0708	1148.6086	1.2676	7.21E-04	9.30E-03
<i>Slc15a2</i>	107.7285	259.3998	1.2678	5.97E-04	8.02E-03
<i>Scarf1</i>	68.1303	164.6011	1.2726	5.05E-06	1.75E-04
<i>Myh7b</i>	21.6080	52.2482	1.2738	2.73E-04	4.41E-03
<i>C1qtnf4</i>	26.0488	62.9870	1.2738	1.84E-04	3.26E-03
<i>Rasgrp4</i>	159.0005	384.6757	1.2746	5.47E-13	1.47E-10
<i>Sez6</i>	92.9482	225.2304	1.2769	3.18E-04	5.00E-03
<i>Slc43a3</i>	295.0410	715.7006	1.2784	1.80E-14	6.73E-12
<i>Sec14l4</i>	45.2586	109.8199	1.2789	4.38E-05	1.03E-03

<i>Pgm2</i>	1152.3591	2798.4633	1.2800	3.19E-23	3.64E-20
<i>Socs1</i>	51.2319	124.5191	1.2813	6.45E-06	2.13E-04
<i>Lgals3bp</i>	36.3054	88.4206	1.2842	6.65E-04	8.75E-03
<i>Ddit4</i>	1403.6826	3422.7783	1.2860	1.61E-04	2.95E-03
<i>Tbxa2r</i>	12.1833	29.7663	1.2888	5.17E-03	4.01E-02
<i>Irs3</i>	19.8719	48.5891	1.2899	1.67E-03	1.77E-02
<i>Rab20</i>	69.6206	170.6238	1.2932	1.47E-07	9.22E-06
<i>Lrriq3</i>	20.8694	51.1522	1.2934	5.60E-03	4.24E-02
<i>Pear1</i>	23.5493	57.7537	1.2942	2.60E-03	2.43E-02
<i>Ddx4</i>	195.6295	480.9106	1.2976	2.14E-14	7.81E-12
<i>Ndufa4l2</i>	26.9131	66.2245	1.2991	1.27E-03	1.43E-02
<i>Art1</i>	17.5815	43.2702	1.2993	1.95E-03	1.98E-02
<i>Rapgef1</i>	59.4853	146.4776	1.3001	2.04E-04	3.53E-03
<i>Tm6sf1</i>	88.5548	218.1561	1.3007	1.42E-09	1.74E-07
<i>Acadvl</i>	846.8413	2087.9641	1.3019	5.40E-12	1.20E-09
<i>Baiap3</i>	46.4757	114.6325	1.3025	1.02E-05	3.14E-04
<i>Irf1</i>	929.1760	2295.5461	1.3048	3.82E-06	1.42E-04
<i>Oprd1</i>	20.0407	49.5717	1.3066	2.56E-03	2.40E-02
<i>Tmem176a</i>	99.5315	246.5251	1.3085	6.04E-07	2.94E-05
<i>Ccdc73</i>	42.6307	105.5973	1.3086	1.53E-06	6.52E-05
<i>Lmod1</i>	84.8749	210.7086	1.3118	7.91E-05	1.67E-03

<i>Crlf1</i>	11.1503	27.7114	1.3134	1.35E-03	1.50E-02
<i>Gmfg</i>	68.9871	171.6705	1.3152	1.68E-08	1.47E-06
<i>Mov10l1</i>	36.1944	90.1029	1.3158	4.92E-03	3.87E-02
<i>Gm11532</i>	18.1326	45.1757	1.3170	4.57E-03	3.66E-02
<i>Prkg2</i>	54.6984	136.3323	1.3176	1.17E-05	3.46E-04
<i>Aldh3a2</i>	1455.4729	3630.5007	1.3187	2.80E-10	4.30E-08
<i>Olfr1372-ps1</i>	32.7261	81.6800	1.3195	3.45E-05	8.49E-04
<i>Nfe2l3</i>	58.4043	146.1699	1.3235	1.99E-07	1.18E-05
<i>Nol4l</i>	399.9905	1001.3654	1.3239	5.87E-12	1.29E-09
<i>Kcp</i>	21.2631	53.3241	1.3264	2.61E-04	4.26E-03
<i>Procr</i>	42.8366	108.1258	1.3358	4.87E-06	1.71E-04
<i>Tmem173</i>	55.9971	141.3484	1.3358	3.51E-05	8.59E-04
<i>Stat3</i>	1315.7981	3322.1471	1.3362	1.24E-23	1.54E-20
<i>Gadd45b</i>	246.5319	624.3039	1.3405	1.63E-03	1.73E-02
<i>Sertad4</i>	238.3019	604.1226	1.3421	1.42E-08	1.35E-06
<i>Slfn5</i>	28.1643	71.4040	1.3421	4.59E-03	3.67E-02
<i>Stc1</i>	28.5793	72.6708	1.3464	3.74E-03	3.17E-02
<i>Clic5</i>	196.9318	500.7982	1.3465	7.96E-13	1.96E-10
<i>Lrp8os2</i>	115.7099	294.5424	1.3480	9.81E-06	3.03E-04
<i>Tnnt1</i>	194.4448	495.0678	1.3483	4.23E-04	6.19E-03
<i>1700029J07Rik</i>	25.5091	64.9543	1.3484	1.31E-03	1.47E-02

<i>Snhg14</i>	465.0178	1186.0800	1.3508	5.11E-17	2.92E-14
<i>Tubg2</i>	19.8013	50.5760	1.3529	1.38E-03	1.52E-02
<i>Ccdc155</i>	34.6269	88.5157	1.3540	1.34E-05	3.87E-04
<i>Trim7</i>	15.0719	38.5397	1.3545	1.82E-03	1.89E-02
<i>Mef2c</i>	136.5361	349.1658	1.3546	4.16E-09	4.53E-07
<i>Tex19.2</i>	23.0513	58.9574	1.3548	2.68E-03	2.49E-02
<i>Afap1l2</i>	296.4360	758.3341	1.3551	6.46E-04	8.54E-03
<i>Aebp1</i>	194.6547	498.8102	1.3576	3.32E-09	3.70E-07
<i>Coro2a</i>	119.0473	306.1414	1.3627	2.23E-12	5.29E-10
<i>Tap2</i>	100.9896	260.1466	1.3651	3.64E-04	5.55E-03
<i>Wdr93</i>	26.3734	68.0957	1.3685	5.28E-04	7.29E-03
<i>Tmem59l</i>	60.5859	156.5779	1.3698	1.33E-10	2.14E-08
<i>Parp10</i>	271.3902	702.7218	1.3726	7.99E-06	2.57E-04
<i>G0s2</i>	57.3950	148.8977	1.3753	2.92E-06	1.12E-04
<i>Tapbp</i>	1201.9029	3119.1896	1.3759	1.02E-11	2.03E-09
<i>Gstt3</i>	65.4622	169.9045	1.3760	2.68E-08	2.20E-06
<i>Tlcd2</i>	145.3326	379.8753	1.3862	7.26E-13	1.84E-10
<i>Tmod1</i>	22.0402	57.6148	1.3863	1.21E-03	1.38E-02
<i>Gramd1c</i>	64.1076	167.8579	1.3887	3.39E-07	1.85E-05
<i>C3</i>	8.8574	23.2102	1.3898	4.74E-03	3.76E-02
<i>Emp3</i>	40.1201	105.1875	1.3906	3.55E-05	8.64E-04

<i>AU022751</i>	22.6715	59.5751	1.3938	6.70E-04	8.79E-03
<i>Rec8</i>	634.8332	1670.7360	1.3960	8.88E-05	1.82E-03
<i>H2-T23</i>	68.1957	179.5453	1.3966	2.74E-06	1.06E-04
<i>Tex14</i>	297.1768	782.8015	1.3973	3.23E-15	1.37E-12
<i>Neurod1</i>	149.5025	395.2576	1.4026	6.22E-03	4.57E-02
<i>Echdc3</i>	39.0445	103.7143	1.4094	3.47E-05	8.52E-04
<i>Mlxipl</i>	15.9263	42.3211	1.4100	7.86E-04	9.86E-03
<i>Mycbpap</i>	51.8690	137.9226	1.4109	2.62E-03	2.44E-02
<i>CN725425</i>	41.1493	109.7996	1.4159	6.17E-08	4.42E-06
<i>BB218582</i>	17.8300	47.6122	1.4170	2.25E-03	2.18E-02
<i>Coch</i>	95.7929	255.8283	1.4172	1.98E-07	1.17E-05
<i>Cd68</i>	95.1475	254.3947	1.4188	3.02E-10	4.56E-08
<i>Guca1a</i>	14.1079	37.7434	1.4197	9.29E-04	1.13E-02
<i>A2m</i>	35.6867	95.7462	1.4238	1.33E-04	2.52E-03
<i>Gbp10</i>	23.1910	62.2583	1.4247	5.98E-04	8.02E-03
<i>Gm4779</i>	32.8596	88.2150	1.4247	2.33E-04	3.90E-03
<i>Smc1b</i>	138.1400	372.0931	1.4295	6.57E-08	4.65E-06
<i>Capn12</i>	13.3775	36.0642	1.4308	5.03E-03	3.92E-02
<i>Lrrc18</i>	23.5120	63.4640	1.4325	4.98E-04	7.00E-03
<i>Stx11</i>	22.1439	59.8078	1.4334	3.95E-04	5.87E-03
<i>Crim1</i>	673.4911	1827.8483	1.4404	1.11E-23	1.54E-20

<i>Dennd2d</i>	31.3768	85.3514	1.4437	4.18E-06	1.51E-04
<i>Pomc</i>	36.3267	98.8407	1.4441	6.83E-05	1.47E-03
<i>Plekhg1</i>	842.5648	2297.8430	1.4474	1.32E-24	2.01E-21
<i>Best1</i>	17.2363	47.1499	1.4518	1.34E-03	1.49E-02
<i>Fmo5</i>	18.9025	51.7318	1.4525	3.15E-03	2.79E-02
<i>Ctso</i>	69.3127	190.0267	1.4550	2.17E-07	1.27E-05
<i>Bin2</i>	73.4192	201.6352	1.4575	1.29E-12	3.13E-10
<i>Phyhip</i>	60.0957	165.6012	1.4624	4.43E-07	2.35E-05
<i>Psmb9</i>	38.3846	106.2119	1.4683	3.36E-06	1.26E-04
<i>Zmat1</i>	51.1781	142.0068	1.4724	1.30E-06	5.69E-05
<i>Gm807</i>	25.9127	72.0367	1.4751	2.25E-03	2.18E-02
<i>Gm11837</i>	11.6316	32.3721	1.4767	1.73E-03	1.82E-02
<i>Dlec1</i>	25.4386	70.8651	1.4781	5.48E-04	7.49E-03
<i>Nrk</i>	1371.8020	3841.5138	1.4856	6.12E-08	4.42E-06
<i>Airn</i>	38.5382	108.2488	1.4900	1.15E-04	2.26E-03
<i>Myo15</i>	8.6792	24.4667	1.4952	5.88E-03	4.40E-02
<i>Rdm1</i>	302.5323	853.5434	1.4964	1.97E-05	5.32E-04
<i>Fgl1</i>	30.4290	86.1578	1.5015	5.63E-05	1.26E-03
<i>Ppp1r3g</i>	10.8504	30.7368	1.5022	6.27E-03	4.59E-02
<i>H2-K1</i>	643.4523	1829.4098	1.5075	7.79E-29	1.78E-25
<i>Slc47a2</i>	9.2398	26.3309	1.5108	2.15E-03	2.11E-02

<i>Slc41a2</i>	15.8627	45.2684	1.5129	8.02E-05	1.69E-03
<i>Sowaha</i>	20.4636	58.5389	1.5163	8.56E-05	1.77E-03
<i>Fmnl1</i>	10.3123	29.5253	1.5176	1.27E-03	1.43E-02
<i>Cd74</i>	32.8159	93.9795	1.5180	2.13E-05	5.68E-04
<i>Tfr2</i>	10.9322	31.3568	1.5202	6.00E-04	8.03E-03
<i>Adamtsl4</i>	35.3812	101.4973	1.5204	1.70E-05	4.74E-04
<i>Ndrp1</i>	314.0184	905.2255	1.5274	7.50E-04	9.57E-03
<i>Espn</i>	77.2468	223.9492	1.5356	7.21E-12	1.57E-09
<i>Fgf11</i>	35.8035	103.9357	1.5375	1.61E-08	1.45E-06
<i>Egr1</i>	109.9002	319.9696	1.5417	1.30E-09	1.62E-07
<i>1810010H24Rik</i>	31.8293	93.0381	1.5475	3.15E-06	1.20E-04
<i>Sgcd</i>	23.2656	68.0467	1.5483	5.77E-03	4.35E-02
<i>Lrrc8e</i>	14.7978	43.3032	1.5491	1.56E-03	1.67E-02
<i>Tmem106a</i>	91.5503	268.2538	1.5510	2.88E-11	5.26E-09
<i>Tex11</i>	109.6107	323.9817	1.5635	1.08E-04	2.14E-03
<i>2010300C02Rik</i>	57.5807	170.3895	1.5652	2.21E-08	1.87E-06
<i>Tdrd5</i>	215.4523	637.7114	1.5655	8.30E-17	4.60E-14
<i>Lgr6</i>	26.9717	79.8790	1.5664	5.29E-05	1.20E-03
<i>Arg1</i>	27.7105	82.3121	1.5707	4.26E-04	6.21E-03
<i>Gm13032</i>	9.7940	29.1604	1.5740	6.97E-03	4.95E-02
<i>Selplg</i>	11.9085	35.5029	1.5759	2.83E-03	2.58E-02

<i>8030474K03Rik</i>	56.7760	169.4069	1.5771	4.36E-03	3.52E-02
<i>Fkbp7</i>	45.3390	135.2932	1.5773	5.94E-07	2.91E-05
<i>Usp18</i>	20.5880	61.4854	1.5784	1.44E-03	1.58E-02
<i>Cyp2s1</i>	21.8175	65.2885	1.5813	1.00E-06	4.56E-05
<i>Smoc2</i>	48.0060	144.2187	1.5870	4.52E-04	6.50E-03
<i>Gm42875</i>	12.2748	36.8948	1.5877	5.32E-03	4.10E-02
<i>Itga2b</i>	22.7369	68.8497	1.5984	5.10E-05	1.16E-03
<i>Got1l1</i>	108.2364	328.2837	1.6008	3.98E-11	7.05E-09
<i>Pik3ap1</i>	29.3725	89.3040	1.6043	4.44E-05	1.04E-03
<i>Gabra4</i>	39.8208	121.1466	1.6052	2.46E-07	1.41E-05
<i>Amhr2</i>	22.2889	67.8457	1.6059	2.86E-06	1.11E-04
<i>Ace</i>	28.5789	87.2020	1.6094	2.62E-05	6.76E-04
<i>Gm13261</i>	16.8305	51.5073	1.6137	1.02E-04	2.04E-03
<i>Ppp1r14a</i>	107.4669	329.0723	1.6145	1.10E-05	3.30E-04
<i>Unc93b1</i>	138.9831	430.1786	1.6300	1.41E-17	8.89E-15
<i>Ocln</i>	405.0820	1255.8874	1.6324	7.66E-27	1.56E-23
<i>Padi2</i>	38.5120	119.4937	1.6336	5.37E-07	2.70E-05
<i>Gm1564</i>	143.8182	446.3871	1.6340	2.23E-03	2.16E-02
<i>Prss50</i>	15.1094	47.0728	1.6395	2.53E-06	9.93E-05
<i>Gbp9</i>	117.5802	366.4245	1.6399	9.71E-14	2.92E-11
<i>Abcd2</i>	440.2904	1376.0000	1.6440	4.50E-05	1.05E-03

<i>Abcc3</i>	22.6884	71.1285	1.6485	6.60E-06	2.17E-04
<i>Bcl3</i>	27.4150	86.1482	1.6519	2.55E-06	9.99E-05
<i>Scn7a</i>	25.9852	81.6607	1.6520	1.52E-04	2.82E-03
<i>Trim12c</i>	217.3670	683.4468	1.6527	9.12E-14	2.82E-11
<i>Gsap</i>	59.0266	185.7533	1.6540	2.70E-10	4.18E-08
<i>Rnf112</i>	13.7531	43.4426	1.6594	5.20E-04	7.22E-03
<i>Parp4</i>	226.2777	714.9850	1.6598	2.22E-04	3.78E-03
<i>Tmem140</i>	60.7659	192.7629	1.6655	3.53E-07	1.92E-05
<i>Ldb3</i>	24.0169	76.2446	1.6666	1.12E-05	3.35E-04
<i>Cyct</i>	187.9921	598.8772	1.6716	1.26E-23	1.54E-20
<i>Pramef12</i>	530.7252	1690.7487	1.6716	1.31E-08	1.27E-06
<i>Cpxm2</i>	23.8546	76.2073	1.6757	1.89E-03	1.94E-02
<i>Sox30</i>	7.4306	23.8624	1.6832	3.37E-03	2.94E-02
<i>Pgam2</i>	27.3781	87.9307	1.6833	5.49E-06	1.86E-04
<i>Dnah10</i>	36.6451	117.9424	1.6864	2.20E-07	1.28E-05
<i>Zbtb7c</i>	16.8676	54.3472	1.6879	4.33E-04	6.29E-03
<i>Wt1</i>	81.9033	264.9011	1.6935	1.21E-17	7.87E-15
<i>Sycp1</i>	14.3892	46.6417	1.6966	4.38E-06	1.58E-04
<i>4930447C04Rik</i>	190.0210	618.4815	1.7026	1.64E-11	3.05E-09
<i>Dlgap1</i>	32.4896	105.7816	1.7030	2.24E-04	3.81E-03
<i>Rnf180</i>	112.7086	367.3762	1.7047	8.87E-14	2.79E-11

<i>Fbxo40</i>	50.0988	163.5486	1.7069	2.22E-03	2.16E-02
<i>Dmrt1</i>	503.2347	1646.0333	1.7097	2.30E-13	6.48E-11
<i>Trim14</i>	10.1200	33.1617	1.7123	2.42E-03	2.30E-02
<i>Hpse</i>	52.0954	171.0412	1.7151	3.04E-07	1.69E-05
<i>Cacng6</i>	75.4822	247.8513	1.7153	3.43E-17	2.02E-14
<i>Elf4</i>	155.8689	514.3941	1.7225	1.58E-06	6.69E-05
<i>Rgs22</i>	28.2553	93.8887	1.7324	1.27E-06	5.55E-05
<i>Skap1</i>	12.8588	43.0239	1.7424	7.73E-04	9.77E-03
<i>Gm15286</i>	7.4915	25.1192	1.7455	2.26E-03	2.18E-02
<i>Helt</i>	19.6683	65.9861	1.7463	4.28E-03	3.48E-02
<i>Dmrta1</i>	40.8700	137.1443	1.7466	3.19E-06	1.20E-04
<i>Fam65c</i>	25.3599	85.1906	1.7481	4.93E-05	1.13E-03
<i>Icam5</i>	8.6324	29.0806	1.7522	2.35E-03	2.25E-02
<i>Bdkrb2</i>	12.6364	42.5824	1.7527	3.28E-03	2.87E-02
<i>Aipl1</i>	12.6320	42.6371	1.7550	1.11E-03	1.29E-02
<i>Rasd1</i>	12.6334	42.7090	1.7573	2.45E-04	4.05E-03
<i>Cyp2d22</i>	15.7570	53.5550	1.7650	5.42E-04	7.42E-03
<i>Gpr155</i>	60.6368	206.9286	1.7709	7.23E-11	1.20E-08
<i>Ifih1</i>	120.9784	412.9371	1.7712	5.55E-13	1.47E-10
<i>Nmnat3</i>	5.5858	19.0857	1.7727	5.52E-03	4.18E-02
<i>Dnaja4</i>	150.0869	513.1397	1.7736	4.68E-08	3.51E-06

<i>Gng13</i>	9.2614	31.6975	1.7751	2.76E-03	2.54E-02
<i>Paqr5</i>	6.4121	21.9655	1.7764	4.72E-03	3.74E-02
<i>Mcoln2</i>	12.1618	41.9013	1.7846	1.99E-03	2.01E-02
<i>Zc3h6</i>	119.4633	415.1793	1.7972	9.15E-18	6.19E-15
<i>Cox4i2</i>	8.0879	28.1889	1.8013	4.87E-03	3.83E-02
<i>Trim30a</i>	9.3480	32.5976	1.8020	5.38E-03	4.12E-02
<i>Sptbn5</i>	13.8214	48.3175	1.8056	8.02E-06	2.58E-04
<i>Pnma5</i>	83.8672	294.4904	1.8120	1.35E-04	2.55E-03
<i>9530082P21Rik</i>	17.0226	59.8346	1.8135	5.54E-05	1.25E-03
<i>Fbxo2</i>	80.7816	284.0876	1.8142	1.84E-09	2.18E-07
<i>Psmb8</i>	107.7042	379.2427	1.8160	2.07E-05	5.57E-04
<i>Dnah11</i>	82.5439	291.3954	1.8197	4.26E-11	7.48E-09
<i>Adam2</i>	11.8076	42.2096	1.8379	8.50E-05	1.76E-03
<i>Evpl</i>	81.8040	294.4664	1.8479	1.20E-21	1.10E-18
<i>Asah2</i>	60.7828	219.1670	1.8503	4.12E-12	9.30E-10
<i>Rtp4</i>	19.9585	72.1918	1.8548	3.17E-05	7.87E-04
<i>Syt17</i>	25.5605	92.6454	1.8578	2.36E-08	1.97E-06
<i>Txnip</i>	3165.2228	11520.0925	1.8638	4.32E-04	6.28E-03
<i>Ier3</i>	71.0148	260.0723	1.8727	1.92E-03	1.96E-02
<i>Lox</i>	17.1449	62.8973	1.8752	9.18E-05	1.87E-03
<i>Sphkap</i>	33.9468	126.2096	1.8945	5.62E-07	2.81E-05

<i>Isg15</i>	24.1103	89.6640	1.8949	9.00E-06	2.82E-04
<i>Dhrs7</i>	207.0718	772.3037	1.8990	1.01E-34	3.70E-31
<i>Slc6a13</i>	14.1055	53.0192	1.9103	3.91E-05	9.30E-04
<i>C920025E04Rik</i>	14.5326	54.9855	1.9198	2.30E-04	3.87E-03
<i>Sycp2</i>	17.1026	65.0339	1.9270	3.19E-07	1.75E-05
<i>H2-T10</i>	54.1102	206.7339	1.9338	1.88E-08	1.63E-06
<i>Trim5</i>	12.7533	48.7525	1.9346	3.89E-05	9.30E-04
<i>Kcnn4</i>	3.9240	15.0442	1.9388	1.47E-03	1.60E-02
<i>Rhbdl3</i>	91.1471	350.9383	1.9449	4.97E-20	3.95E-17
<i>4933427D06Rik</i>	13.7317	52.8937	1.9456	2.73E-03	2.51E-02
<i>Sp140</i>	16.1356	62.2683	1.9483	8.31E-05	1.73E-03
<i>Gm9112</i>	78.5342	303.5714	1.9506	2.31E-14	8.11E-12
<i>H2-M3</i>	23.1739	89.8534	1.9551	1.18E-07	7.74E-06
<i>Gm42637</i>	10.5917	41.1081	1.9565	8.09E-04	1.01E-02
<i>Ifi27</i>	26.7647	104.1312	1.9600	5.45E-06	1.85E-04
<i>Lat</i>	25.6801	100.2235	1.9645	8.84E-12	1.81E-09
<i>Nxn12</i>	5.8393	22.8355	1.9674	2.71E-03	2.51E-02
<i>Lpar3</i>	31.4491	123.0933	1.9687	1.08E-08	1.07E-06
<i>Catsperg1</i>	26.0305	102.0202	1.9706	1.02E-10	1.66E-08
<i>Gcnt4</i>	111.3340	437.5631	1.9746	2.48E-03	2.35E-02
<i>Dmkn</i>	12.7041	50.1178	1.9800	4.81E-04	6.81E-03

<i>Irf6</i>	461.7431	1823.5981	1.9816	6.48E-10	9.04E-08
<i>Proca1</i>	16.6519	65.9908	1.9866	4.10E-06	1.49E-04
<i>Ighm</i>	59.3574	236.5316	1.9945	3.24E-04	5.09E-03
<i>Cerkl</i>	14.5511	58.4832	2.0069	4.25E-05	1.00E-03
<i>Aldoc</i>	215.6836	867.6424	2.0082	1.69E-15	7.71E-13
<i>1700024P16Rik</i>	5.5765	22.4680	2.0104	5.38E-03	4.12E-02
<i>Shcbp1l</i>	7.8388	31.6050	2.0114	1.52E-03	1.64E-02
<i>Ifi35</i>	104.6149	424.3176	2.0201	2.25E-05	5.96E-04
<i>Tns4</i>	22.1813	90.3173	2.0257	6.48E-07	3.13E-05
<i>Neurog3</i>	83.0923	341.6931	2.0399	9.85E-06	3.03E-04
<i>Gbp4</i>	138.2273	570.4679	2.0451	1.85E-15	8.24E-13
<i>Atp1b2</i>	122.2184	505.9941	2.0497	1.20E-04	2.34E-03
<i>Cntnap1</i>	20.0997	83.2184	2.0497	1.10E-06	4.89E-05
<i>Slc17a7</i>	57.7501	240.0947	2.0557	2.21E-15	9.60E-13
<i>Uba7</i>	16.6261	69.5880	2.0654	1.89E-05	5.15E-04
<i>Tgfb1</i>	520.8911	2180.3083	2.0655	1.52E-13	4.41E-11
<i>Ltk</i>	11.2558	47.3135	2.0716	4.03E-06	1.48E-04
<i>Spink2</i>	6.3931	26.9344	2.0749	6.91E-04	9.01E-03
<i>Izumo1</i>	20.5900	86.9188	2.0777	3.67E-08	2.86E-06
<i>Oasl2</i>	223.0380	941.7511	2.0781	5.22E-11	8.99E-09
<i>Abcg3</i>	4.4569	18.8252	2.0786	2.39E-03	2.28E-02

<i>Gal3st1</i>	24.9507	105.4646	2.0796	4.80E-07	2.50E-05
<i>Nmur2</i>	12.6664	53.5625	2.0802	3.65E-04	5.55E-03
<i>Nxf3</i>	115.1203	487.2829	2.0816	1.93E-26	3.52E-23
<i>Mgarp</i>	165.9103	705.5638	2.0884	1.45E-35	6.64E-32
<i>Izumo1r</i>	6.9493	29.8709	2.1038	5.28E-04	7.29E-03
<i>Parp14</i>	246.5764	1061.3226	2.1058	1.89E-22	2.03E-19
<i>Stra8</i>	87.5600	377.2841	2.1073	6.48E-03	4.69E-02
<i>Tgm2</i>	298.4437	1297.0796	2.1197	1.88E-05	5.13E-04
<i>Nfix</i>	19.3604	84.5951	2.1275	3.29E-08	2.61E-06
<i>Gm15283</i>	8.9702	39.4527	2.1369	1.41E-03	1.55E-02
<i>1810041L15Rik</i>	155.0780	684.4664	2.1420	2.89E-06	1.11E-04
<i>Snai2</i>	16.6801	73.6261	2.1421	5.14E-06	1.77E-04
<i>Fstl4</i>	41.9548	185.6131	2.1454	2.62E-12	6.09E-10
<i>Stk31</i>	11.5873	51.4926	2.1518	7.99E-06	2.57E-04
<i>Cd274</i>	36.4580	162.7085	2.1580	1.33E-06	5.76E-05
<i>Gbp3</i>	239.5297	1074.5647	2.1655	1.73E-20	1.44E-17
<i>Lyve1</i>	7.5901	34.1101	2.1680	1.39E-03	1.53E-02
<i>Meiob</i>	8.7682	39.4210	2.1686	2.21E-06	8.85E-05
<i>H2-Aa</i>	9.2964	42.3075	2.1862	1.70E-04	3.06E-03
<i>Dmrtc1b</i>	21.3668	97.2520	2.1864	4.08E-07	2.18E-05
<i>Inca1</i>	23.1858	106.6915	2.2021	4.35E-10	6.26E-08

<i>Noxa1</i>	5.0155	23.1439	2.2062	1.91E-03	1.95E-02
<i>Gfra3</i>	22.7472	105.5811	2.2146	2.25E-07	1.30E-05
<i>Pdk4</i>	43.3203	201.8718	2.2203	1.26E-07	8.11E-06
<i>Dsc3</i>	5.0131	23.4586	2.2263	4.11E-04	6.07E-03
<i>Gbp6</i>	7.7075	36.2657	2.2343	6.92E-04	9.01E-03
<i>Tgtp1</i>	11.4743	54.7080	2.2533	2.99E-04	4.76E-03
<i>Hs3st4</i>	16.4733	78.7340	2.2569	2.33E-08	1.95E-06
<i>Erich3</i>	5.4428	26.0528	2.2590	5.03E-03	3.92E-02
<i>Zbp1</i>	32.6508	157.6930	2.2719	6.18E-08	4.42E-06
<i>Gbp2</i>	638.2094	3085.4140	2.2734	3.75E-15	1.56E-12
<i>Cntd1</i>	32.5003	158.2836	2.2840	8.76E-10	1.15E-07
<i>Ptrf</i>	753.6068	3690.6393	2.2920	7.47E-29	1.78E-25
<i>Gbp8</i>	19.5336	95.7148	2.2928	1.02E-06	4.58E-05
<i>Gbp2b</i>	508.7398	2499.3653	2.2966	3.73E-22	3.78E-19
<i>Abhd3</i>	13.8024	67.8264	2.2969	8.39E-09	8.42E-07
<i>C1ra</i>	9.8832	48.6397	2.2991	5.69E-05	1.27E-03
<i>Ccr7</i>	17.6914	88.1887	2.3175	1.03E-06	4.64E-05
<i>H2-T24</i>	6.3883	31.9598	2.3228	1.43E-03	1.57E-02
<i>Dmrtc1a</i>	4.9966	25.3599	2.3435	4.44E-03	3.57E-02
<i>Gsdmd</i>	48.8375	250.6210	2.3594	4.89E-11	8.50E-09
<i>Ifi47</i>	8.0243	41.2272	2.3611	1.60E-04	2.92E-03

<i>Dmrtb1</i>	130.3161	683.9977	2.3920	3.40E-09	3.77E-07
<i>Igtp</i>	140.2607	747.0062	2.4130	1.00E-16	5.38E-14
<i>G730013B05Rik</i>	7.7897	41.6581	2.4190	4.02E-05	9.53E-04
<i>Al481877</i>	12.1689	65.1723	2.4211	1.15E-05	3.41E-04
<i>Usp26</i>	251.0676	1349.9356	2.4267	2.90E-07	1.64E-05
<i>4930524B15Rik</i>	3.5815	19.2581	2.4268	1.61E-03	1.72E-02
<i>Mat1a</i>	18.7438	101.4092	2.4357	8.18E-06	2.62E-04
<i>Pla2g2f</i>	15.9243	86.1939	2.4364	5.04E-07	2.58E-05
<i>Rasl10a</i>	17.7248	95.9877	2.4371	3.82E-11	6.85E-09
<i>Gbp7</i>	357.2126	1936.0299	2.4382	6.25E-42	3.81E-38
<i>Fer1l4</i>	2.5065	13.6946	2.4498	6.18E-03	4.55E-02
<i>Cyp4v3</i>	24.6408	135.4510	2.4587	8.00E-12	1.68E-09
<i>Pyroxd2</i>	3.6331	20.1263	2.4698	4.25E-03	3.46E-02
<i>Sgcg</i>	5.2364	29.0494	2.4719	1.82E-03	1.89E-02
<i>Irgm2</i>	119.7274	679.6037	2.5049	4.00E-14	1.33E-11
<i>Gm11413</i>	7.7405	43.9678	2.5059	1.23E-05	3.61E-04
<i>Gm1141</i>	78.6071	455.5574	2.5349	1.38E-11	2.62E-09
<i>Il12rb1</i>	6.3815	37.7044	2.5628	5.34E-06	1.83E-04
<i>Asb9</i>	55.0431	330.3876	2.5855	2.87E-05	7.23E-04
<i>Hrasls</i>	4.7503	29.4810	2.6337	5.69E-07	2.81E-05
<i>Tnfsf10</i>	10.8710	68.6165	2.6581	7.81E-07	3.69E-05

<i>Irf7</i>	4.1776	26.4221	2.6610	1.42E-03	1.56E-02
<i>Rsad2</i>	130.1580	825.0134	2.6642	3.02E-10	4.56E-08
<i>Lgi3</i>	3.3703	21.5882	2.6793	1.99E-03	2.01E-02
<i>Gm23833</i>	4.1309	26.6453	2.6894	2.60E-03	2.43E-02
<i>Clec1a</i>	11.1293	74.1915	2.7369	1.09E-07	7.20E-06
<i>Gm44</i>	8.8175	60.0158	2.7669	7.72E-07	3.65E-05
<i>Gm26868</i>	2.7601	19.1104	2.7916	1.36E-03	1.52E-02
<i>Cytip</i>	9.6156	67.0765	2.8024	8.45E-08	5.82E-06
<i>Ddx60</i>	95.9453	722.5454	2.9128	5.86E-13	1.51E-10
<i>Gm2420</i>	3.5465	27.5058	2.9553	2.61E-05	6.72E-04
<i>Gbp11</i>	16.3073	128.0661	2.9733	4.53E-08	3.43E-06
<i>Atcayos</i>	2.2039	17.4212	2.9827	2.76E-05	7.04E-04
<i>Hsd11b1</i>	41.7933	352.0992	3.0746	4.51E-16	2.17E-13
<i>Prss38</i>	2.5182	21.4179	3.0883	3.22E-05	7.97E-04
<i>Erg</i>	17.4494	150.6751	3.1102	3.27E-03	2.87E-02
<i>Esr1</i>	6.6491	61.3878	3.2067	6.87E-09	7.01E-07
<i>Ifit1</i>	7.6910	83.4372	3.4394	6.04E-11	1.02E-08
<i>Adm</i>	33.9373	374.1789	3.4628	7.38E-10	9.92E-08
<i>Ramp1</i>	2.5041	28.9935	3.5333	1.36E-05	3.94E-04
<i>Casp4</i>	1.3825	16.1626	3.5474	5.35E-03	4.11E-02
<i>Alox12b</i>	2.2788	29.3741	3.6882	3.61E-05	8.74E-04

<i>Ifit3</i>	1.8706	31.4014	4.0693	1.12E-05	3.35E-04
<i>Gm13404</i>	0.8613	18.6097	4.4334	5.76E-06	1.93E-04
<i>B830012L14Rik</i>	6.1211	0.0000	#NAME?	2.11E-03	2.09E-02

FDR, False discovery rate; FC, Fold change.

**Appendix 2 List of genes with altered expression levels upon *Gcn5* loss
in day 3 EBs identified by RNAseq (FDR 0.05, FC2)**

Gene name	Normalized expression		Log2ratio	P-value	FDR
	<i>Gcn5</i> ^{fx/fx}	<i>Gcn5</i> ^{-/-}			
<i>H19</i>	295.7229	39.5608	-2.9021	4.47E-04	1.84E-02
<i>Mid2</i>	22.2336	50.6207	1.1870	1.57E-03	4.59E-02
<i>Gm38393</i>	1476.4408	2955.2626	1.0012	3.28E-09	2.00E-06
<i>Nfix</i>	21.1839	59.8629	1.4987	6.82E-05	4.63E-03
<i>Ptrf</i>	459.9491	932.0316	1.0189	3.17E-07	7.51E-05
<i>Sgce</i>	249.6504	573.1940	1.1991	2.02E-12	3.35E-09
<i>Ndrg1</i>	656.7510	2437.9021	1.8922	2.91E-05	2.44E-03
<i>Trh</i>	9789.4798	4550.6930	-1.1051	5.47E-06	7.49E-04
<i>Scube2</i>	57.4297	15.1001	-1.9272	1.11E-05	1.25E-03
<i>Tex14</i>	387.3497	855.7284	1.1435	2.25E-11	2.41E-08
<i>lfi35</i>	86.5145	308.3013	1.8333	6.40E-05	4.42E-03
<i>Phox2b</i>	12.4354	0.5961	-4.3828	9.69E-04	3.19E-02
<i>St3gal1</i>	26.2187	54.6358	1.0593	1.82E-03	4.97E-02
<i>Pax5</i>	29.8262	7.2078	-2.0490	3.85E-06	5.66E-04
<i>Stc1</i>	129.8966	344.9942	1.4092	7.19E-04	2.60E-02
<i>Cd34</i>	99.9102	214.2235	1.1004	8.33E-05	5.42E-03
<i>Mpp2</i>	180.3525	404.6391	1.1658	5.71E-08	1.96E-05

<i>Aldoc</i>	909.9353	2177.9662	1.2591	2.15E-07	5.53E-05
<i>Tns4</i>	9.7900	32.6697	1.7386	1.30E-04	7.34E-03
<i>H13</i>	1182.0507	575.5301	-1.0383	1.46E-12	2.65E-09
<i>Aim1</i>	95.0254	207.5686	1.1272	1.22E-05	1.30E-03
<i>P4ha1</i>	1985.6404	4031.5676	1.0217	4.32E-04	1.80E-02
<i>Grb10</i>	11086.8733	1345.4841	-3.0427	6.58E-23	4.00E-19
<i>Slc5a4b</i>	91.5091	245.5334	1.4239	4.70E-07	1.04E-04
<i>Upp1</i>	3509.6201	7527.8257	1.1009	1.26E-03	3.89E-02
<i>Id2</i>	214.1148	77.5601	-1.4650	3.86E-07	8.91E-05
<i>Ace</i>	27.5621	103.0379	1.9024	1.08E-06	2.03E-04
<i>Tekt1</i>	10.0719	31.9644	1.6661	1.51E-03	4.46E-02
<i>Abcc3</i>	64.1262	137.7773	1.1034	8.70E-04	3.00E-02
<i>Myh3</i>	67.0591	164.8064	1.2973	2.19E-06	3.67E-04
<i>Krt19</i>	149.2674	346.1946	1.2137	4.30E-04	1.80E-02
<i>Kat2a</i>	2227.8727	701.2760	-1.6676	3.98E-32	7.26E-28
<i>Dhrs7</i>	626.2132	1524.7409	1.2838	9.67E-19	2.52E-15
<i>Meg3</i>	410.5595	18.8993	-4.4412	1.64E-11	1.87E-08
<i>Rnf180</i>	90.5018	189.8833	1.0691	7.74E-06	9.73E-04
<i>Fst</i>	328.7240	148.3242	-1.1481	1.58E-06	2.74E-04
<i>Otx2</i>	290.1915	141.1145	-1.0401	2.17E-04	1.06E-02
<i>Angpt1</i>	53.3111	9.0722	-2.5549	5.58E-04	2.18E-02

<i>Fbxo32</i>	359.3874	176.5819	-1.0252	1.41E-08	6.58E-06
<i>Col2a1</i>	865.9088	422.0682	-1.0367	1.35E-05	1.40E-03
<i>C3</i>	23.7365	82.7934	1.8024	1.46E-05	1.47E-03
<i>Psmb8</i>	46.6289	165.3420	1.8262	1.41E-05	1.44E-03
<i>Tap2</i>	82.7309	205.5175	1.3128	3.03E-04	1.38E-02
<i>Pdgfrb</i>	25.8384	62.9024	1.2836	1.79E-03	4.91E-02
<i>Dmrt1</i>	1342.9145	2874.4468	1.0979	8.00E-07	1.68E-04
<i>Pik3ap1</i>	8.4033	26.9442	1.6810	6.79E-04	2.50E-02
<i>Il1r2</i>	11.9409	36.9845	1.6310	1.75E-03	4.84E-02
<i>Epha4</i>	703.4733	182.3822	-1.9475	8.29E-08	2.65E-05
<i>Ifih1</i>	47.5933	129.4857	1.4440	1.10E-08	5.52E-06
<i>Nmi</i>	78.3630	167.5192	1.0961	1.53E-04	8.28E-03
<i>Neb</i>	105.8289	243.3978	1.2016	8.70E-07	1.76E-04
<i>Meis2</i>	1236.1904	287.7491	-2.1030	9.16E-06	1.09E-03
<i>Chst1</i>	62.7585	132.1654	1.0745	7.25E-05	4.84E-03
<i>Zbp1</i>	17.3788	62.1533	1.8385	1.28E-05	1.34E-03
<i>Ctso</i>	20.5854	46.6214	1.1794	2.81E-04	1.30E-02
<i>Gbp3</i>	94.1590	341.8391	1.8601	4.00E-14	8.10E-11
<i>Gbp2</i>	303.3540	839.8920	1.4692	1.04E-07	3.15E-05
<i>Dmrtb1</i>	145.2507	456.5793	1.6523	1.55E-05	1.53E-03
<i>Rhd</i>	65.3627	139.0487	1.0891	6.20E-04	2.34E-02

<i>Espn</i>	336.9615	731.2654	1.1178	4.89E-08	1.75E-05
<i>Hes3</i>	21.3594	1.3014	-4.0367	4.79E-08	1.75E-05
<i>Prkg2</i>	41.2820	85.6695	1.0533	9.21E-04	3.08E-02
<i>Fgf5</i>	219.1651	92.2737	-1.2480	3.27E-04	1.45E-02
<i>Oasl2</i>	225.2595	606.4064	1.4287	2.42E-06	3.84E-04
<i>Ptn</i>	478.2054	187.6812	-1.3493	1.74E-05	1.66E-03
<i>Slc13a4</i>	30.9451	80.7136	1.3831	1.90E-05	1.79E-03
<i>Plxnd1</i>	235.1387	475.2960	1.0153	4.53E-08	1.68E-05
<i>Tdrd12</i>	423.2191	937.6618	1.1477	3.99E-10	3.31E-07
<i>Asb9</i>	45.7565	184.9153	2.0148	1.16E-03	3.65E-02
<i>Cdyl2</i>	310.0220	676.8534	1.1265	5.18E-04	2.05E-02
<i>Psmb10</i>	513.8166	1049.4042	1.0302	7.05E-04	2.57E-02
<i>Car12</i>	167.6581	354.2381	1.0792	1.17E-07	3.47E-05
<i>Rasl10a</i>	24.9890	75.0985	1.5875	1.39E-05	1.43E-03
<i>Parp14</i>	157.5274	482.8653	1.6160	3.38E-14	7.69E-11
<i>Nkx6-1</i>	16.3448	2.9697	-2.4605	1.11E-03	3.53E-02
<i>Lpar3</i>	13.4404	47.0794	1.8085	3.15E-06	4.71E-04
<i>Apln</i>	76.6080	201.0613	1.3921	3.62E-08	1.46E-05
<i>Mgarp</i>	351.1918	734.0375	1.0636	1.62E-11	1.87E-08
<i>Ephx3</i>	186.5985	417.0694	1.1603	1.00E-05	1.16E-03
<i>Cdkn1c</i>	616.6902	163.4825	-1.9154	9.78E-22	4.46E-18

<i>Pcdh18</i>	194.3579	71.6024	-1.4406	3.39E-05	2.72E-03
<i>Ddx60</i>	45.7988	204.5236	2.1589	4.06E-08	1.57E-05
<i>Rapgef11</i>	71.7653	159.9583	1.1563	8.64E-04	2.99E-02
<i>Tlcd2</i>	159.4359	332.9265	1.0622	2.36E-08	1.03E-05
<i>Stx11</i>	21.7452	57.3821	1.3999	7.29E-04	2.63E-02
<i>Prss23</i>	119.3074	40.4708	-1.5597	1.01E-04	6.17E-03
<i>Cbx4</i>	72.6579	150.5833	1.0514	2.48E-05	2.20E-03
<i>Gbp7</i>	127.0694	402.6418	1.6639	1.23E-19	3.75E-16
<i>Gbp2b</i>	227.0553	654.1423	1.5266	5.78E-11	5.85E-08
<i>Cyp2s1</i>	68.4012	176.9613	1.3713	1.37E-06	2.44E-04
<i>Map7d2</i>	397.3767	804.7087	1.0180	1.46E-10	1.35E-07
<i>Sox15</i>	55.6940	112.4348	1.0135	8.79E-04	3.02E-02
<i>Dlgap3</i>	765.9737	300.7296	-1.3488	4.57E-07	1.03E-04
<i>Zc3h6</i>	141.7489	314.4933	1.1497	2.96E-08	1.23E-05
<i>Gm9785</i>	4.3222	28.5719	2.7248	8.69E-04	3.00E-02
<i>Neurog3</i>	116.4951	307.4676	1.4002	1.61E-03	4.67E-02
<i>Sowaha</i>	30.2589	94.6631	1.6454	4.48E-06	6.38E-04
<i>Smtnl2</i>	1032.3725	2351.8311	1.1878	4.02E-06	5.85E-04
<i>Fam83h</i>	534.5661	234.3295	-1.1898	2.04E-06	3.48E-04
<i>Ppp1r3b</i>	118.2135	238.3038	1.0114	6.33E-04	2.37E-02
<i>Gap43</i>	82.8168	35.9024	-1.2058	9.40E-04	3.12E-02

<i>Nccrp1</i>	34.4972	3.3456	-3.3662	1.36E-06	2.44E-04
<i>Sp8</i>	338.7400	108.0426	-1.6486	4.05E-06	5.85E-04
<i>Prss50</i>	98.4685	222.1058	1.1735	2.48E-05	2.20E-03
<i>Gal3st1</i>	43.8119	129.3119	1.5615	3.52E-05	2.80E-03
<i>Fam161a</i>	62.5269	126.7662	1.0196	4.52E-04	1.84E-02
<i>Sarm1</i>	96.8237	216.1714	1.1587	1.30E-06	2.42E-04
<i>Pnma5</i>	86.4028	372.7974	2.1092	1.21E-05	1.30E-03
<i>Sv2c</i>	34.5522	107.3978	1.6361	1.22E-04	7.03E-03
<i>4933427D06Rik</i>	26.5821	132.1078	2.3132	4.43E-04	1.83E-02
<i>Usp26</i>	576.8641	2633.6663	2.1908	2.53E-06	3.93E-04
<i>Kdm5d</i>	197.1656	404.3364	1.0361	1.62E-04	8.59E-03
<i>A930024E05Rik</i>	327.0260	157.4958	-1.0541	9.30E-05	5.84E-03
<i>Nxf3</i>	89.3717	388.9137	2.1216	1.64E-26	1.49E-22
<i>Inca1</i>	29.5235	64.8825	1.1360	9.17E-04	3.08E-02
<i>Tmem140</i>	11.3854	28.7399	1.3359	1.25E-03	3.87E-02
<i>H2-Q7</i>	143.8002	292.8012	1.0259	4.00E-05	3.05E-03
<i>Lsamp</i>	0.6802	7.6615	3.4937	7.08E-04	2.57E-02
<i>Sox21</i>	339.4044	106.9601	-1.6659	7.04E-07	1.49E-04
<i>Usp17lb</i>	40.3897	12.8864	-1.6481	1.43E-03	4.30E-02
<i>Parp10</i>	233.4522	471.6549	1.0146	4.37E-04	1.81E-02
<i>Ifi27</i>	7.5372	24.1861	1.6821	9.73E-04	3.20E-02

<i>Efcab1</i>	27.3559	58.1989	1.0891	1.02E-03	3.35E-02
<i>Il3ra</i>	88.5823	30.5425	-1.5362	1.19E-05	1.29E-03
<i>Uba1y</i>	208.8711	434.7815	1.0577	9.14E-07	1.83E-04
<i>Irgm2</i>	99.3136	265.9235	1.4209	1.32E-05	1.37E-03
<i>Fbxo47</i>	67.2402	151.2119	1.1692	2.29E-05	2.08E-03
<i>Rgma</i>	353.6609	159.8469	-1.1457	1.40E-05	1.43E-03
<i>Rbm44</i>	562.3924	1137.7533	1.0165	6.56E-08	2.21E-05
<i>Zscan4f</i>	133.7923	38.1506	-1.8102	3.21E-04	1.43E-02
<i>Cebpd</i>	173.7531	85.6049	-1.0213	1.95E-04	9.83E-03
<i>Nup62cl</i>	218.9731	453.1032	1.0491	3.87E-05	2.97E-03
<i>Gm1141</i>	151.0135	405.4066	1.4247	3.43E-05	2.75E-03
<i>Gm9</i>	0.3023	9.1533	4.9202	1.54E-03	4.50E-02
<i>Lrp8os2</i>	59.5906	137.4819	1.2061	5.56E-05	4.01E-03
<i>Rec114</i>	131.5090	283.5878	1.1086	5.23E-04	2.06E-02
<i>1810010H24Rik</i>	38.3081	80.6864	1.0747	9.18E-04	3.08E-02
<i>Cntd1</i>	54.6588	131.6818	1.2685	4.56E-04	1.85E-02
<i>Igtp</i>	146.7145	331.5726	1.1763	2.71E-05	2.33E-03
<i>Gbp4</i>	73.5510	221.4101	1.5899	1.11E-09	8.33E-07
<i>H2-T10</i>	33.0454	74.9007	1.1805	8.93E-04	3.04E-02
<i>Hist3h2bb-ps</i>	461.3166	1079.6088	1.2267	3.45E-12	5.23E-09
<i>Kis2</i>	558.4567	250.8900	-1.1544	6.75E-07	1.45E-04

<i>2700033N17Rik</i>	28.6467	7.8726	-1.8635	4.41E-04	1.82E-02
<i>BC064078</i>	51.8482	17.9813	-1.5278	8.27E-05	5.42E-03
<i>Zscan4d</i>	113.2395	35.3590	-1.6792	3.52E-04	1.53E-02
<i>Peg10</i>	2280.4827	6904.8484	1.5983	5.30E-04	2.08E-02
<i>Mirg</i>	237.1671	7.2003	-5.0417	2.47E-21	8.99E-18
<i>Rian</i>	2408.3454	107.2252	-4.4893	1.16E-09	8.33E-07
<i>G730013B05Rik</i>	4.0055	23.6903	2.5643	5.70E-05	4.07E-03
<i>Gm26945</i>	32.4924	2.3032	-3.8184	4.23E-06	6.07E-04
<i>B830012L14Rik</i>	17.1328	1.2220	-3.8095	1.29E-03	3.95E-02
<i>Tcf24</i>	51.5219	111.3713	1.1121	1.05E-03	3.39E-02
<i>Snrpn</i>	1040.7031	2155.8370	1.0507	1.03E-06	1.97E-04
<i>Gm37899</i>	77.0838	5.3044	-3.8612	1.32E-06	2.43E-04
<i>Pcdhga11</i>	59.7718	25.4418	-1.2323	1.68E-03	4.75E-02
<i>Gbp10</i>	15.0419	63.1312	2.0694	1.34E-06	2.44E-04
<i>Gm2762</i>	93.6145	201.5682	1.1065	3.03E-05	2.51E-03

FDR, False discovery rate; FC, Fold change.

Appendix 3 List of genes with decreased H3K9ac levels in promoter region upon *Gcn5* loss in day 5 EBs (FDR0.05)

Gene name	Distance to TSS	Gene name	Distance to TSS	Gene name	Distance to TSS
<i>Mir363</i>	-471	<i>Gtf2e1</i>	0	<i>Rad51ap1</i>	0
<i>Ints7</i>	0	<i>Rpl37a</i>	0	<i>Arhgef7</i>	0
<i>Prr11</i>	0	<i>Mak16</i>	0	<i>Dscr3</i>	0
<i>Efnb2</i>	0	<i>Mir7067</i>	0	<i>Chchd4</i>	0
<i>Fbxl18</i>	0	<i>Snora81</i>	0	<i>Thap1</i>	0
<i>Sugt1</i>	0	<i>1700001G1</i> <i>7Rik</i>	0	<i>Cep44</i>	0
<i>Ankrd28</i>	0	<i>Vps35</i>	0	<i>Pik3r2</i>	0
<i>Lins</i>	0	<i>Snord2</i>	0	<i>Nsl1</i>	0
<i>Rab13</i>	0	<i>Mcm5</i>	0	<i>Qtrtd1</i>	0
<i>Snora74a</i>	0	<i>Tbc1d31</i>	0	<i>Snord83b</i>	-8
<i>Ubr5</i>	0	<i>Acd</i>	0	<i>Snora7a</i>	0
<i>Cnnm2</i>	0	<i>Mir18b</i>	0	<i>Dusp4</i>	0
<i>Zcchc4</i>	0	<i>Rnf165</i>	0	<i>Gm10052</i>	0
<i>Cirh1a</i>	0	<i>Zwilch</i>	0	<i>Enkd1</i>	0
<i>Eif4a2</i>	0	<i>C130036L2</i> <i>4Rik</i>	0	<i>Kis2</i>	0

<i>Gapdh</i>	0	<i>Cadps</i>	0	<i>Rpl4</i>	0
<i>Snord45b</i>	0	<i>Naa40</i>	0	<i>Eef1g</i>	0
<i>Snrpa1</i>	0	<i>Rpl7l1</i>	0	<i>Xpc</i>	0
<i>Gldc</i>	0	<i>Rpl3</i>	0	<i>Upf3a</i>	0
<i>Sall2</i>	0	<i>Urb2</i>	0	<i>Srm</i>	0
<i>Wdr76</i>	0	<i>Mthfd2</i>	0	<i>2810428l15R ik</i>	0
<i>Snord16a</i>	0	<i>Mar11</i>	0	<i>Rpl18a</i>	0
<i>Eif4ebp1</i>	0	<i>Ncl</i>	0	<i>Rnf20</i>	0
<i>Prim2</i>	0	<i>Slc20a2</i>	0	<i>Mcm6</i>	0
<i>Nqo1</i>	0	<i>Rps9</i>	0	<i>Smim19</i>	0
<i>B230354K17 Rik</i>	0	<i>Prkdc</i>	0	<i>Cript</i>	0
<i>Gnl3</i>	0	<i>Pola1</i>	0	<i>Fmn2</i>	0
<i>Mir7238</i>	0	<i>Cdc5l</i>	0	<i>Srp19</i>	0
<i>Spns1</i>	0	<i>Hells</i>	0	<i>Lincenc1</i>	0
<i>Rabggtb</i>	0	<i>2610015P0 9Rik</i>	0	<i>Dtl</i>	0
<i>Rnf150</i>	0	<i>Gins2</i>	0	<i>Uba52</i>	0
<i>Mir1949</i>	0	<i>Tuba1b</i>	0	<i>Taf5l</i>	0
<i>Hnrnpa1</i>	0	<i>Pard6a</i>	0	<i>Asb7</i>	0

<i>Sox1</i>	0	<i>Bcat1</i>	0	<i>Hsbp1</i>	0
<i>Ccdc115</i>	0	<i>Gm12191</i>	0	<i>Mt2</i>	0
<i>Setbp1</i>	0	<i>Cxcr4</i>	0	<i>Zfp524</i>	0
<i>lpo9</i>	0	<i>Set</i>	0	<i>Mir92-2</i>	-310
<i>Bdh1</i>	0	1600020E0 <i>1Rik</i>	0	<i>Tatdn3</i>	0
<i>Ap4m1</i>	0	<i>Klf2</i>	0	<i>Afg3l1</i>	0
<i>Fbxo8</i>	0	1110038B1 <i>2Rik</i>	0	<i>Chtf8</i>	0
<i>Bccip</i>	0	<i>Hspe1</i>	0	<i>Tex30</i>	0
<i>Snord47</i>	0	<i>Snord19</i>	0	<i>Orc6</i>	0
<i>Tardbp</i>	0	2310035C2 <i>3Rik</i>	0	<i>Huwe1</i>	0
4930429B21 <i>Rik</i>	0	<i>Rpl30</i>	0	<i>Rmi2</i>	0
<i>Txn14b</i>	0	<i>Cct2</i>	0	<i>Cenpq</i>	0
<i>Eno1b</i>	0	<i>Gm31763</i>	0	<i>Aldh6a1</i>	0
<i>Zbtb37</i>	0	<i>Tmem183a</i>	0	<i>Orc1</i>	0
<i>Osbp1a</i>	0	<i>Uros</i>	0	<i>Nat10</i>	0
<i>Mir301</i>	-347	<i>Ska2</i>	0	<i>Snord45c</i>	0
<i>Mir8109</i>	0	<i>Mad1l1</i>	0	<i>Eno1</i>	0

<i>Rplp2</i>	0	<i>Bola1</i>	0	<i>Rps27</i>	0
<i>Nmnat2</i>	0	<i>Snhg1</i>	0	<i>Apba1</i>	0
<i>Snhg4</i>	0	<i>Zranb3</i>	0	2500002B13 <i>Rik</i>	0
<i>Paxip1</i>	0	<i>Dhx38</i>	0	<i>Anapc4</i>	0
<i>Snord43</i>	0	<i>Pigf</i>	0	<i>Snord52</i>	0
<i>Zfyve26</i>	0	<i>Rad51b</i>	0	<i>Mir1967</i>	0
<i>Ipo5</i>	0	<i>Lsm3</i>	0	<i>Pign</i>	0
<i>Cbx5</i>	0	<i>Grb10</i>	0	<i>Utp14a</i>	0
<i>Msmo1</i>	0	<i>Timeless</i>	0	<i>Cox20</i>	0
<i>Dpp7</i>	0	<i>Carf</i>	0	<i>Ankrd10</i>	0
<i>Pcna</i>	0	2210408I21 <i>Rik</i>	0	<i>Pcbp1</i>	0
<i>Lin52</i>	0	<i>Hspd1</i>	0	<i>Mcm4</i>	0
<i>Gas5</i>	0	<i>Slc3a2</i>	0	<i>Snora33</i>	0
<i>Ifi30</i>	0	<i>Aars</i>	0	<i>Rps21</i>	0
<i>Ptp4a1</i>	0	<i>Rabl3</i>	0	<i>Atp6v1b2</i>	0
<i>Snord82</i>	0	<i>Ankrd32</i>	0	<i>Pbrm1</i>	0
<i>Cstf2</i>	0	<i>U2surp</i>	0	<i>Sap30</i>	0
4933405L10 <i>Rik</i>	0	<i>Rps27rt</i>	0	<i>Gm5643</i>	0

<i>R3hdm1</i>	0	<i>Mcm7</i>	0	<i>Snord22</i>	0
<i>Mir106a</i>	0	<i>Tmem43</i>	0	<i>Mut</i>	0
<i>Rps12</i>	0	<i>Rps5</i>	0	<i>Mcm2</i>	0
<i>Gins1</i>	0	<i>Mfap1a</i>	0	<i>2010320M18</i> <i>Rik</i>	0
<i>Mir3091</i>	0	<i>Gja1</i>	0	<i>Snord100</i>	0
<i>Mir20b</i>	-46	<i>D6Wsu163</i> <i>e</i>	0	<i>Gm13363</i>	0
<i>Mir19b-2</i>	-172	<i>Nuf2</i>	0	<i>Slc18a1</i>	0
<i>Zmat3</i>	0	<i>Prpf38a</i>	0	<i>Imp4</i>	0
<i>Lipt1</i>	0	<i>Rps6ka2</i>	0	<i>Fiz1</i>	0
<i>Mir124a-3</i>	0	<i>Rpl32</i>	0	<i>Dhps</i>	0
<i>Wdr12</i>	0	<i>Snora52</i>	0		
<i>Snora68</i>	0	<i>Impa2</i>	0		

FDR, False discovery rate.

BIBLIOGRAPHY

1. Strahl, B. D., and C. D. Allis. 2000. The language of covalent histone modifications. *Nature* 403: 41-45.
2. Kouzarides, T. 2007. Chromatin modifications and their function. *Cell* 128: 693-705.
3. Lawrence, M., S. Daujat, and R. Schneider. 2016. Lateral Thinking: How Histone Modifications Regulate Gene Expression. *Trends Genet* 32: 42-56.
4. Bannister, A. J., and T. Kouzarides. 2011. Regulation of chromatin by histone modifications. *Cell Res* 21: 381-395.
5. Mujtaba, S., L. Zeng, and M. M. Zhou. 2007. Structure and acetyl-lysine recognition of the bromodomain. *Oncogene* 26: 5521-5527.
6. Nakamura, T., J. Blechman, S. Tada, T. Rozovskaia, T. Itoyama, F. Bullrich, A. Mazo, C. M. Croce, B. Geiger, and E. Canaani. 2000. huASH1 protein, a putative transcription factor encoded by a human homologue of the *Drosophila* ash1 gene, localizes to both nuclei and cell-cell tight junctions. *Proc Natl Acad Sci U S A* 97: 7284-7289.
7. Li, Y., H. Wen, Y. Xi, K. Tanaka, H. Wang, D. Peng, Y. Ren, Q. Jin, S. Y. Dent, W. Li, H. Li, and X. Shi. 2014. AF9 YEATS domain links

- histone acetylation to DOT1L-mediated H3K79 methylation. *Cell* 159: 558-571.
8. Brownell, J. E., J. Zhou, T. Ranalli, R. Kobayashi, D. G. Edmondson, S. Y. Roth, and C. D. Allis. 1996. Tetrahymena histone acetyltransferase A: a homolog to yeast Gcn5p linking histone acetylation to gene activation. *Cell* 84: 843-851.
 9. Wu, P. Y., C. Ruhlmann, F. Winston, and P. Schultz. 2004. Molecular architecture of the *S. cerevisiae* SAGA complex. *Mol Cell* 15: 199-208.
 10. Brand, M., C. Leurent, V. Mallouh, L. Tora, and P. Schultz. 1999. Three-dimensional structures of the TAFII-containing complexes TFIID and TFTC. *Science* 286: 2151-2153.
 11. Wang, L., and S. Y. Dent. 2014. Functions of SAGA in development and disease. *Epigenomics* 6: 329-339.
 12. Xu, W., D. G. Edmondson, and S. Y. Roth. 1998. Mammalian GCN5 and P/CAF acetyltransferases have homologous amino-terminal domains important for recognition of nucleosomal substrates. *Mol Cell Biol* 18: 5659-5669.
 13. Ogryzko, V. V., T. Kotani, X. Zhang, R. L. Schiltz, T. Howard, X. J. Yang, B. H. Howard, J. Qin, and Y. Nakatani. 1998. Histone-like TAFs within the PCAF histone acetylase complex. *Cell* 94: 35-44.
 14. Koutelou, E., C. L. Hirsch, and S. Y. Dent. 2010. Multiple faces of the SAGA complex. *Curr Opin Cell Biol* 22: 374-382.

15. Zhao, D., H. Guan, S. Zhao, W. Mi, H. Wen, Y. Li, Y. Zhao, C. D. Allis, X. Shi, and H. Li. 2016. YEATS2 is a selective histone crotonylation reader. *Cell Res* 26: 629-632.
16. McMahon, S. B., M. A. Wood, and M. D. Cole. 2000. The essential cofactor TRRAP recruits the histone acetyltransferase hGCN5 to c-Myc. *Mol Cell Biol* 20: 556-562.
17. Gamper, A. M., and R. G. Roeder. 2008. Multivalent binding of p53 to the STAGA complex mediates coactivator recruitment after UV damage. *Mol Cell Biol* 28: 2517-2527.
18. Liu, X., M. Vorontchikhina, Y. L. Wang, F. Faiola, and E. Martinez. 2008. STAGA recruits Mediator to the MYC oncoprotein to stimulate transcription and cell proliferation. *Mol Cell Biol* 28: 108-121.
19. Liu, X., J. Tesfai, Y. A. Evrard, S. Y. Dent, and E. Martinez. 2003. c-Myc transformation domain recruits the human STAGA complex and requires TRRAP and GCN5 acetylase activity for transcription activation. *J Biol Chem* 278: 20405-20412.
20. Lang, S. E., S. B. McMahon, M. D. Cole, and P. Hearing. 2001. E2F transcriptional activation requires TRRAP and GCN5 cofactors. *J Biol Chem* 276: 32627-32634.
21. Krebs, A. R., K. Karmodiya, M. Lindahl-Allen, K. Struhl, and L. Tora. 2011. SAGA and ATAC histone acetyl transferase complexes regulate

distinct sets of genes and ATAC defines a class of p300-independent enhancers. *Mol Cell* 44: 410-423.

22. Lee, T. I., H. C. Causton, F. C. Holstege, W. C. Shen, N. Hannett, E. G. Jennings, F. Winston, M. R. Green, and R. A. Young. 2000. Redundant roles for the TFIID and SAGA complexes in global transcription. *Nature* 405: 701-704.
23. Bonnet, J., C. Y. Wang, T. Baptista, S. D. Vincent, W. C. Hsiao, M. Stierle, C. F. Kao, L. Tora, and D. Devys. 2014. The SAGA coactivator complex acts on the whole transcribed genome and is required for RNA polymerase II transcription. *Genes Dev* 28: 1999-2012.
24. Xu, W., D. G. Edmondson, Y. A. Evrard, M. Wakamiya, R. R. Behringer, and S. Y. Roth. 2000. Loss of Gcn5l2 leads to increased apoptosis and mesodermal defects during mouse development. *Nat Genet* 26: 229-232.
25. Bu, P., Y. A. Evrard, G. Lozano, and S. Y. Dent. 2007. Loss of Gcn5 acetyltransferase activity leads to neural tube closure defects and exencephaly in mouse embryos. *Mol Cell Biol* 27: 3405-3416.
26. Wilde, J. J., J. A. Siegenthaler, S. Y. Dent, and L. A. Niswander. 2017. Diencephalic Size Is Restricted by a Novel Interplay Between GCN5 Acetyltransferase Activity and Retinoic Acid Signaling. *J Neurosci* 37: 2565-2579.

27. Tudor, M., P. J. Murray, C. Onufryk, R. Jaenisch, and R. A. Young. 1999. Ubiquitous expression and embryonic requirement for RNA polymerase II coactivator subunit Srb7 in mice. *Genes Dev* 13: 2365-2368.
28. Lin, W., G. Srajer, Y. A. Evrard, H. M. Phan, Y. Furuta, and S. Y. Dent. 2007. Developmental potential of Gcn5(-/-) embryonic stem cells in vivo and in vitro. *Dev Dyn* 236: 1547-1557.
29. Martinez-Cerdeno, V., J. M. Lemen, V. Chan, A. Wey, W. Lin, S. R. Dent, and P. S. Knoepfler. 2012. N-Myc and GCN5 regulate significantly overlapping transcriptional programs in neural stem cells. *PLoS One* 7: e39456.
30. Jin, Q., C. Wang, X. Kuang, X. Feng, V. Sartorelli, H. Ying, K. Ge, and S. Y. Dent. 2014. Gcn5 and PCAF regulate PPARgamma and Prdm16 expression to facilitate brown adipogenesis. *Mol Cell Biol* 34: 3746-3753.
31. Smith, A. G. 2001. Embryo-derived stem cells: of mice and men. *Annu Rev Cell Dev Biol* 17: 435-462.
32. Boyer, L. A., T. I. Lee, M. F. Cole, S. E. Johnstone, S. S. Levine, J. P. Zucker, M. G. Guenther, R. M. Kumar, H. L. Murray, R. G. Jenner, D. K. Gifford, D. A. Melton, R. Jaenisch, and R. A. Young. 2005. Core transcriptional regulatory circuitry in human embryonic stem cells. *Cell* 122: 947-956.

33. Chen, X., H. Xu, P. Yuan, F. Fang, M. Huss, V. B. Vega, E. Wong, Y. L. Orlov, W. Zhang, J. Jiang, Y. H. Loh, H. C. Yeo, Z. X. Yeo, V. Narang, K. R. Govindarajan, B. Leong, A. Shahab, Y. Ruan, G. Bourque, W. K. Sung, N. D. Clarke, C. L. Wei, and H. H. Ng. 2008. Integration of external signaling pathways with the core transcriptional network in embryonic stem cells. *Cell* 133: 1106-1117.
34. Rossant, J. 2008. Stem cells and early lineage development. *Cell* 132: 527-531.
35. Young, R. A. 2011. Control of the embryonic stem cell state. *Cell* 144: 940-954.
36. Hirsch, C. L., Z. Coban Akdemir, L. Wang, G. Jayakumaran, D. Trcka, A. Weiss, J. J. Hernandez, Q. Pan, H. Han, X. Xu, Z. Xia, A. P. Salinger, M. Wilson, F. Vizeacoumar, A. Datti, W. Li, A. J. Cooney, M. C. Barton, B. J. Blencowe, J. L. Wrana, and S. Y. Dent. 2015. Myc and SAGA rewire an alternative splicing network during early somatic cell reprogramming. *Genes Dev* 29: 803-816.
37. Kim, J., A. B. Cantor, S. H. Orkin, and J. Wang. 2009. Use of in vivo biotinylation to study protein-protein and protein-DNA interactions in mouse embryonic stem cells. *Nat Protoc* 4: 506-517.
38. Bernstein, B. E., T. S. Mikkelsen, X. Xie, M. Kamal, D. J. Huebert, J. Cuff, B. Fry, A. Meissner, M. Wernig, K. Plath, R. Jaenisch, A. Wagschal, R. Feil, S. L. Schreiber, and E. S. Lander. 2006. A bivalent

chromatin structure marks key developmental genes in embryonic stem cells. *Cell* 125: 315-326.

39. Voigt, P., W. W. Tee, and D. Reinberg. 2013. A double take on bivalent promoters. *Genes Dev* 27: 1318-1338.
40. Loh, Y. H., Q. Wu, J. L. Chew, V. B. Vega, W. Zhang, X. Chen, G. Bourque, J. George, B. Leong, J. Liu, K. Y. Wong, K. W. Sung, C. W. Lee, X. D. Zhao, K. P. Chiu, L. Lipovich, V. A. Kuznetsov, P. Robson, L. W. Stanton, C. L. Wei, Y. Ruan, B. Lim, and H. H. Ng. 2006. The Oct4 and Nanog transcription network regulates pluripotency in mouse embryonic stem cells. *Nat Genet* 38: 431-440.
41. Arman, E., R. Haffner-Krausz, Y. Chen, J. K. Heath, and P. Lonai. 1998. Targeted disruption of fibroblast growth factor (FGF) receptor 2 suggests a role for FGF signaling in pregastrulation mammalian development. *Proc Natl Acad Sci U S A* 95: 5082-5087.
42. Chazaud, C., Y. Yamanaka, T. Pawson, and J. Rossant. 2006. Early lineage segregation between epiblast and primitive endoderm in mouse blastocysts through the Grb2-MAPK pathway. *Dev Cell* 10: 615-624.
43. Feldman, B., W. Poueymirou, V. E. Papaioannou, T. M. DeChiara, and M. Goldfarb. 1995. Requirement of FGF-4 for postimplantation mouse development. *Science* 267: 246-249.

44. Georgiades, P., and J. Rossant. 2006. Ets2 is necessary in trophoblast for normal embryonic anteroposterior axis development. *Development* 133: 1059-1068.
45. Kang, M., V. Garg, and A. K. Hadjantonakis. 2017. Lineage Establishment and Progression within the Inner Cell Mass of the Mouse Blastocyst Requires FGFR1 and FGFR2. *Dev Cell* 41: 496-510 e495.
46. Yamanaka, Y., F. Lanner, and J. Rossant. 2010. FGF signal-dependent segregation of primitive endoderm and epiblast in the mouse blastocyst. *Development* 137: 715-724.
47. Ciruna, B., and J. Rossant. 2001. FGF signaling regulates mesoderm cell fate specification and morphogenetic movement at the primitive streak. *Dev Cell* 1: 37-49.
48. Lanner, F., and J. Rossant. 2010. The role of FGF/Erk signaling in pluripotent cells. *Development* 137: 3351-3360.
49. Kunath, T., M. K. Saba-EI-Leil, M. Almousailleakh, J. Wray, S. Meloche, and A. Smith. 2007. FGF stimulation of the Erk1/2 signalling cascade triggers transition of pluripotent embryonic stem cells from self-renewal to lineage commitment. *Development* 134: 2895-2902.
50. Ying, Q. L., J. Wray, J. Nichols, L. Battle-Morera, B. Doble, J. Woodgett, P. Cohen, and A. Smith. 2008. The ground state of embryonic stem cell self-renewal. *Nature* 453: 519-523.

51. Li, S., D. Edgar, R. Fassler, W. Wadsworth, and P. D. Yurchenco. 2003. The role of laminin in embryonic cell polarization and tissue organization. *Dev Cell* 4: 613-624.
52. Giancotti, F. G. 2014. Deregulation of cell signaling in cancer. *FEBS Lett* 588: 2558-2570.
53. Dang, C. V. 2012. MYC on the path to cancer. *Cell* 149: 22-35.
54. Kim, D., G. Pertea, C. Trapnell, H. Pimentel, R. Kelley, and S. L. Salzberg. 2013. TopHat2: accurate alignment of transcriptomes in the presence of insertions, deletions and gene fusions. *Genome Biol* 14: R36.
55. Mudge, J. M., and J. Harrow. 2015. Creating reference gene annotation for the mouse C57BL6/J genome assembly. *Mamm Genome* 26: 366-378.
56. Anders, S., P. T. Pyl, and W. Huber. 2015. HTSeq--a Python framework to work with high-throughput sequencing data. *Bioinformatics* 31: 166-169.
57. Anders, S., and W. Huber. 2010. Differential expression analysis for sequence count data. *Genome Biol* 11: R106.
58. de Hoon, M. J., S. Imoto, J. Nolan, and S. Miyano. 2004. Open source clustering software. *Bioinformatics* 20: 1453-1454.
59. Saldanha, A. J. 2004. Java Treeview--extensible visualization of microarray data. *Bioinformatics* 20: 3246-3248.

60. Subramanian, A., P. Tamayo, V. K. Mootha, S. Mukherjee, B. L. Ebert, M. A. Gillette, A. Paulovich, S. L. Pomeroy, T. R. Golub, E. S. Lander, and J. P. Mesirov. 2005. Gene set enrichment analysis: a knowledge-based approach for interpreting genome-wide expression profiles. *Proc Natl Acad Sci U S A* 102: 15545-15550.
61. Wen, H., Y. Li, Y. Xi, S. Jiang, S. Stratton, D. Peng, K. Tanaka, Y. Ren, Z. Xia, J. Wu, B. Li, M. C. Barton, W. Li, H. Li, and X. Shi. 2014. ZMYND11 links histone H3.3K36me3 to transcription elongation and tumour suppression. *Nature* 508: 263-268.
62. Langmead, B., C. Trapnell, M. Pop, and S. L. Salzberg. 2009. Ultrafast and memory-efficient alignment of short DNA sequences to the human genome. *Genome Biol* 10: R25.
63. Zhang, Y., T. Liu, C. A. Meyer, J. Eeckhoute, D. S. Johnson, B. E. Bernstein, C. Nusbaum, R. M. Myers, M. Brown, W. Li, and X. S. Liu. 2008. Model-based analysis of ChIP-Seq (MACS). *Genome Biol* 9: R137.
64. Consortium, E. P. 2012. An integrated encyclopedia of DNA elements in the human genome. *Nature* 489: 57-74.
65. Robinson, M. D., D. J. McCarthy, and G. K. Smyth. 2010. edgeR: a Bioconductor package for differential expression analysis of digital gene expression data. *Bioinformatics* 26: 139-140.

66. Kent, W. J., C. W. Sugnet, T. S. Furey, K. M. Roskin, T. H. Pringle, A. M. Zahler, and D. Haussler. 2002. The human genome browser at UCSC. *Genome Res* 12: 996-1006.
67. Auerbach, R. K., B. Chen, and A. J. Butte. 2013. Relating genes to function: identifying enriched transcription factors using the ENCODE ChIP-Seq significance tool. *Bioinformatics* 29: 1922-1924.
68. McCarthy, R. L., A. D. Duncan, and M. C. Barton. 2017. Sample Preparation for Mass Cytometry Analysis. *J Vis Exp*.
69. McCarthy, R. L., D. H. Mak, J. K. Burks, and M. C. Barton. 2017. Rapid monoisotopic cisplatin based barcoding for multiplexed mass cytometry. *Sci Rep* 7: 3779.
70. Dignam, J. D., R. M. Lebovitz, and R. G. Roeder. 1983. Accurate transcription initiation by RNA polymerase II in a soluble extract from isolated mammalian nuclei. *Nucleic Acids Res* 11: 1475-1489.
71. Cong, L., F. A. Ran, D. Cox, S. Lin, R. Barretto, N. Habib, P. D. Hsu, X. Wu, W. Jiang, L. A. Marraffini, and F. Zhang. 2013. Multiplex genome engineering using CRISPR/Cas systems. *Science* 339: 819-823.
72. Tomida, J., K. Takata, S. S. Lange, A. C. Schibler, M. J. Yousefzadeh, S. Bhetawal, S. Y. Dent, and R. D. Wood. 2015. REV7 is essential for DNA damage tolerance via two REV3L binding sites in mammalian DNA polymerase zeta. *Nucleic Acids Res* 43: 1000-1011.

73. Kamiya, D., S. Banno, N. Sasai, M. Ohgushi, H. Inomata, K. Watanabe, M. Kawada, R. Yakura, H. Kiyonari, K. Nakao, L. M. Jakt, S. Nishikawa, and Y. Sasai. 2011. Intrinsic transition of embryonic stem-cell differentiation into neural progenitors. *Nature* 470: 503-509.
74. Patient, R. K., and J. D. McGhee. 2002. The GATA family (vertebrates and invertebrates). *Curr Opin Genet Dev* 12: 416-422.
75. Yao, Y. 2017. Laminin: loss-of-function studies. *Cell Mol Life Sci* 74: 1095-1115.
76. Kurokawa, D., N. Takasaki, H. Kiyonari, R. Nakayama, C. Kimura-Yoshida, I. Matsuo, and S. Aizawa. 2004. Regulation of Otx2 expression and its functions in mouse epiblast and anterior neuroectoderm. *Development* 131: 3307-3317.
77. Sumi, T., S. Oki, K. Kitajima, and C. Meno. 2013. Epiblast ground state is controlled by canonical Wnt/beta-catenin signaling in the postimplantation mouse embryo and epiblast stem cells. *PLoS One* 8: e63378.
78. Yamanaka, Y., A. Ralston, R. O. Stephenson, and J. Rossant. 2006. Cell and molecular regulation of the mouse blastocyst. *Dev Dyn* 235: 2301-2314.
79. Spitzer, M. H., and G. P. Nolan. 2016. Mass Cytometry: Single Cells, Many Features. *Cell* 165: 780-791.

80. Qiu, P., E. F. Simonds, S. C. Bendall, K. D. Gibbs, Jr., R. V. Bruggner, M. D. Linderman, K. Sachs, G. P. Nolan, and S. K. Plevritis. 2011. Extracting a cellular hierarchy from high-dimensional cytometry data with SPADE. *Nat Biotechnol* 29: 886-891.
81. Suganuma, T., J. L. Gutierrez, B. Li, L. Florens, S. K. Swanson, M. P. Washburn, S. M. Abmayr, and J. L. Workman. 2008. ATAC is a double histone acetyltransferase complex that stimulates nucleosome sliding. *Nat Struct Mol Biol* 15: 364-372.
82. Spedale, G., H. T. Timmers, and W. W. Pijnappel. 2012. ATAC-king the complexity of SAGA during evolution. *Genes Dev* 26: 527-541.
83. Urbanek, P., I. Fetka, M. H. Meisler, and M. Busslinger. 1997. Cooperation of Pax2 and Pax5 in midbrain and cerebellum development. *Proc Natl Acad Sci U S A* 94: 5703-5708.
84. Lee, H. J., N. Y. Choi, S. W. Lee, K. Ko, T. S. Hwang, D. W. Han, J. Lim, H. R. Scholer, and K. Ko. 2016. Epigenetic alteration of imprinted genes during neural differentiation of germline-derived pluripotent stem cells. *Epigenetics* 11: 177-183.
85. Szabo, N. E., T. Zhao, M. Cankaya, T. Theil, X. Zhou, and G. Alvarez-Bolado. 2009. Role of neuroepithelial Sonic hedgehog in hypothalamic patterning. *J Neurosci* 29: 6989-7002.
86. Tefft, J. D., M. Lee, S. Smith, M. Leinwand, J. Zhao, P. Bringas, Jr., D. L. Crowe, and D. Warburton. 1999. Conserved function of mSpry-2, a

murine homolog of *Drosophila* sprouty, which negatively modulates respiratory organogenesis. *Curr Biol* 9: 219-222.

87. Wu, Q., L. Zhang, P. Su, X. Lei, X. Liu, H. Wang, L. Lu, Y. Bai, T. Xiong, D. Li, Z. Zhu, E. Duan, E. Jiang, S. Feng, M. Han, Y. Xu, F. Wang, and J. Zhou. 2015. MSX2 mediates entry of human pluripotent stem cells into mesendoderm by simultaneously suppressing SOX2 and activating NODAL signaling. *Cell Res* 25: 1314-1332.
88. Brewer, J. R., P. Mazot, and P. Soriano. 2016. Genetic insights into the mechanisms of Fgf signaling. *Genes Dev* 30: 751-771.
89. Guy, G. R., R. A. Jackson, P. Yusoff, and S. Y. Chow. 2009. Sprouty proteins: modified modulators, matchmakers or missing links? *J Endocrinol* 203: 191-202.
90. Yu, Y., S. O. Yoon, G. Poulogiannis, Q. Yang, X. M. Ma, J. Villen, N. Kubica, G. R. Hoffman, L. C. Cantley, S. P. Gygi, and J. Blenis. 2011. Phosphoproteomic analysis identifies Grb10 as an mTORC1 substrate that negatively regulates insulin signaling. *Science* 332: 1322-1326.
91. Desbuquois, B., N. Carre, and A. F. Burnol. 2013. Regulation of insulin and type 1 insulin-like growth factor signaling and action by the Grb10/14 and SH2B1/B2 adaptor proteins. *FEBS J* 280: 794-816.
92. Ornitz, D. M., and N. Itoh. 2015. The Fibroblast Growth Factor signaling pathway. *Wiley Interdiscip Rev Dev Biol* 4: 215-266.

93. Huang, C., K. Jacobson, and M. D. Schaller. 2004. MAP kinases and cell migration. *J Cell Sci* 117: 4619-4628.
94. Huff, J. 2015. The Airyscan detector from ZEISS: confocal imaging with improved signal-to-noise ratio and super-resolution. *Nat Methods* 12.
95. Loebel, D. A., J. B. Studdert, M. Power, T. Radziewicz, V. Jones, L. Coultas, Y. Jackson, R. S. Rao, K. Steiner, N. Fossat, L. Robb, and P. P. Tam. 2011. Rho maintains the epithelial architecture and facilitates differentiation of the foregut endoderm. *Development* 138: 4511-4522.
96. Sakai, T., S. Li, D. Docheva, C. Grashoff, K. Sakai, G. Kostka, A. Braun, A. Pfeifer, P. D. Yurchenco, and R. Fassler. 2003. Integrin-linked kinase (ILK) is required for polarizing the epiblast, cell adhesion, and controlling actin accumulation. *Genes Dev* 17: 926-940.
97. Binetruy, B., L. Heasley, F. Bost, L. Caron, and M. Aouadi. 2007. Concise review: regulation of embryonic stem cell lineage commitment by mitogen-activated protein kinases. *Stem Cells* 25: 1090-1095.
98. Bernstein, E., A. A. Caudy, S. M. Hammond, and G. J. Hannon. 2001. Role for a bidentate ribonuclease in the initiation step of RNA interference. *Nature* 409: 363-366.
99. Weidgang, C. E., R. Russell, P. R. Tata, S. J. Kuhl, A. Illing, M. Muller, Q. Lin, C. Brunner, T. M. Boeckers, K. Bauer, A. E. Kartikasari, Y. Guo, M. Radenz, C. Bernemann, M. Weiss, T. Seufferlein, M. Zenke, M.

- Iacovino, M. Kyba, H. R. Scholer, M. Kuhl, S. Liebau, and A. Kleger. 2013. TBX3 Directs Cell-Fate Decision toward Mesendoderm. *Stem Cell Reports* 1: 248-265.
100. Komander, D., M. J. Clague, and S. Urbe. 2009. Breaking the chains: structure and function of the deubiquitinases. *Nat Rev Mol Cell Biol* 10: 550-563.
 101. Kuo, M. H., J. E. Brownell, R. E. Sobel, T. A. Ranalli, R. G. Cook, D. G. Edmondson, S. Y. Roth, and C. D. Allis. 1996. Transcription-linked acetylation by Gcn5p of histones H3 and H4 at specific lysines. *Nature* 383: 269-272.
 102. Wang, Y. L., F. Faiola, M. Xu, S. Pan, and E. Martinez. 2008. Human ATAC Is a GCN5/PCAF-containing acetylase complex with a novel NC2-like histone fold module that interacts with the TATA-binding protein. *J Biol Chem* 283: 33808-33815.
 103. Snezhkina, A. V., G. S. Krasnov, A. V. Lipatova, A. F. Sadritdinova, O. L. Kardymon, M. S. Fedorova, N. V. Melnikova, O. A. Stepanov, A. R. Zaretsky, A. D. Kaprin, B. Y. Alekseev, A. A. Dmitriev, and A. V. Kudryavtseva. 2016. The Dysregulation of Polyamine Metabolism in Colorectal Cancer Is Associated with Overexpression of c-Myc and C/EBPbeta rather than Enterotoxigenic Bacteroides fragilis Infection. *Oxid Med Cell Longev* 2016: 2353560.

104. Pikman, Y., A. Puissant, G. Alexe, A. Furman, L. M. Chen, S. M. Frumm, L. Ross, N. Fenouille, C. F. Bassil, C. A. Lewis, A. Ramos, J. Gould, R. M. Stone, D. J. DeAngelo, I. Galinsky, C. B. Clish, A. L. Kung, M. T. Hemann, M. G. Vander Heiden, V. Banerji, and K. Stegmaier. 2016. Targeting MTHFD2 in acute myeloid leukemia. *J Exp Med* 213: 1285-1306.
105. Ben-Yosef, T., A. Eden, and N. Benvenisty. 1998. Characterization of murine BCAT genes: Bcat1, a c-Myc target, and its homolog, Bcat2. *Mamm Genome* 9: 595-597.
106. Li, Z., S. Van Calcar, C. Qu, W. K. Cavenee, M. Q. Zhang, and B. Ren. 2003. A global transcriptional regulatory role for c-Myc in Burkitt's lymphoma cells. *Proc Natl Acad Sci U S A* 100: 8164-8169.
107. Grandori, C., S. M. Cowley, L. P. James, and R. N. Eisenman. 2000. The Myc/Max/Mad network and the transcriptional control of cell behavior. *Annu Rev Cell Dev Biol* 16: 653-699.
108. Lehtinen, L., K. Ketola, R. Makela, J. P. Mpindi, M. Viitala, O. Kallioniemi, and K. Iljin. 2013. High-throughput RNAi screening for novel modulators of vimentin expression identifies MTHFD2 as a regulator of breast cancer cell migration and invasion. *Oncotarget* 4: 48-63.
109. Zhou, W., X. Feng, C. Ren, X. Jiang, W. Liu, W. Huang, Z. Liu, Z. Li, L. Zeng, L. Wang, B. Zhu, J. Shi, J. Liu, C. Zhang, Y. Liu, and K. Yao.

2013. Over-expression of BCAT1, a c-Myc target gene, induces cell proliferation, migration and invasion in nasopharyngeal carcinoma. *Mol Cancer* 12: 53.
110. Charalambous, M., F. M. Smith, W. R. Bennett, T. E. Crew, F. Mackenzie, and A. Ward. 2003. Disruption of the imprinted Grb10 gene leads to disproportionate overgrowth by an Igf2-independent mechanism. *Proc Natl Acad Sci U S A* 100: 8292-8297.
111. Gerdts, J., D. W. Summers, J. Milbrandt, and A. DiAntonio. 2016. Axon Self-Destruction: New Links among SARM1, MAPKs, and NAD⁺ Metabolism. *Neuron* 89: 449-460.
112. Walker, L. J., D. W. Summers, Y. Sasaki, E. J. Brace, J. Milbrandt, and A. DiAntonio. 2017. MAPK signaling promotes axonal degeneration by speeding the turnover of the axonal maintenance factor NMNAT2. *Elife* 6.
113. Yao, Y., W. Li, J. Wu, U. A. Germann, M. S. Su, K. Kuida, and D. M. Boucher. 2003. Extracellular signal-regulated kinase 2 is necessary for mesoderm differentiation. *Proc Natl Acad Sci U S A* 100: 12759-12764.
114. Tsai, W. B., I. Aiba, Y. Long, H. K. Lin, L. Feun, N. Savaraj, and M. T. Kuo. 2012. Activation of Ras/PI3K/ERK pathway induces c-Myc stabilization to upregulate argininosuccinate synthetase, leading to arginine deiminase resistance in melanoma cells. *Cancer Res* 72: 2622-2633.

115. Smith, K. N., A. M. Singh, and S. Dalton. 2010. Myc represses primitive endoderm differentiation in pluripotent stem cells. *Cell Stem Cell* 7: 343-354.
116. Scognamiglio, R., N. Cabezas-Wallscheid, M. C. Thier, S. Altamura, A. Reyes, A. M. Prendergast, D. Baumgartner, L. S. Carnevalli, A. Atzberger, S. Haas, L. von Paleske, T. Boroviak, P. Worsdorfer, M. A. Essers, U. Klotz, R. N. Eisenman, F. Edenhofer, P. Bertone, W. Huber, F. van der Hoeven, A. Smith, and A. Trumpp. 2016. Myc Depletion Induces a Pluripotent Dormant State Mimicking Diapause. *Cell* 164: 668-680.
117. Baudino, T. A., C. McKay, H. Pendeville-Samain, J. A. Nilsson, K. H. Maclean, E. L. White, A. C. Davis, J. N. Ihle, and J. L. Cleveland. 2002. c-Myc is essential for vasculogenesis and angiogenesis during development and tumor progression. *Genes Dev* 16: 2530-2543.
118. Davis, A. C., M. Wims, G. D. Spotts, S. R. Hann, and A. Bradley. 1993. A null c-myc mutation causes lethality before 10.5 days of gestation in homozygotes and reduced fertility in heterozygous female mice. *Genes Dev* 7: 671-682.
119. Charron, J., B. A. Malynn, P. Fisher, V. Stewart, L. Jeannotte, S. P. Goff, E. J. Robertson, and F. W. Alt. 1992. Embryonic lethality in mice homozygous for a targeted disruption of the N-myc gene. *Genes Dev* 6: 2248-2257.

120. Sawai, S., A. Shimono, Y. Wakamatsu, C. Palmes, K. Hanaoka, and H. Kondoh. 1993. Defects of embryonic organogenesis resulting from targeted disruption of the N-myc gene in the mouse. *Development* 117: 1445-1455.
121. Stanton, B. R., A. S. Perkins, L. Tessarollo, D. A. Sassoon, and L. F. Parada. 1992. Loss of N-myc function results in embryonic lethality and failure of the epithelial component of the embryo to develop. *Genes Dev* 6: 2235-2247.
122. Trimarchi, J. M., and J. A. Lees. 2002. Sibling rivalry in the E2F family. *Nat Rev Mol Cell Biol* 3: 11-20.
123. Swiss, V. A., and P. Casaccia. 2010. Cell-context specific role of the E2F/Rb pathway in development and disease. *Glia* 58: 377-390.
124. Plasschaert, R. N., and M. S. Bartolomei. 2015. Tissue-specific regulation and function of Grb10 during growth and neuronal commitment. *Proc Natl Acad Sci U S A* 112: 6841-6847.
125. Serra, V., P. J. Eichhorn, C. Garcia-Garcia, Y. H. Ibrahim, L. Prudkin, G. Sanchez, O. Rodriguez, P. Anton, J. L. Parra, S. Marlow, M. Scaltriti, J. Perez-Garcia, A. Prat, J. Arribas, W. C. Hahn, S. Y. Kim, and J. Baselga. 2013. RSK3/4 mediate resistance to PI3K pathway inhibitors in breast cancer. *J Clin Invest* 123: 2551-2563.
126. She, P., T. M. Reid, S. K. Bronson, T. C. Vary, A. Hajnal, C. J. Lynch, and S. M. Hutson. 2007. Disruption of BCATm in mice leads to

increased energy expenditure associated with the activation of a futile protein turnover cycle. *Cell Metab* 6: 181-194.

127. Pai, Y. J., K. Y. Leung, D. Savery, T. Hutchin, H. Prunty, S. Heales, M. E. Brosnan, J. T. Brosnan, A. J. Copp, and N. D. Greene. 2015. Glycine decarboxylase deficiency causes neural tube defects and features of non-ketotic hyperglycinemia in mice. *Nat Commun* 6: 6388.
128. Hu, C., L. Fan, P. Cen, E. Chen, Z. Jiang, and L. Li. 2016. Energy Metabolism Plays a Critical Role in Stem Cell Maintenance and Differentiation. *Int J Mol Sci* 17: 253.
129. Anjum, R., and J. Blenis. 2008. The RSK family of kinases: emerging roles in cellular signalling. *Nat Rev Mol Cell Biol* 9: 747-758.
130. Conacci-Sorrell, M., C. Ngouenet, and R. N. Eisenman. 2010. Myc-nick: a cytoplasmic cleavage product of Myc that promotes alpha-tubulin acetylation and cell differentiation. *Cell* 142: 480-493.
131. Patel, J. H., Y. Du, P. G. Ard, C. Phillips, B. Carella, C. J. Chen, C. Rakowski, C. Chatterjee, P. M. Lieberman, W. S. Lane, G. A. Blobel, and S. B. McMahon. 2004. The c-MYC oncoprotein is a substrate of the acetyltransferases hGCN5/PCAF and TIP60. *Mol Cell Biol* 24: 10826-10834.
132. Martinez-Balbas, M. A., U. M. Bauer, S. J. Nielsen, A. Brehm, and T. Kouzarides. 2000. Regulation of E2F1 activity by acetylation. *EMBO J* 19: 662-671.

133. Kim, J. H., B. Kim, L. Cai, H. J. Choi, K. A. Ohgi, C. Tran, C. Chen, C. H. Chung, O. Huber, D. W. Rose, C. L. Sawyers, M. G. Rosenfeld, and S. H. Baek. 2005. Transcriptional regulation of a metastasis suppressor gene by Tip60 and beta-catenin complexes. *Nature* 434: 921-926.
134. Sierra, J., T. Yoshida, C. A. Joazeiro, and K. A. Jones. 2006. The APC tumor suppressor counteracts beta-catenin activation and H3K4 methylation at Wnt target genes. *Genes Dev* 20: 586-600.
135. Guelman, S., K. Kozuka, Y. Mao, V. Pham, M. J. Solloway, J. Wang, J. Wu, J. R. Lill, and J. Zha. 2009. The double-histone-acetyltransferase complex ATAC is essential for mammalian development. *Mol Cell Biol* 29: 1176-1188.
136. Yamauchi, T., J. Yamauchi, T. Kuwata, T. Tamura, T. Yamashita, N. Bae, H. Westphal, K. Ozato, and Y. Nakatani. 2000. Distinct but overlapping roles of histone acetylase PCAF and of the closely related PCAF-B/GCN5 in mouse embryogenesis. *Proc Natl Acad Sci U S A* 97: 11303-11306.
137. Fazzio, T. G., J. T. Huff, and B. Panning. 2008. An RNAi screen of chromatin proteins identifies Tip60-p400 as a regulator of embryonic stem cell identity. *Cell* 134: 162-174.
138. Jin, Q., L. Zhuang, B. Lai, C. Wang, W. Li, B. Dolan, Y. Lu, Z. Wang, K. Zhao, W. Peng, S. Y. Dent, and K. Ge. 2014. Gcn5 and PCAF

negatively regulate interferon-beta production through HAT-independent inhibition of TBK1. *EMBO Rep* 15: 1192-1201.

139. Makedis, M. M., and K. M. Downs. 2013. Widespread but tissue-specific patterns of interferon-induced transmembrane protein 3 (IFITM3, FRAGILIS, MIL-1) in the mouse gastrula. *Gene Expr Patterns* 13: 225-239.

VITA

Li Wang was born in Luo Yang, People's Republic of China on December 7, 1976, the daughter of Xinhua Zhang and Jiyuan Wang. After completing her work at the First High School of Luo Yang City, Henan in 1995, she entered the Health Science Center of Peking University in Beijing. She received the degree of Bachelor of Science with a major in pharmacology from Peking University in July 2000. For the next six years, she worked as a research associate in the State Key Laboratory of Natural and Biomimetic Drugs at the School of Pharmacy of Peking University. In October of 2006 she joined the Pharmacovigilance group in the headquarters of Eisai Co., Ltd, Tokyo, Japan, as an auditor for monitoring the effects of licensed medical products. In August of 2010, she entered The University of Texas MD Anderson Cancer Center UTHHealth Graduate School of Biomedical Sciences.